8-2007

Analysis of Simulated Electromyography (EMG) Signals Using Integrated Computer Muscle Model

Mohammad Abdul Ahad
University of Tennessee - Knoxville

To the Graduate Council:

I am submitting herewith a dissertation written by Mohammad Abdul Ahad entitled "Analysis of Simulated Electromyography (EMG) Signals Using Integrated Computer Muscle Model." I have examined the final electronic copy of this dissertation for form and content and recommend that it be accepted in partial fulfillment of the requirements for the degree of Doctor of Philosophy, with a major in Electrical Engineering.

Mohammad Ferdjallah, Major Professor

We have read this dissertation and recommend its acceptance:

Aly Fathy, Michael J. Roberts, Jack F. Wasserman

Accepted for the Council:

Carolyn R. Hodges

Vice Provost and Dean of the Graduate School

(Original signatures are on file with official student records.)

To the Graduate Council:

I am submitting herewith a dissertation written by Mohammad Abdul Ahad entitled "Analysis of Simulated Electromyography (EMG) Signals Using Integrated Computer Muscle Model". I have examined the final electronic copy of this dissertation for form and content and recommend that it be accepted in partial fulfillment of the requirements for the degree of Doctor of Philosophy, with a major in Electrical Engineering.

Mohammad Ferdjallah, Major Professor

We have read this dissertation
And recommend its acceptance:

Aly Fathy

Michael J. Roberts

Jack F. Wasserman

Accepted for the Council:

Carolyn Hodges

Vice Provost and Dean of the Graduate School

(Original signatures are on file with official student records)

ANALYSIS OF SIMULATED ELECTROMYOGRAPHY (EMG) SIGNALS USING INTEGRATED COMPUTER MUSCLE MODEL

A Thesis
Presented For the
Doctor of Philosophy
Degree

The University of Tennessee, Knoxville

Mohammad Abdul Ahad
August 2007

Dedicated to my parents

Acknowledgement

There are a number of people that I need to mention without whose help this work would never have seen the light. First of all, my academic advisor Dr. Mohammed Ferdjallah whose constant encouragement and thoughtful guidance were key to the success of this dissertation. He introduced me to this fascinating world of Bioengineering and taught me all the basics of this interesting field. He made me a thinker, writer and scientist. I would also like to thank the committee members Drs Aly Fathy, Michael Roberts and Jack Wasserman who in different situations, helped and guided me for the successful completion of this dissertation. I'm grateful to my group members Moshiur Rahman and Abdullah Zaman for their technical and moral support. I would also like to thank Ashraf and many other friends for their encouragement. All of my family members especially my late brother-in-law Abul Mansur were a source of constant encouragement and their confidence in me was unwavering. Last but not the least, I thank my wife Faiza, who always believed in me and supported me through thick and thin.

Table of Contents

List of Tables

List of Figures

CHAPTER 1

1. Motivation and Problem Statement

1.1 Introduction

Electromyography (EMG) is a technique used to study the activity of muscle through detection and analysis of the electrical signals generated during muscular contractions. Electromyographic activity is recorded from skeletal muscles to obtain information about their anatomy and physiology. Electromyography, in interplay with various anatomical techniques, provides the present knowledge of the structural organization and the nervous control of muscle. EMG is the prime source of information about the status of the neuromuscular system, and EMG has developed into a diagnostic tool that allows the clinician to follow changes in nerve and muscle caused by neuromuscular diseases.

EMG provides both invasive and noninvasive means for the study of muscular functions [1, 2]. It is also useful in interpreting pathologic states of musculoskeletal or neuromuscular systems [3, 4]. In particular, EMG offers valuable information concerning the timing of muscular activity and its relative intensity [5, 6]. Standard EMG is typically recorded from fine wire or two surface electrodes placed at discrete sites over a muscle or muscle belly. Currently surface grid electrode EMG is widely used.

The cell bodies of these neurons reside in the brainstem and spinal cord. The interfacing fiber between motor neuron and muscle is called axon. At the distal end, an axon divides

into many terminal branches. Each terminal branch innervates a group of muscle fibers. When a nerve signal approaches the end of an axon, it spreads out over all its terminal branches and stimulates all the muscle fibers supplied by them. So, all the excited muscle fibers contract almost simultaneously. Since they behave as a single functional unit, one nerve fiber and all the muscle fibers innervated by it are called a motor unit (MU) [7, 8]. Generally, the muscle fibers of a motor unit are distributed throughout muscle rather than being clustered together. The fine control of the muscle force is performed through the intricate mechanism and interaction of the brain and muscle. During contraction, these motor units are recruited systematically and the recruited motor units discharge in a train of pulses in a complex manner [9, 10]. The recorded EMG is the temporal summation of all the recruited motor unit action potential trains. Because movement is controlled by motor unit activity, an understanding of motor unit physiology can have a significant impact on the evaluation and treatment of movement disorders.

The neuromuscular system is an intricate physiological organization of brain, nerve and muscle. These neural control properties are not well understood mostly because of the experimental difficulties in quantifying the neural input to the muscle. Moreover, the muscle itself is a complex system. It is necessary to address these complexities as accurately as possible. Understanding of these complex systems facilitates the understanding of EMG generation, which is a highly complex signal by itself.

1.2 Application of EMG Signal

The main reason for the interest in EMG signal analysis is in clinical diagnosis and biomedical applications. EMG is used clinically for the diagnosis of neurological and neuromuscular problems. The shapes and firing rates of motor unit action potentials (MUAPs) in EMG signals provide an important source of information for the diagnosis of neuromuscular disorders. The field of management and rehabilitation of motor disability is identified as one of the important application areas. It is used diagnostically by gait laboratories and by clinicians trained in the use of biofeedback or ergonomic assessment. EMG is also used in many types of research laboratories, including those involved in biomechanics, neuromuscular physiology, movement disorders, postural control, physical therapy, and many others. Electromyography signals can also be used for Evolvable Hardware Chip (EHW) development, and modern human computer interaction [11]. Moreover, EMG covers nerve conduction studies - testing the electrical function of nerves in the limbs. The most frequent reason for nerve conduction studies is to look for evidence of a trapped nerve. Carpal tunnel syndrome is the type of nerve entrapment most frequently seen in clinical neurophysiology. Nerve conduction testing is also used to test for and evaluate a whole range of other nerve disorders. If a limb is injured, this technique can be used to test for nerve damage. The studies can give valuable information about which nerves are involved and how severely they have been injured. Nerve conduction studies are also used in the diagnosis of peripheral neuropathies. This is a group of conditions in which, instead of a single nerve being involved, there is a generalised abnormality of the nerves in the limbs. Nerve conduction

studies in these cases may show several types of abnormality - slowing of nerve conduction or a decrease in the size of the electrical signals or both. The exact pattern of these abnormalities will help to classify the type of peripheral neuropathy.

1.3 Techniques of EMG Acquisition

Fine wire needle electrode and surface electrodes are two ways to collect EMG data. Fine wire electrodes require a needle for insertion into the belly of the muscle. The advantages of fine wire electrodes are an increased bandwidth, a more specific pick-up area, ability to test deep muscles, isolation of specific muscle parts of large muscles, and ability to test small muscles which would be impossible to detect with a surface electrode due to cross-talk. But there are some disadvantages using the fine wire electrodes. The needle insertion causes discomfort. This discomfort can increase the tightness or spasticity in the muscles. The electrodes are less repeatable as it is very difficult to place the needle in the same area of the muscle each time. On the other hand, with the surface electrodes there is minimal pain with application, they are more reproducible, easy to apply, and they are very good for movement applications. The disadvantages of surface electrodes are that they have a large pick-up area and therefore, have more potential for cross talk from adjacent muscles. Nevertheless the surface grid electrode technology is becoming popular now a days.

There are two techniques for surface electrode EMG that are widely used. They are, differential electrode and surface grid electrode configuration. Because the EMG signal is low in amplitude with respect to other ambient signals on the surface of the skin, it is

convenient to detect it with a differential configuration. That is, two detection surfaces are used and the two detected signals are subtracted prior to being amplified. In this differential configuration, the shape and area of the detection surfaces and the distance between the detection surfaces are important factors because they affect the amplitude and the frequency content of the signal. The differential arrangement acts as a comb band-pass filter to the electrical signal seen by the detection surfaces. The Double differential technique is widely used to reduce and possibly eliminate crosstalk in the EMG signal detected with surface electrodes. This technique consists of using a surface electrode having three detection surfaces equally spaced apart. Figure 1 shows the configuration of a double-differential surface electrode technique. Two differential signals are obtained from detection surfaces 1 and 2, and detection surfaces 2 and 3. Then a differential signal is obtained from these two. Thus, the EMG signal undergoes two levels of differentiation. This procedure has the advantage of decreasing considerably the pick-up volume of the three-bar electrode, thus filtering out the signals from further distances often corresponding to those emanating from other muscles.

Single Motor unit analysis is a key attraction of multichannel surface grid electrode EMG. Moreover, multichannel EMG allows the construction of higher order electrode montages for spatial filtering, which facilitate the study and mapping of muscle's spatial functional properties [12]. Multichannel surface EMG provides spatial or topographical information from a muscle. A Myoelectric signal recorded over the muscle surface changes with the anatomical position of that muscle. Single-site recording thus do not have the complete information of the investigated muscle and

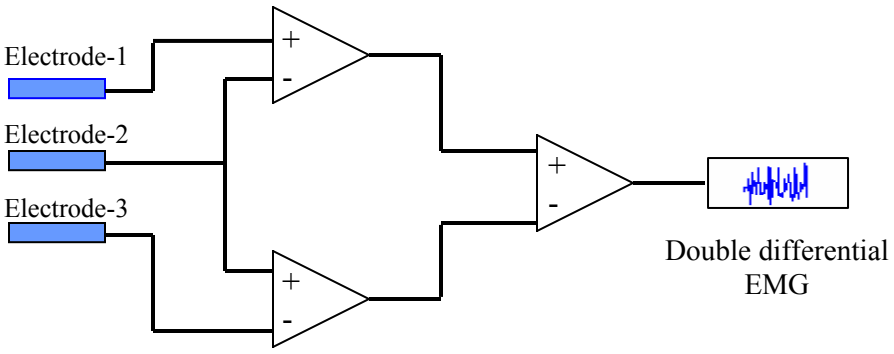

Figure 1.1: Double differential technique for EMG acquisition

may lead to erroneous interpretation of the EMG signals and eventually unnecessary surgery especially in the case of Carpometacarpal (CMC) degenerative joint disease (DJD), which is very common in the aging hands [13]. Thus the multichannel grid electrode EMG system has promising future in electro-diagnostic research.

1.4 System Development of Multichannel EMG

Figure 1.2 shows a block diagram of multichannel EMG acquiring technique. This EMG unit uses a 60-channel configuration for EMG data collection. EMG signals are on the order of milivolt; hence they are vulnerable to many types of electronic noise. A pre-amplification stage is necessary to enhance the performance of the filtering stage. EMG data are needed to be amplified and filtered out for further processing. So a front-end instrumentation consisting of an amplifier and a lowpass filter has been designed [14]. 60 steel (6X10grid) pins are inserted into a 8cmX8cm plastic paper so that these pins are insulated from each other. Each individual electrode has a diameter of 1mm and these pins are placed 2.5mm apart from each other. 60-channel bus-type ribbon cable is used to connect those pins to the front-end instrument.

1.4.1Front-end Instrumentation

A pre-amplification stage is necessary to enhance the performance of the filtering stage. For pre-amplification, a power instrumentation amplifier (Burr-Brown's INA2126) is used. This dual (two amplifier in a single chip) precision instrumentation amplifier is

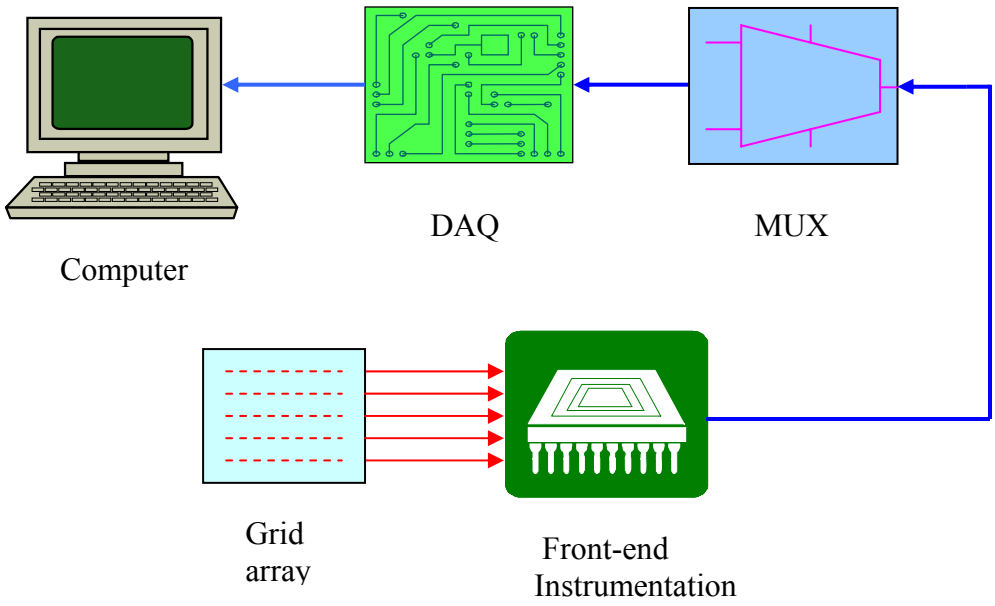

Figure 1.2: A block diagram for surface EMG acquisition technique

capable of accurate, low noise differential signal acquisition. Its two-op-amp design provides excellent performance with very low quiescent current. This combined with wide operating voltage range of ±13.5V to ±18V, makes it ideal for portable instrumentation and data acquisition systems. Gain can be set from 5V/V to 10000V/V with a single external resistor R_g using the following gain equation:

$$G = \frac{V_o}{V_{in^+} - V_{in^-}} = 5 + \frac{80K}{R_g} \quad (1)$$

The gain was set by an external resistor to 120 with common-mode rejection of 94 dB and 9 KHz of bandwidth.

1.4.2 Filtering stage

An ideal lowpass filter passes all frequencies below its cutoff frequency with a uniform gain and phase change. It also totally suppresses all frequencies above the cutoff frequency. Although the realization of such a filter is impossible, practical filters can be designed and implemented to satisfy at least the most crucial design requirements. A filter design, which provides the maximum degree of pass-band flatness is the Butterworth design. The Butterworth filter has a gain characteristic, which rolls off slowly near the cutoff, approaching the asymptotic slope only at frequencies well above the cutoff. Moreover, the Butterworth is the design which least affects the phase of those signals whose spectral components all fall within the pass-band of the filter. The Sallen and Key circuit whose simplicity, stability and ease of adjustment have made it an extremely popular circuit as a basic low-pass filter will be used for this filter design,

which is shown in Figure 3. The operational amplifier in the circuit is actually the pre-amplification stage described above and thus the filter is designed at the top of the amplifier. The operational amplifier is configured in the voltage-follower configuration, which has a closed loop gain of unity, very high input impedance and nearly zero output impedance. For an ideal operational amplifier, the input resistance of its terminals is infinite. Therefore, the sum of the two entering currents at each terminal must be zero. The voltage transfer function of this circuit, using the Laplace Transform, can be expressed as:

$$H(s) = \frac{V_o}{V_{in}} = \frac{1}{s^2(C_1C_2R_1R_2) + sC_2(R_1 + R_2) + 1} \qquad (2)$$

The following nominal values can be calculated for a 2500Hz cutoff frequency:

$R_1=R_2=R=100K\Omega$ and $C_1=900pf$ *and C2=450pf*

The small values of the capacitors C_1 and C_2 ensure linearity and stability of the filter. Since the filter is designed as follower for the pre-amplifier, which has very low output resistance ($<<1\Omega$), the value of the resistance R_1 is less affected. Consequently the cutoff frequency as well as the performance of the filter is not affected. Figure 4 shows the frequency response of the filter described above.

1.4.3 Building of the Front-end Interface

After the pre-signal processing in the front-end instrument, the data are passed through the multiplexer. We used the AMUX-64T of National Instrument, which is a front-end Analog multiplexer that quadruples the number of analog input signals that can be

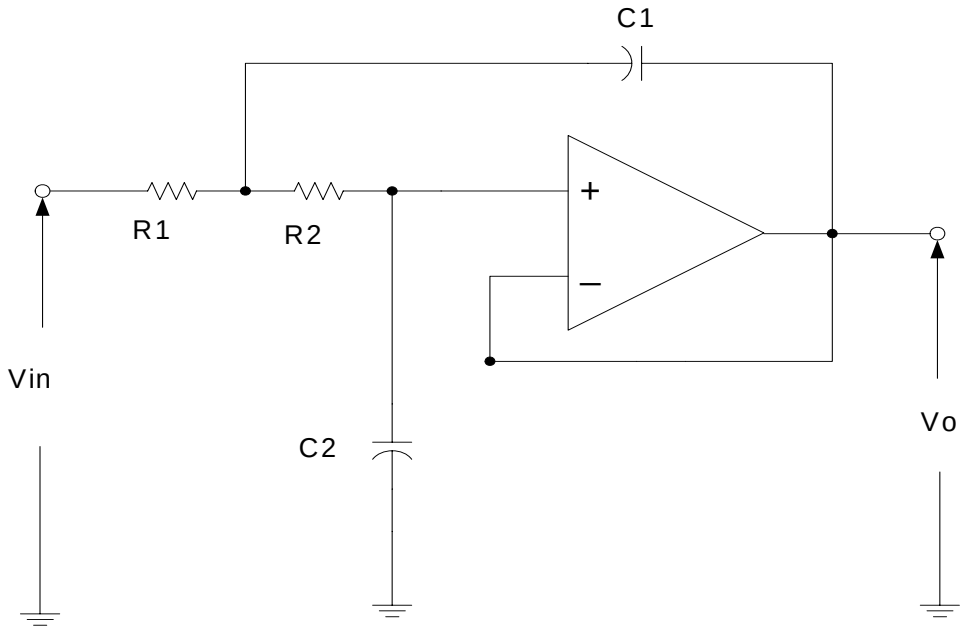

Figure 1.3: A Sallen and Key type Butterworth filter

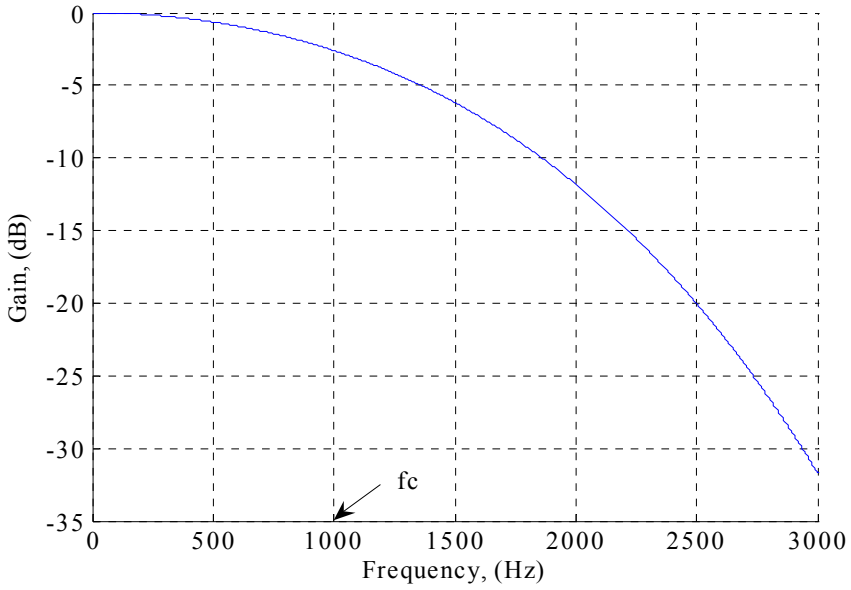

Figure 1.4: Frequency response of the Butterworth filter

digitized with a National Instruments DAQ board. The AMUX-64T has 16 separate four-to-one analog multiplexer circuits and has 64 single-ended or 32 differential channels. It can be powered by the computer through the DAQ board or with a 5V battery.

The Data Acquisition Board used is the National Instrument's AT-MIO-16E-1 which delivers high-performance, reliable data acquisition capabilities to meet a wide range of application requirements. It has a 12- bit resolution with 16 single-ended analog inputs. The maximum sampling rate it can provide is 1.5 MS/s. This device features both analog and digital triggering capability, as well as two 12-bit analog outputs, two 24-bit 20MHz counter/timers and 8 digital I/O lines.

The whole EMG mapping system circuit board has been developed using the following connection between all the modules as shown below. The EMG signals acquired through the grid electrodes are amplified and filtered out by the front-end instrumentation. These analog signals are then received by the DAQ board through the MUX circuitry and converted to digital signals to be processed by the computer.

1.5 Review of the Previous Research on EMG

A number of investigators worked mostly on the development of generating the single muscle fiber action potential. Several approaches have been presented to simulate the extra-cellular potential by volume conduction theory [5, 15, 16]. In 1947, Loerente de No [6] first introduced the idea of intercellular and extra cellar potential. In 1969, Paul

Rosenfalck [17] first presented the mathematical analysis of the spread of action potential within nerve and muscle fibers. Based on Maxwell's field equation, he developed the relationship between the extra cellular and intracellular potential. In 1974, Plonsey [16] formulated this relationship as a free space source-sink relationship. In 1981, Andreassen et al [18] extended this model by approximating the muscle structure with an anisotropic volume conductor model. In 1983, Nandedkar and Stalberg [19] introduced a line source model with a simplified approach of the transfer function of the medium. They utilized the concept of potential produced by a point source located at the origin of cylindrical coordinate system. In 1990, Gootzen et al [20] reported the influence of the finite dimension of volume conductor and fiber length on single-fiber action potential. Their described model is found to be capable of generating a surface motor unit action potential, which showed a very good resemblance with measured signal. In 1999, Merletti et al [21] investigated the relationship between the parameters of the active motor unit by using mathematical model of surface electromyographic signal. In 2001, Farina et al [22] proposed a new model of EMG signal generation and detection by describing the volume conductor as an inhomogeneous and anisotropic medium constituted by muscle, fat and skin tissue. He presented the transfer function in the form of two-dimensional filter function. Later on, most of the modeling studies were focused around the precise representation of multiple layer volume conductor model [2,11].

Not too many researchers worked on the development of the motor unit pool in a muscle mostly because there was lack of information about the motor unit physiology although there has been an extensive amount of literature devoted to investigating the various

properties of a motor unit. These studies have demonstrated that the histochemical, morphological and physiological properties of motor units vary across the motor unit pool of a muscle (23, 24, 25). These studies have also found that the properties of the motor unit pool vary dramatically between different muscles by their number, size and recruitment threshold. However, the muscle fibers belonging to a motor unit feature many common characteristics (23). The fibers of a motor unit are scattered throughout a broad region of muscle and intermingled with fibers belonging to many other motor units (23). Henneman and his colleagues [25] demonstrated that there is a unique relationship between motoneuron size and the motor unit's recruitment threshold, which is well known as size principle that states that in a pool of motor units, recruitment occurs in the order of increasing size of the motor unit during contractions. It has been demonstrated that variable inputs to the motor unit pool allow the nervous system to vary the rate coding and recruitment strategies used during any specific task [24, 26, 27]. Several investigators have also proposed that the rate coding and recruitment strategies used during a specific task can be altered with training (28, 29, 30). The firing rates of earlier recruited motor units are greater than those of later recruited motor units at any given force value [31, 32]. However, some others found the opposite characteristics in some muscles.

During the past century a large number of mathematical models have been developed to gain a better understanding of the various neurornuscular factors, which result in the mechanical output of muscle. These models vary widely from models of single cross-bridge interactions to models of complex kinematical movements involving large

numbers of muscles [33]. Kernell [34] employed a relatively simple computational algorithm to imitate experimentally-observed recruitment and firing rate behaviors in a small pool of motoneurons. In 1988, Stein et al [35] presented the intrinsic motoneuron properties in more mechanistic models. While reporting on the EMG signal generation, some common assumptions were made which seem contrary to the known experimental results. Some [36, 37] researchers assumed the same shape for all motor unit action potential whereas others [19,38] thought all motor units discharged in the same frequency. In 1993, Fuglevand et al [31] and Stashuk [32] presented a more realistic model than others but did not incorporate the effect of different types of fibers, which influence the EMG generation significantly. Their model also did not consider the multilayer model of human muscle.

1.6 Problem Statement

An EMG is the recorded electrical signals, which represent the activities of skeletal muscle due to the stimulation by nerves. Muscle fibers are organized into many functional units, which are called motor units. A single-fiber action potential is the recorded extra cellular potential due to the propagation of the transmembrane current through the muscle fiber. The motor unit action potential is the summation of all the single fiber action potentials belonging to that motor unit. During contraction, the nervous system controls the number and patterns of motor unit recruitment as well as their rate and pattern of discharge from a pool of the motor units in a muscle group.

EMG is the temporal addition of all motor unit potentials at each of the motor unit's recruitment and firing frequency level.

By extensive survey of the current literature of experimental findings on motor unit physiology, it becomes necessary to incorporate and utilize all the latest findings in developing a muscle model for EMG generation. A muscle model developed with rigorous detail of the physiological behavior will be highly beneficial in clinical neuromuscular assessment. A good amount of research is dedicated to the development of EMG signal decomposition techniques. However without a reliable and a comprehensive model of muscle EMG generation, clinical representation of the outcome of these researches will not be accurate.

Thus, the main objective of this dissertation is to develop simulation techniques for EMG generation using a muscle model. A muscle model for EMG generation consists of two separate models. The first required model is a single-fiber action potential model to generate motor unit action potential and the other is a motor unit pool model, which will predict the motor unit recruitment and the firing frequency of each of the motor units for a certain level of force on the muscle. So the specific aims for this dissertation are as follows:

1. A single muscle fiber action potential model
2. Motor unit pool model
3. EMG generation using the single fiber action potential model and the motor unit pool model for various recruitments and firing frequency patterns

4. Analyze the generated EMG amplitude and spectrum for change in various physiological and recording factors and also for aging

Chapter Two presents a brief discussion about the muscle physiology and the conception of motor unit. For any biological system design, it is critically important to understand the physiological behavior of the system. This is also true for skeletal muscle and its modeling. Different constituent parts of muscle as well as motor unit are described. The distribution and size of motor units inside a muscle and the distribution and size of muscle fibers inside a motor unit are also discussed based on recent conceptual development of the motor unit physiology, which is the most fascinating and complicated issue to describe while developing a muscle model. This chapter also describes the biophysical and bio-chemical phenomena of the generation and propagation of action potentials inside a muscle fiber.

To develop a muscle model, it is essential to model a single-muscle fiber action potential using mathematical representations of muscle fiber's intercellular potential and muscle's electrophysiological behavior. ***Chapter Three*** provides an analytical solution of the single fiber action potential for muscle in the absence of fat and skin layer and also for multilayer model with fat and skin. The following physiological factors and the factors related to the recording of the potential affect the modeling of a single fiber action potential:

- Distribution of diameter of the muscle fibers
- Distribution of endplate and tendon of the fibers

- Finite length of the fiber
- Thickness of fat and skin tissue layers
- Spatial configuration and localization of the recording electrodes
- Distance of the muscle fiber and the recording electrode
- Sampling frequency

By considering these factors, a simulation algorithm is developed to generate a profile of single fiber muscle action potential using published anatomical and clinical data.

As EMG is the summation of all the recruited motor unit action potentials at their firing frequencies, it is necessary to predict each of the motor unit's recruitment level and pattern and the rate at which each of them fires. ***Chapter Four*** describes a motor unit pool model, which predicts the motor unit recruitment and the firing rate pattern. The model requires following physiological considerations:

- Number of motor units in a muscle and the physiological phenomenon of total number of fibers innervated by each motor unit
- Spatial distribution pattern of each motor unit and the fibers inside the motor unit
- Different types of fiber, their diameter and percentage concentration in a muscle
- Recruitment pattern of motor units (spatial coding)
- Firing rate and pattern of each motor unit (temporal coding)

The related data about the motor unit physiology were collected from published experimental medical work. A general motor unit pool model is developed to accommodate any change of above physiological factors.

In ***Chapter Five,*** models described in chapter three and four are utilized to generate EMG signals during voluntary contraction. The contraction is assumed to rise linearly in one second at a particular level and remain at that level for remaining time of the simulation. The generated EMG signal is temporal addition of each motor unit action potential trains. For a different level of voluntary contraction, the EMG signals are generated to investigate the relationship between force and different parameters of EMG signal and its spectrum. Various recruitment patterns and different firing frequency distribution behavior are tested using the model for steady-state contraction level. Results are verified with the published experimental results.

Application of the EMG model and the validation of the model with the published experimental results are described in ***Chapter Six***. Neuromuscular system behavior during aging is assessed and the muscle model developed in earlier chapter is remodeled for the age related alterations in the muscle structure and physiologic behavior. For comparison, both young and elderly muscle of tibialis anterior has been simulated for EMG generation. Changes in the EMG parameters in aging muscle are also analyzed and compared with that of young muscle.

In this chapter, a human aging process model is also developed, which shows how with age, humans lose the strength. Using this model, the effects of aging on compound muscle action potential (CMAP), which is the addition of all the muscle fiber action potential in a muscle group, is analyzed. Different CMAP metrics such as peak-to-peak amplitude, area under the curve, rise time and mean frequency of the CMAP waveform

are analyzed and compared between young and elderly persons. The changing patterns of these metrics during aging are investigated.

Finally a conclusion is made in ***Chapter Seven***, which summarizes the work in this dissertation and discusses the limitations of this muscle EMG model. Future recommendation is also provided to overcome the shortcomings of this work and a discussion is made of the future applications that this model can offer.

CHAPTER 2

2. Muscle Physiology

2.1 Introduction

Virtually all of our dynamic interactions with the environment involve muscle tissue. Muscle helps us to posture, to produce force to work in our daily life. Three types of muscle tissues exist in human body. They are skeletal striated muscle, 2) cardiac striated muscle and, 3) smooth non-striated muscle. Without these muscle tissues, nothing in the body would move. Skeletal muscle tissue moves the body by pulling on bones of the skeleton, making it possible for us to do our daily work. Cardiac muscle tissue pushes blood through the circulatory system. Smooth muscle tissue pushes fluids and solids along the digestive tract, regulates the diameters of small arteries, and performs a variety of other functions. In particular, skeletal muscles do the following functions:

1. Produce skeletal movement
2. Maintain posture and body position
3. Maintain body temperature
4. Support soft tissues
5. Guard entrances and exits

Three layers of connective tissue are part of each muscle [39, 40]: (1) an outer epimysium, (2) a central perimysium, and (3) an inner endomysium. These are shown in Figure 2.1. The entire muscle is surrounded by the epimysium dense layer of collagen

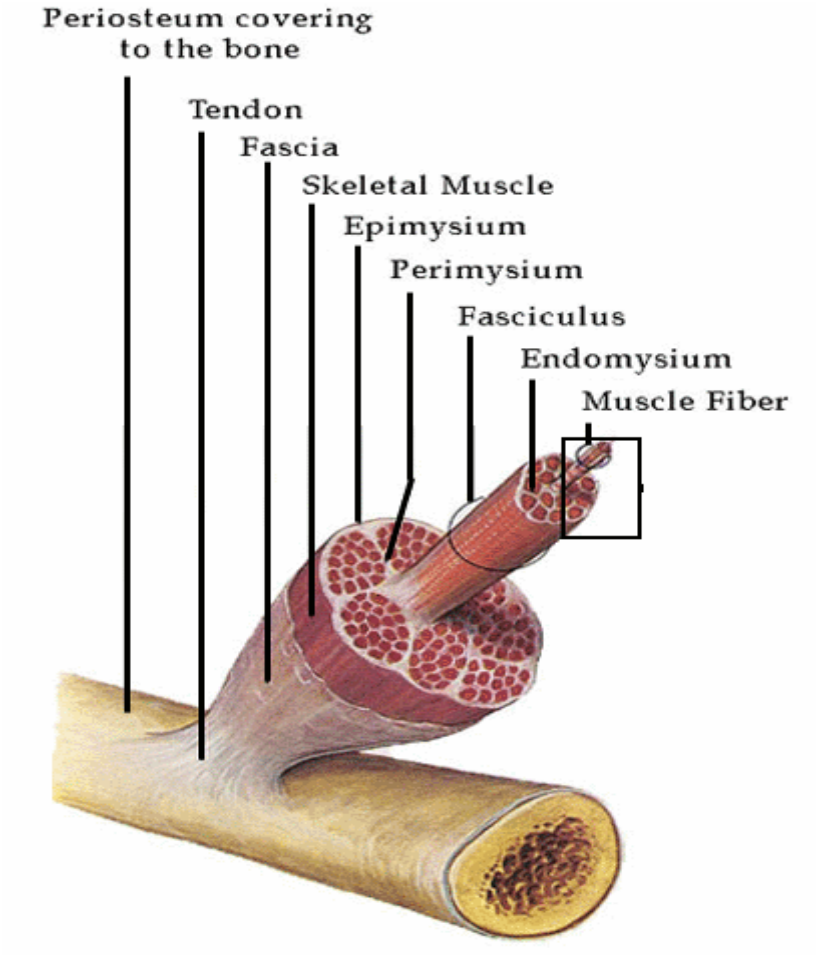

Figure 2.1: Different layers of a muscle [40].

fibers. The epimysium separates the muscle from surrounding tissues and organs. The connective tissue fibers of the perimysium divide the skeletal muscle into a series of compartments, each containing a bundle of muscle fibers called a *fascicle*. Within a fascicle, the delicate connective tissue of the endomysium surrounds the individual skeletal muscle fibers and interconnects adjacent muscle fibers. Scattered between the endomysium and the muscle fibers are satellite cells, embryonic stem cells that function in the repair of damaged muscle tissue. At each end of the muscle, the collagen fibers of the epimysium, perimysium, and endomysium come together to form a bundle known as a tendon. Tendons usually attach skeletal muscles to bones. Any contraction of the muscle will exert a pull on its tendon and thereby on the attached bone. Skeletal muscles contract only under stimulation from the central nervous system. Axons, or nerve fibers, penetrate the epimysium, branch through the perimysium, and enter the endomysium to innervate individual muscle fibers. Skeletal muscles are often called voluntary muscles, because we have voluntary control over their contractions.

2.2 Muscle Fibers

A muscle fiber is a single cell of a muscle. Muscle fibers contain many myofibrils, the contractile unit of muscles. Muscle fibers are long and a single fiber can reach a length of 30 cm. Skeletal muscle fibers can be divided into two basic types, type-I (slow-twitch fibers) and type-II (fast twitch fibers). They can also be grouped according to what kind of tissue they are found in, namely, skeletal muscle, cardiac muscle and smooth muscle [41, 42, 43]. Type-I muscle fibers (slow-oxidative fibers) use primarily cellular

respiration and as a result, have relatively high endurance. To support their high-oxidative metabolism, these muscle fibers typically have large amount of myoglobin, many mitochondria, and many blood capillaries, generate ATP by aerobic system, thus known as oxidative fiber. Type-I muscle fibers are typically found in muscles of animals that require endurance.

Type-II muscle fibers use primarily anaerobic metabolism and have relatively low endurance. These muscle fibers are typically used during tasks requiring short bursts of strength, such as sprints or weightlifting. Type-II muscle fibers cannot sustain contraction for significant lengths of time and get fatigued faster. There are two sub classes of type-II muscle fibers. They are type-IIA (fast oxidative) and type-IIB (fast glycolytic). Type IIB tire the fastest and are the prevalent type in sedentary individuals. Some research suggests that these subtypes can switch with training to some degree. Table 2.1 shows all the properties of different types of fibers.

2.2.1 Endplate

Skeletal muscle fibers contract only under the control of the nervous system. Communication between the nervous system and a skeletal muscle fiber occurs at a specialized intercellular connection known as a neuromuscular junction (Figure 2.2), or myoneural junction. A single axon branches within the perimysium to form a number of fine branches. Each branch ends at an expanded synaptic terminal. The cytoplasm of the synaptic terminal contains mitochondria and vesicles filled with molecules of acetylcholine, or ACh. Acetylcholine is a neurotransmitter, a chemical released by a

Table 2-1: Difference between different types of fibers in a muscle

Muscle Properties	Type-I fiber	Type-IIA fiber	Type-IIB fiber
Contraction time	Slow	Fast	Very fast
Size of motor neuron	Small	Large	Very large
Resistance to fatigue	High	Intermediate	Low
Activity used for	Aerobic long term	Anaerobic short term	Anaerobic
Force Production	Low	High	Very high
Mitochondria density	High	High	Low
Oxidative capacity	High	High	Low

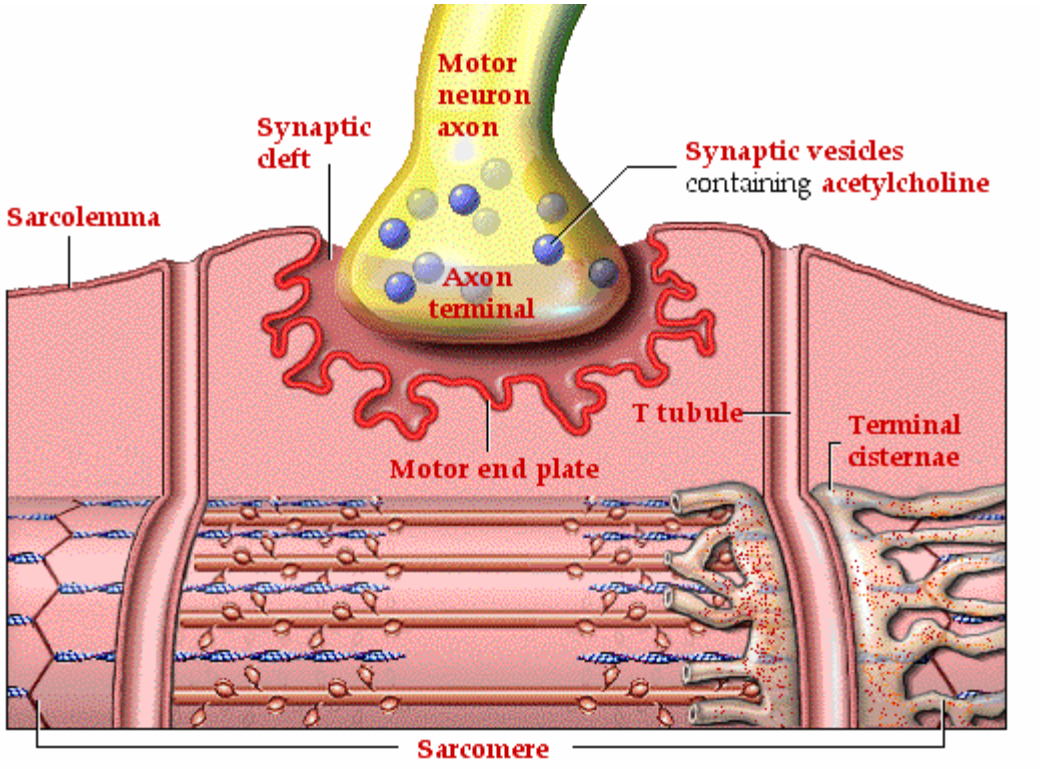

Figure 2.2: Structure of the muscle endplate

neuron to change the membrane properties of another cell. In this case, the release of ACh from the synaptic terminal can alter the permeability of the sarcolemma and trigger the contraction of the muscle fiber. The synaptic cleft, a narrow space, separates the synaptic terminal of the neuron from the opposing sarcolemmal surface. This surface, which contains membrane receptors that bind ACh, is known as the motor end plate. The endplate is that specialized region between the motor nerve terminal and the muscle fiber that mediates neuromuscular transmission. Therefore, the endplate region on the muscle fiber contains some receptors. When these receptors are activated successfully, the result is an endplate potential. An action potential is generated right after the endplate potential is generated and this action potential spreads down the length of the muscle fiber. As the action potential travels down the muscle fiber membrane, the contractile apparatus is activated in turn. The endplate zone in a healthy muscle is fairly homogeneous in that the endplates are usually at the mid portion along the length of the muscle fibers. This may vary depending on the shape of the muscle. Such positioning of the endplates allows greater efficiency in the bidirectional spread of the action potential along the length of the muscle fiber membrane. The mean position of the endplates is defined as a percentage p of a basic muscle length L (default values: p = 50%). Endplates are generally considered as scattered and normally distributed around this mean position. The default distribution has been taken as Gaussian with zero mean, SD = 1mm, range = ±3.

2.2.2 Tendon

A tendon (or sinew) is a tough band of fibrous connective tissue that connects muscle to bone. They are similar to ligaments except that ligaments join one bone to another.

Tendons are designed to withstand tension. Tendons connect muscles to bones. A combination of tendons and muscles can only exert a pulling force. The distribution of the location of tendons at the end of the fiber is homogeneous.

2.2.3 Muscle Fiber Diameter

Different types of fibers have different fiber diameters. In most of the muscle, histochemical analysis showed that type-II fiber diameter is bigger than the type-I fiber diameter. Muscle fiber diameter differs from muscle to muscle as well. The range of fiber diameter varies from 25 μm to 110 μm in different skeletal muscles. The distribution of fiber diameter is Gaussian inside a motor unit [44]. Lange et al. (45.) showed that the spread in MFCV followed a normal (Gaussian) distribution in the biceps brachii at different contraction levels (0-100% MVC) of short duration (1.5 s).

2.2.4 Muscle Fiber Numbers and Distribution

Muscle fiber numbers vary according to the size of the muscle. The bigger the muscle, the bigger the number of fibers in that muscle is. However type-I and type-II fiber number differ in a muscle and differ from muscle to muscle as well. For example in Bicep Brachii muscle group of young adults, 50% of the total fiber is type-I and 50% is type-II, whereas in Tibialis Anterior muscle, only 28% of the total number of fibers is type-I and the remaining are type-II fibers [46, 47]. Fibers are distributed uniformly throughout the muscle cross section.

2.3 Nervous System

The nervous system is both the controlling and communications system of the body. This system consists of a large number of excitable connected cells called neurons that communicate with different parts of the body by means of electrical signals, which are rapid and specific. The nervous system consists of three main parts: the brain, the spinal cord and the peripheral nerves. The neurons are the basic structural unit of the nervous system and vary considerably in size and shape. Neurons are highly specialized cells that conduct messages in the form of nerve impulses from one part of the body to another. Neurons are branches into smaller neurons to innervate the muscle fibers.

2.3.1 Motor Units

Motor units are the functional block of the muscular system. The force that a muscle produces depends on the percentage of the number of motor units that are active at that time. The motor unit (MU) is a part of the neuromuscular system that contains an anterior horn cell, its axon, and all of the muscle fibers that it innervates (Figure2.3), including the axon's specialized point of connection to the muscle fibers, the neuromuscular junction at the endplate. As motoneuron branches and innervates muscle fibers, one motoneuron innervates either type-I or type-II fibers. Thus motor unit could be either type-I or type-II category. Characteristics of two types of motor units are shown in Table 2.2. All muscles consist of a number of motor units and the fibers belonging to a motor unit are dispersed and intermingle amongst fibers of other units. The muscle fibers belonging to one motor unit can be spread throughout part, or most of the entire muscle, depending on the number of fibers and size of the muscle. When a motor neuron is

Table 2-2: Characteristics of two types of motor units

Characteristics	Type-I motor unit	Type-II motor unit
Properties of neuron cell diameter	Small	Large
Conduction velocity	Fast	Very fast
Ease of excitability	High	Low
Number of fibers	Few	Many
Fiber diameter	Moderate	Larger
Force of unit	Low	High
Contraction velocity	Moderate	Fast
Fatigability	Low	High

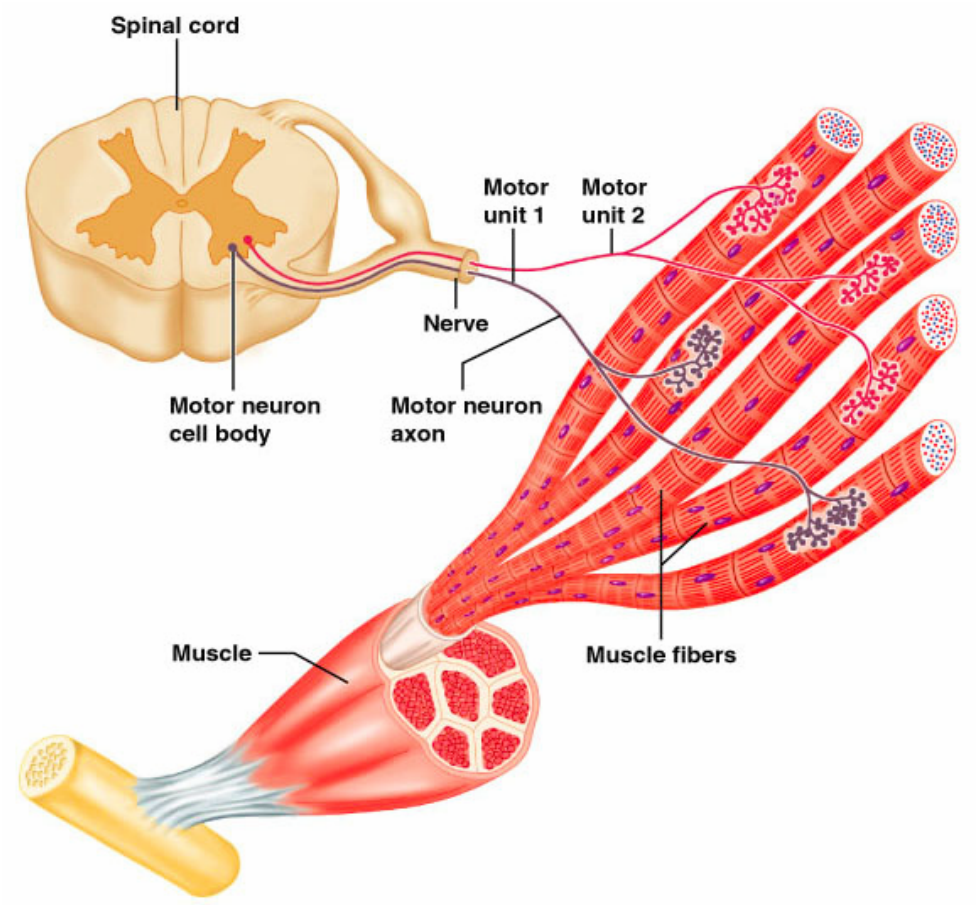

Figure 2.3: A complete neuromuscular system

activated, all of the muscle fibers innervated by the motor neuron are stimulated and contract. The activation of one motoneuron will result in a weak but distributed muscle contraction. The activation of more motor neurons will result in more muscle fibers being activated, and therefore a stronger muscle contraction. This also result is the ability of the muscle to make various patterns of contraction under the control of the upper motor neurons in the central nervous system (CNS) [48]. Groups of motor units often work together to coordinate the contractions of a single muscle. The output of a single motor unit is referred to as "all or none". This means that either all fibers in the unit contract or none do. The number of muscle fibers within each unit can vary [Table 2.3]. The bigger unit of the thigh muscles such as the gastrocnemious muscle can have thousands of fibers in each unit whereas eye muscles might have ten. In general, the number of muscle fibers innervated by a motor unit is a function of a muscle's need for refined motion. Muscles requiring more refined motion have motor units that innervate fewer muslce fibers. Motor units are distributed randomly inside the muscle [24]. Within a muscle, the ratio of the diameter of smaller and the bigger motor units can vary up to 1:10. The most consistant finding in the motor unit physiology is that motor unit properties have skewed nature of distribution [49]. Thus, it can be stated that most of the motor units will have smaller diameters and very few will have bigger diameters and this relationship can be expressed by the following equation:

$$d_i = d_{\min} e^{\frac{\ln(R)}{n} \cdot i} \tag{3}$$

where,

d_i = diameter of the ith motor unit

d_{min} = diameter of the smallest motor unit

R = ratio of biggest and the smallest motor unit diameter

n = number of motor units

2.3.2 Motor Unit Numbers

The number of motor units also varies with the size of the muscle. In human skeletal muscles, motor unit numbers can vary from 50 motor units in smaller muscle to 900 motor units in the larger muscle groups.

2.3.3 Innervations Ratio

The numbers of fibers innervated by each motoneuron differ from each other in a muscle. The innervation ratio indicates the average number of muscle fibers that, under normal conditions with respond to the action potential discharged by a single motor neuron. The data suggest that smaller muscles, such as the intrinsic hand muscles, tend to have lower innervation ratios. There is a negative correlation between the values of the innervation ratio and how finely movement can be controlled. In muscles where innervation ratios are low, it is possible to produce very fine motion. This is because each neuron is responsible for only a small increment in force. On the other hand, when the innervation ratio is large, each neuron can initiate a very large step in force. The variation in innervation ratios is one of the most significant factors that contribute to differences in motor unit force [50, 51, 52]. Such a distribution can be represented as an exponential form as [24, 49] (Figure 2.4):

$$y_i = ae^{\frac{\ln(R)}{n}.i} \quad (4)$$

where: y_i is the force or innervation number of motor unit i

a is the force or innervation number for the smallest unit

R is the ratio of the innvervation numbers for the largest and the smallest units

n is the total number of motor units

Figure 2.5 shows the number of motor units that innervate the different fiber types. Although the muscle (for example Tibialis Anterior) is comprised of 70% type-I and 30% type-II fibers, 396 motor units are of type-I and only 34 of them are type-II motor units in a pool of 430 motor units.

2.4 Biophysical Phenomenon of Action Potential

Each muscle or nerve cell has membranes, which introduces a structural barrier to limit the movement of some ions, but permits others to diffuse freely from in and out of the cell. This selective permeability creates a potential difference across the membrane. At resting muscle there are more sodium (Na^+) and chloride (Cl^-) ions in the extra cellular fluid outside the cell than inside the cell and excess amount of potassium (K+) ions and proteins in the intracellular fluid within the cell than that of extra cellular medium [53].

At resting potential some potassium channels are open but the voltage-gated sodium channels are closed. Even though no net current is flowing, the major ion species moving

Table 2-3: Total number of motor units in different group of muscle and total number of muscle fibers in a motor unit.

Name of muscle group	Number of motor units	Number of fibers/motor unit
Bicep brachii	750	774
Tibialis Anterior	445	562
Gastrocnemius	580	1720
First dorsal interosseous	119	340

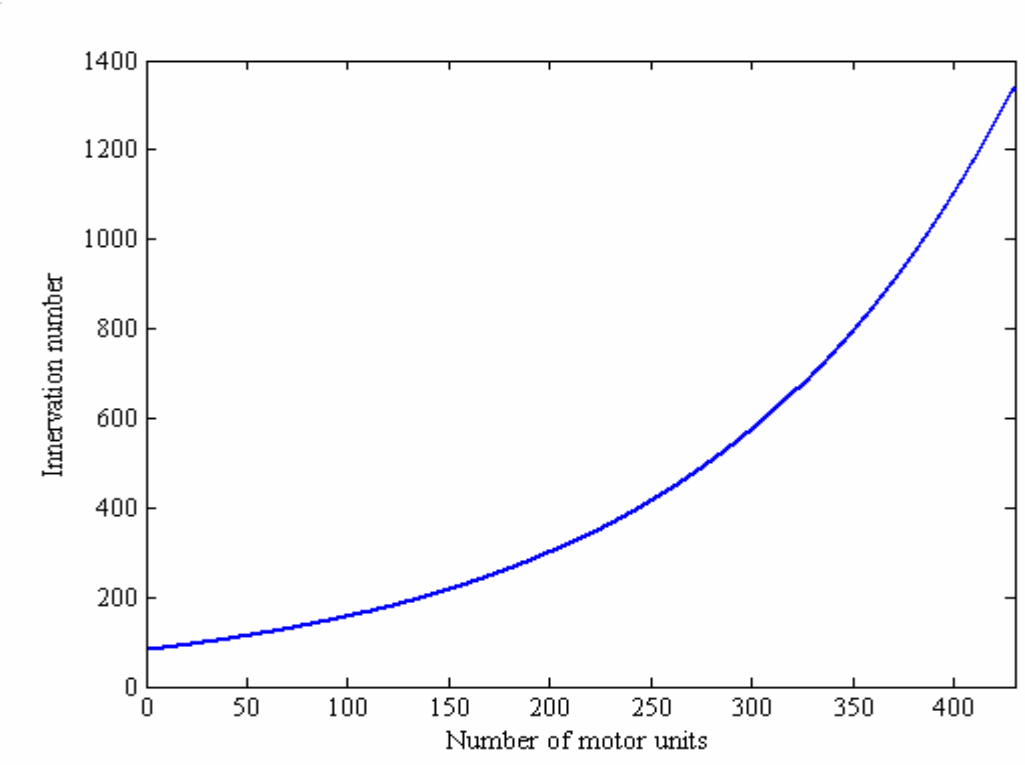

Figure 2.4: Innervation number of the different motor units in a muscle

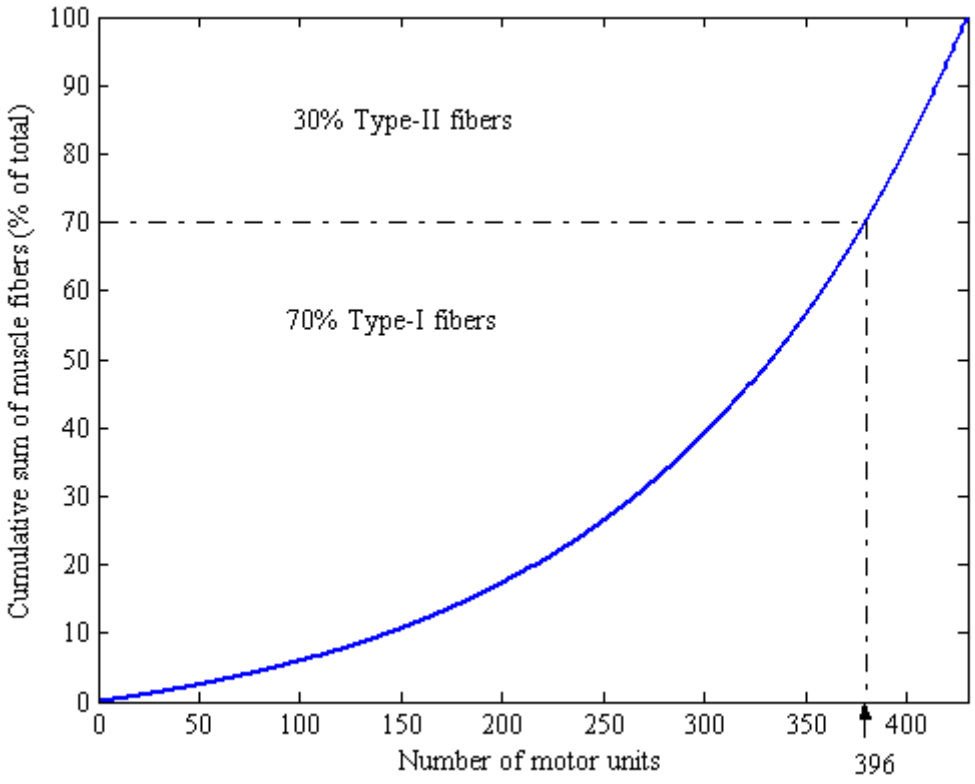

Figure 2.5: Distribution of number of different types of motor units in a muscle

across the membrane is potassium, thus pulling the resting potential close to the K^+ equilibrium potential. The potential difference that exists across the membrane of all cells is usually negative inside the cell with respect to the outside. The membrane is said to be polarized. The potential difference across the membrane at rest is called the resting and is approximately –90 mV in neurons, with the negative sign indicating that the inside of the cell is negative with respect to the outside.

A local membrane depolarization caused by an excitatory stimulus causes some voltage-gated sodium channels in the neuron cell surface membrane to open and therefore Na^+ ions diffuse in through the channels along their electrochemical gradient. Being positively charged, they begin a reversal in the potential difference across the membrane from negative to positive-inside.

As Na^+ ions enter and the membrane potential becomes less negative, more sodium channels open, causing an even greater influx of Na^+ ions. This is an example of positive feedback. As more sodium channels open, the sodium current dominates over the potassium leak current and the membrane potential becomes positive inside.

As voltage-gated potassium channels open, there is a large outward movement of K^+ ions driven by the potassium concentration gradient and initially favored by the positive-inside electrical gradient. As K^+ ions diffuse out, this movement of positive charge causes a reversal of the membrane potential to negative-inside and repolarization of the neuron back towards the large negative-inside resting potential. Figure (2.6) shows an action potential and all its phases.

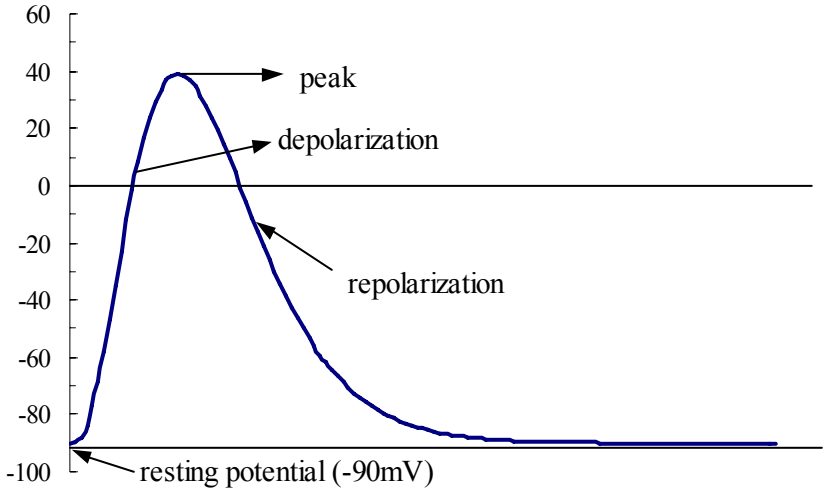

Figure 2.6: Different phases of an action potential generated inside the fiber

CHAPTER 3

3. Muscle Computer Model

3.1 Introduction

The quantitative description of intracellular and extracellular fields of a single circular cylindrical fiber, resulting from the propagation of an action potential is of obvious interest in electro-physiology. A mathematical analytical model of muscle fiber action potential is the first step in the modeling of the muscle and thus simulation and analysis of EMG signals. The analytic modeling technique enhances the application of EMG signal, reduces the complexity of performing tedious and expensive experimental measurements. Analytical solutions are valuable to determine the theoretical dependence of the solution on specific parameters of the system. It reduces the computational time and thus accelerates the development of different DSP algorithm for post processing of measured signals.

3.2 Muscle Modeling

Electromyography (EMG) provides noninvasive means for the study of muscular functions during biofeedback training, activities of sports or daily living. It is also useful in interpreting pathologic states of musculoskeletal or neuromuscular systems. Surface myoelectric signals (SEMG) are recorded in motor nerve conduction studies, fatigue studies and in kinesiologic studies. A surface motor unit action potential (MUAP) is the summation of the spatially and temporally dispersed action potentials of individual

muscle fibers belonging to the motor unit within the uptake area of the recording surface electrode [19, 55]. Compound muscle action potentials (CMAPs) represent the summation of a number of motor unit action potentials [56]. For modeling the motor unit action potentials, it is essential to simulate a single fiber action potential [19,57]. Several approaches have been investigated and documented. Models based on the mathematical expression describing the single fiber action potential using volume conduction theory are very complex and computationally time consuming [58, 59]. In simplified models, the transmembrane current have been approximated as dipole or tripole sources propagating from the neuromuscular endplate toward the tendons [20]. The dipole model generated only biphasic potentials, whereas the transmembrane current profile is usually triphasic. The tripole model is found to be unsuitable when the electrode is very close to the muscle fiber. Nonetheless, the later model has been used in larger muscle models considering the transmembrane current as discrete point sources along the axis of the muscle fiber for a finite fiber within a finite volume conductor [20]. The influence of the finite dimensions of the volume conductor, however, has small effects on the amplitudes of SMUPs. The volume conductor discrimination diminishes when motor units are farther from the detecting electrode [20]. Consequently, a less computationally demanding model, which consists of a line source model within a finite fiber length and an infinite homogenous volume conductor, is used in this study. Figure 3.1 shows a muscle model where fibers are randomly distributed inside motor units. The fibers are assumed to lie inside the motor unit as parallel to the surface of the muscle. The isotropic layers of fat and skin tissues lie above the anisotropic layers of muscle. The size and

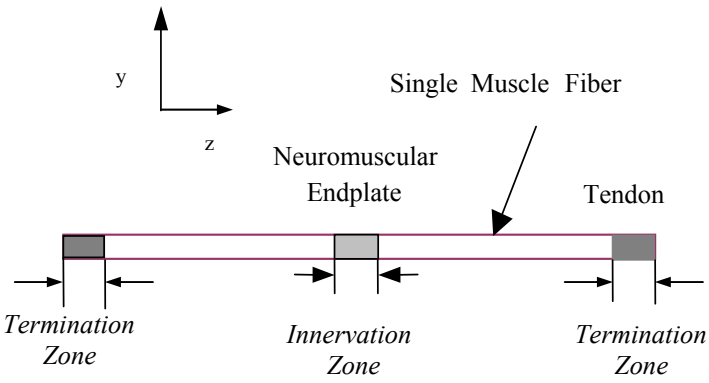

Figure 3.1: A single fiber action potential model

distribution of individual muscle fibers are adapted from anatomical and clinical data. The assumptions used in deriving a single fiber action potential are as follows:

- Muscle is infinitely extended radially
- Muscle Fiber is cylindrical
- Radius of the fiber is much smaller than the length of the fiber
- There is no capacitive effect on the volume conductor
- Muscle fibers lie parallel to the surface of the muscle

The time-varying fields associated with electromyographic currents are considered low-frequency fields, and thus, the wavelength of the harmonic fields is considerably larger than the dimensions of human muscles. The electrical field distribution can be approximated by a static field satisfying the time-varying boundary conditions. For a region with homogeneous conductivity σ the relationship between field potential, φ and volume source density, I_V can be stated using Poisson's equation as:

$$\nabla.(\sigma.\nabla\varphi) = -I_V \tag{5}$$

$$\text{ie.}\ \nabla^2\varphi = -\frac{I_V}{\sigma} \tag{6}$$

Where $\nabla^2 = \frac{\partial^2}{\partial x^2} + \frac{\partial^2}{\partial y^2} + \frac{\partial^2}{\partial z^2}$ is a three dimensional differential operator.

A linear differential equation written in the general form is as follows:

$$L(x)u(x) = f(x) \tag{7}$$

where L(x) is a linear differential operator,

$$L(x) = D^n + a_{n-1}(t)D^{n-1} + \ldots\ldots + a_0(t) \tag{8}$$

and $u(x)$ is the unknown function and $f(x)$ is a known non-homogeneous term.

Solution of equation (8) can be written as:

$$u(x) = L^{-1}(x)f(x) \tag{9}$$

where L^{-1} is the inverse of the differential operator L. Since L is a differential operator, it is reasonable to expect its inverse to be an integral operator and the usual properties of inverse hold,

$$LL^{-1} = L^{-1}L = I \tag{10}$$

where I is the identity operator. More specifically we define the inverse operator as:

$$u(x) = L^{-1}f = \int G(x;x')f(x')dx' \tag{11}$$

where the kernel G(x; x′) is the Green's function associated with the differential operator L.

Let $L = \nabla^2$, a three dimensional differential operator. So the potential of the Poisson's equation (6) can be written as:

$$\varphi = L^{-1}(-\frac{I_V}{\sigma}) \tag{12}$$

So by using equation (12), we can write:

$$\varphi(p) = \int G(p;p')I_V(p')dV(p') \tag{13}$$

So Green's function gives the potential at the point p due to a point charge at the point p' based on the assumption of quasi-stationary condition, which means that wave propagation effects, capacitive effects and inductive effect can be ignored in the calculation of potential.

An important special case of Poisson's equation occurs when the source density I_V is zero everywhere in a region of interest i.e. sources lie outside or at the boundary of this identified region. In the case of muscle fiber, the sources are concentrated on the membrane of the active fiber, and in this case Poisson's equation becomes Laplace's equation, which is:

$$\nabla^2 \varphi = 0 \tag{14}$$

$$\text{i.e.,} \frac{\partial^2 \varphi(x,y,z)}{\partial x^2} + \frac{\partial \varphi(x,y,z)}{\partial y^2} + \frac{\partial^2 \varphi(x,y,z)}{\partial z^2} = 0 \tag{15}$$

This equation can be written in cylindrical coordinates as:

$$\nabla^2 \varphi(r,z) = \frac{\partial^2 \varphi(r,z)}{\partial r^2} + \frac{1}{r}\frac{\partial \varphi(r,z)}{\partial r} + \frac{1}{r^2}\frac{\partial^2 \varphi}{\partial \theta^2} + \frac{\partial^2 \varphi(r,z)}{\partial z^2} = 0\,; \tag{16}$$

Assuming rotational symmetry, we get:

$$\nabla^2 \varphi(r,z) = \frac{\partial^2 \varphi(r,z)}{\partial r^2} + \frac{1}{r}\frac{\partial \varphi(r,z)}{\partial r} + \frac{\partial^2 \varphi(r,z)}{\partial z^2} = 0 \tag{17}$$

where $r = \sqrt{x^2 + y^2}$

Taking Fourier Transform of Equation (17) only along the z-axis, we get:

$$\frac{\partial^2 \Phi(r,\omega)}{\partial^2 r} + \frac{1}{r}\frac{\partial \Phi(r,\omega)}{\partial r} - \omega^2 \Phi(r,\omega) = 0 \tag{18}$$

Here Φ is the notation for Fourier transforms of extracellular field φ and ω is the spatial angular frequency corresponding to z-axis. The spatial angular frequency is related to the angular frequency k by:

$$\omega = 2\pi k \tag{19}$$

The boundary condition to be satisfied by φ is given by the membrane current i_m:

$$\left.\frac{\partial\varphi(r,z)}{\partial r}\right|_{r=a} = -\frac{i_m(z)}{\sigma_e} \tag{20}$$

The general solution of the Equation (14) can be represented by Bessel function as shown by [60]:

$$\Phi(r,\omega) = C_1(\omega).I_0(r\omega) + C_2(\omega).K_0(r|\omega|) \tag{21}$$

where I_n and K_n are modified Bessel functions and $C_1(\omega)$ and $C_2(\omega)$ are functions to be determined from the boundary conditions. The solution of the equation can be found utilizing the properties of Bessel functions. Before proceeding towards the solution of Equation (21), the field of isotropic extracellular medium, it is important to address the anisotropic behavior of the extracellular medium or the volume conductor of the muscle. Muscle fibers are separated by thin layers of extracellular fluid and each fiber is surrounded by a membrane. Extracellular fluid has high conductivity compared to the conductivity of the membranes. As a result, action potential currents running perpendicular to the fibers are forced to flow mainly in the narrow extracellular space between the fibers. Consequently, the extracellular medium is not adequately described by a uniform conductivity σ_e. An exact calculation of the potential around a muscle fiber in *situ* would require calculation of the currents in the narrow interstitial spaces surrounding the fiber and the currents in the membranes of the nearby fibers, taking electrical properties of passive membranes into account. This is only possible when numerical methods are employed. It is too complicated geometrical to be tractable by analytical methods. However, an approximate solution can be obtained if the extracellular medium is considered homogenous but anisotropic, i.e., with different

conductivities in parallel and perpendicular directions, which are σ_z and σ_r respectively. Thus the conductivity of anisotropic extracelllular medium can be written as:

$$\sigma_e = \begin{bmatrix} \sigma_r & 0 & 0 \\ 0 & \sigma_r & 0 \\ 0 & 0 & \sigma_z \end{bmatrix} \tag{22}$$

Thus Laplace's equation for the single fiber field calculation can be rewritten as:

$$\sigma_r \frac{\partial^2 \varphi(x,y,z)}{\partial x^2} + \sigma_r \frac{\partial \varphi(x,y,z)}{\partial y^2} + \sigma_z \frac{\partial^2 \varphi(x,y,z)}{\partial z^2} = 0 \tag{23}$$

$$\therefore \frac{\partial^2 \varphi(x,y,z)}{\partial x^2} + \frac{\partial \varphi(x,y,z)}{\partial y^2} + \frac{\sigma_z}{\sigma_r} \frac{\partial^2 \varphi(x,y,z)}{\partial z^2} = 0 \tag{24}$$

Let $P = \frac{\sigma_z}{\sigma_r}$, the ratio of longitudinal and radial conductivity. Transferring Equation (24) in the cylindrical co-ordinate system as:

$$\frac{\partial^2 \varphi(r,z)}{\partial r^2} + \frac{1}{r} \cdot \frac{\partial^2 \varphi(r,z)}{\partial r^2} + P \frac{\partial^2 \varphi(r,z)}{\partial z^2} = 0 \tag{25}$$

Taking Fourier transform along z-axis to represent Equation (25) in the spatial frequency domain, we get:

$$\nabla^2 \Phi(r,\omega_z) = \frac{\partial^2 \Phi(r,\omega_z)}{\partial r^2} + \frac{1}{r} \cdot \frac{\partial^2 \Phi(r,\omega_z)}{\partial r^2} - P\omega_z{}^2 \Phi(r,\omega_z) = 0 \tag{26}$$

This is similar to equation (18) and the solution of which can be given again using the modified Bessel function as follows [60]:

$$\Phi(r,\omega_z) = C_1(\omega_z) I_0\left(r\sqrt{P}\omega_z\right) + C_2(\omega_z) K_0\left(r\sqrt{P}|\omega_z|\right) \tag{27}$$

The potential distribution is a continuous decay function with respect to the radius of the cylindrical volume and it approaches to zero at $r \to \infty$. Since $I_0 \to \infty$ for $r \to \infty$, the

general solution turns into,

$$\Phi(r,\omega_z) = C_2(\omega_z) K_0\left(r\sqrt{P}\,|\omega_z|\right) \tag{28}$$

At the interface of intracellular and extracellular medium i.e., at $r = a$, membrane current I_m flows in radial direction and thus can be used as a boundary condition to solve Equation (24) for field potential and can be expressed by membrane current, I_m to get the solution of field potential:

$$\left.\frac{\partial\Phi(r,\omega_z)}{\partial r}\right|_{r=a} = -\frac{I_m(\omega_z)}{\sigma_r} \tag{29}$$

Differentiating Equation (28) and applying the boundary condition, we get:

$$-C_2(\omega_z)\sqrt{P}|\omega_z|K_1(r\sqrt{P}|\omega_z|) = -\frac{I_m(\omega_z)}{\sigma_r} \tag{30}$$

where $r = a$ and $K_0' = -K_1$. Thus,

$$C_2(\omega_z) = \frac{I_m(\omega_z)}{\sigma_r\sqrt{P}|\omega_z|K_1\left(a\sqrt{P}|\omega_z|\right)} \tag{31}$$

Using Equation (31), the solution of extracellular potential for an infinite volume conductor can be written in the spatial frequency domain as [60]:

$$\Phi(r,\omega_z) = \frac{K_0\left(r\sqrt{P}\,|\omega_z|\right)}{\sigma_r\sqrt{P}|\omega_z|K_1\left(a\sqrt{P}|\omega_z|\right)} I_m(\omega_z) \tag{32}$$

Taking the inverse Fourier transform of the Equation (32), the extracellular potential distribution in space domain can be expressed as:

$$\varphi(r,z) = \frac{1}{2\pi\sigma_r}\int_{-\infty}^{\infty}\frac{K_0\left(r\sqrt{P}\,|\omega_z|\right)}{\sqrt{P}|\omega_z|K_1\left(a\sqrt{P}|\omega_z|\right)} I_m(\omega_z)\, e^{-i\,\omega_z z}\, d\omega_z \tag{33}$$

Equation (33) can be solved by evaluating Bessel's function, K_0 and K_1 and discrete Fourier transform of the membrane current I_m. Moreover, the FFT can be applied directly to Equation (32) to solve the inverse Fourier transform to get $\varphi(r,z)$. Although this technique can readily be applied, it is important and handy to derive a straight-forward and simple expression for the extracellular field potential for better understanding. For this purpose, we can write the Equation (32) as:

$$\Phi(r,\omega_z) = W(r,\omega_z)\cdot I_m(\omega_z) \tag{34}$$

where,
$$W(r,\omega_z) = \frac{K_0\left(r\sqrt{P}|\omega_z|\right)}{\sigma_r\sqrt{P}|\omega_z|K_1\left(a\sqrt{P}|\omega_z|\right)} \tag{35}$$

Using the Inverse Fourier Transform and the convolution property on Equation (34) we find [60,19]:

$$\varphi(r,z) = w(r,z) * i_m(z) = \int_{-\infty}^{\infty} i_m(s).w(r,z-s)ds \tag{36}$$

where, '*' denotes the convolution operator and $w(r,z)$ is called the weighting function or the transfer function of the volume conductor. This function is similar to the Green's function in Equation (13).

Thus the extracellular potential $\varphi(r, z)$ can be calculated by convolving the weighting function $h(r, z)$ with the membrane current $i_m(z)$. As the radial distance r is increased the weighting function gets broadened and diminished in amplitude with the effect that the extracellular potential also is broadened and diminished in amplitude. The weighting function W in Equation (35) can be redefined by introduction of an approximation to the

weighting function. Transmembrane current flows due to the intracellular potential generated between inside and outside the cell. In human muscle, it is found that the intracellular potential is a low frequency field, which is less than 10 KHz in frequency domain. This frequency is equivalent to 2500 cycle/m in spatial frequency domain. Thus,

$$\omega_z = 2\pi k \le 2\pi.2500 \text{ rad/sec.} \tag{37}$$

The average diameter of human muscle fiber is 55 μm or radius a = 28 μm, which gives:

$$|a\omega_z| \le 2\pi.2500.28.10^{-6}$$

$$\text{i.e., } |a\omega_z| \le 0.44 \tag{38}$$

Thus the intercellular potential or the membrane current is zero for frequency more than 10 KHz or

$$I_m(\omega_z) \cong 0 \text{ for } |a\omega_z| > 0.44 \tag{39}$$

Introducing this condition, the weighting function can be approximated as:

$$H(r,\omega_z) = \frac{1}{\sigma_r} \frac{aK_0(r'|\omega_z|)}{a'|\omega_z| K_1(a'|\omega_z|)} \quad for\ |a'\omega_z| \le 0.44 \tag{40}$$

where $a' = a\sqrt{P}$ and $r' = r\sqrt{P}$. From the behavior of the first-order modified Bessel function it is found that the value $a'|\omega_z| K_1(a'|\omega_z|) \to 1$ for $|a'\omega_z| \to 0$. For $|a\omega_z| = 0.44$, $a'|\omega_z| K_1(a'|\omega_z|) = 0.86$. So, ignoring around 14% error it can be assumed that $a'|\omega_z| K_1(a'|\omega_z|) \approx 1$ for $|a'\omega_z| \le 0.44$. This approximation turns the weighting function as:

$$W(r,\omega_z) \approx \frac{1}{\sigma_r} aK_0\left(r'|\omega_z|\right) \tag{41}$$

or by [60], $$w(r,z) = \frac{a}{2\sigma_r} \frac{1}{\sqrt{(r')^2 + z^2}} \tag{42}$$

Thus we finally get the equation for the extracellular potential from Equation (45):

$$\varphi(r,z) = \frac{a}{2\sigma_r} \int_{-\infty}^{\infty} \frac{i_m(s)}{\sqrt{\frac{\sigma_z}{\sigma_r} r^2 + (z-z')^2}} dz' \tag{43}$$

The denominator of Equation (43) can be identified as the distance R between the integration point $P' = (0, z')$ on the fiber axis and the observation point $P = (r, z)$ (Figure 3.2), i.e.,

$$R = |P - P'| = \sqrt{(r')^2 + (z-z')^2} \tag{44}$$

Thus Equation (46) can be written as:

$$\varphi(r,z) = \frac{a}{2\sigma_r} \int_{-\infty}^{\infty} \frac{i_m(z')}{R} dz' \tag{45}$$

From the line source model, we know that total membrane current for a section of the fiber can be denoted as a point source. Again, the potential $V(p)$ from a point source i_0 at the point P' in an infinite volume conductor with conductivity σ_e is:

$$V(p) = \frac{1}{4\pi\sigma_e} \frac{i_0}{R} \tag{46}$$

Accordingly, the potential $\varphi(r,z)$ from a line source on the center of the fiber is:

$$\varphi(r,z) = \frac{1}{4\pi\sigma_e} \int_{-\infty}^{\infty} \frac{2\pi a.i_m(z')dz'}{R} \tag{47}$$

$$= \frac{a}{2\sigma_r} \int_{-\infty}^{\infty} \frac{i_m(z')}{R} dz' \tag{48}$$

which is same as Equation (45). Thus Equation (45) is equivalent to concentrating the membrane current as a line source on the center of the fiber.

3.2.1 Analytical Expression of the Transmembrane Current Source

The ionic currents in the membrane create electrical potentials inside and outside the membrane. The transmembrane current is usually considered as the bioelectrical source of SFAPs. In an approximating description, the current can be represented by a current tripole along the fiber axis [61]. Alternatively, the shape of the intracellular action potential (IAP) can be approximated by a synthetic Gaussian curve [62] or a quasi-continuous function [19, 63]. A discrepancy is always seen between the actual experimental action potential and the simulated one. One of the origins of discrepancy might be an erroneous description of the source. Benno K. van Veen et al [64], studied different sources. First, an analytical description of the intercellular action potential was used. Furthermore, an experimental intercellular potential, a special experimental surface action potential, and a measured transmembrane current scaled to their experimental situation were applied. The results for the experimental IAP were comparable to those with the analytical IAP. The best agreement between experimental and simulated data was found for a measured transmembrane current as source, but differences are still apparent.

The core conductor model applies to a situation where a cylindrical fiber is surrounded by

a cylindrical conductor. If a and b are the radius of the muscle fiber and the surrounding medium respectively, then the resistance per unit length r is given by:

$$r_i = \frac{1}{\sigma_i \pi a^2} \tag{49}$$

Applying Ohm's law to a cross section of the fiber (Figure 3.2) gives:

$$\frac{dv_i(z)}{dz} = -r_i . i_i(z) \tag{50}$$

Kirchhoff's law applied to a cross section of the fiber gives:

$$2\pi . a . i_m(z) = -\frac{di_i(z)}{dz}$$

$$\Rightarrow i_m = \frac{a.\sigma_i}{2} \frac{d^2 v_i(z)}{dz^2} \tag{51}$$

Thus the transmembrane current is then calculated as the second derivative of the intercellular potential. The extracellular action potential from a single muscle fiber is generated by the depolarized and repolarized transmembrane current [61, 65]. The extracellular field can be described either by the intercellular potential or the transmembrane current. Andreassen and Rosenfalck have suggested a mathematical representation of the intercellular action potential from a precise experimental setup. If the muscle fiber is parallel to the z axis and the neuromuscular endplate is located at $z = 0$, then the intracellular potential V_m at a particular point z and time t is given by [65]:

$$V_m(z) = A(\lambda z)^3 e^{-\lambda z} - B \tag{52}$$

Where V_m is the profile of the intracellular action potential along the length of the muscle fiber in the z direction, and $A=96$, a suitable constant to fit the amplitude of the action potential and B is the resting potential of –90mV and $\lambda = 1$. Thus the transmembrane

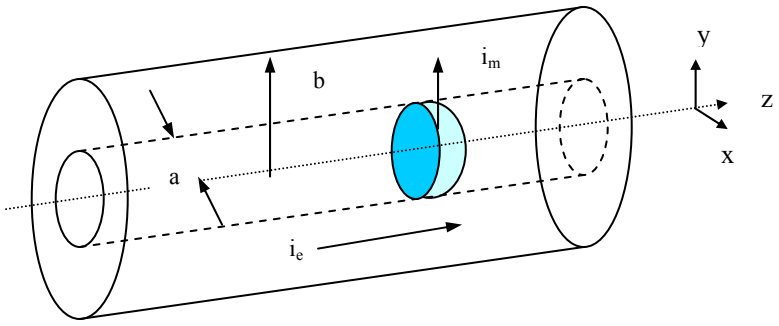

Figure 3.2: A muscle core conductor model

potential becomes:

$$V_m(z) = 96z^3 e^{-z} - 90 \tag{53}$$

Modification of Rosenfalck's model by dividing the time scale by two (or $\lambda = 2$) enhanced the peak-to-peak voltage of the transmembrane current (proportional to the second derivative of the intercellular potential). After this transformation, the simulated data of Nandedkar and Stalberg [19] matched the experimental data. Their empirical equation was:

$$V_m(z) = 768z^3 e^{-2z} - 90 \tag{54}$$

However, after this transformation, their intercellular potential had a duration that was never obtained from experiments [64]. Nevertheless, in this study, Rosenfalck's empirical model of intercellular potential will be used to derive the transmembrane current for the source description of the surface EMG. As described earlier, the transmembrane current is proportional to the second derivative of the intracellular potential:

$$\begin{aligned} i_m(z) &= \frac{a\sigma_i}{2} . \frac{\partial^2 V_m(z)}{\partial z^2} \\ &= \frac{a\sigma_i}{2} . 96e^{-z}[z^3 - 6z^2 + 6z] \end{aligned} \tag{55}$$

where σ_i is the intracellular conductivity, a is the muscle fiber radius. In the particular case where the extra-cellular medium is considered infinite with cylindrical anisotropy, the potential recorded at the surface of the model when a current source travels along the muscle fiber from the neuromuscular endplate toward the tendons can be approximated as:

$$\varphi(r,z) = \frac{\sigma_i a^2}{\sigma_r} * 96 \int_{z_1}^{z_2} \frac{\left[6 - 6z' + (z')^2\right] e^{-z}}{\sqrt{\frac{\sigma_z}{\sigma_r} r^2 + (z - z')^2}} dz' \tag{56}$$

3.2.2 Effects of Endplate and Tendons

At the neuromuscular endplate and muscle fiber endings, the transmembrane current is constrained by the excitation and extinction principles. To account for the finite dimensions of muscle fibers and volume conductor distortions, the excitation and the extinction of the action potential are described as current sources at the neuromuscular endplate and fiber endings. These compensating current sources are calculated such as the total current is zero over the active part of the fiber.

$$\int_{fiber} i_m(z,t)dz = 0 \tag{57}$$

The model is described by a fiber with length L and diameter d which is located at a depth of y_e from the surface of the skin. The endplate is located at the center of the fiber with normal distribution with the innervation zone with a radius of r_e. Similarly the tendons, which are located at the two ends of the fiber, are also distributed uniformly within a radius of r_t. The conduction velocity, v_c, for each fiber is calculated as a linear function of the fiber diameter d (μm), by the empirical formula [19]:

$$v_c = 2.2 + 0.05(d - 25) \tag{58}$$

3.3 Algorithm Used for SFAP Modeling

Following are the steps that are utilized to model a single fiber action potential.

1. Select a sampling frequency, f_s usually 25khz.
2. Spatial frequency is deduced from f_s using

   $\Delta z = \frac{v_c}{f_s} * 1000$ [Δz is in mm], v_c is the conduction velocity of the action potential in the muscle fiber which is related to the fiber diameter by Equation (58).
3. Thus for a length of 'L' fiber, total numbers of points Npt needed for the action potential [these points are from endplate to one side of tendon] is calculated as

   $$Npt = \frac{L}{2 * \Delta z}$$
4. Total number of points to generate the action potential in the endplate zone is N_{ev}. As Plonsy has shown that it takes 5ms for an action potential to generate before it starts propagating. Thus N_{ev} is calculated as

   $$N_{ev} = \frac{5}{dt}$$

   where $dt = \frac{1}{f_s * 1000}$ (dt in ms) and N_{ev} is rounded towards zero.
5. A coordinate system is chosen with center of the coordinate system located at the center of the endplate location of the fiber.
6. Recording electrode position is selected as (x_e, y_e, z_e) where the user selects the position of the electrode.

7. The next step in SFAP modeling is to define the action potential source as transmembrane current $i_m(z)$. The samples of $i_m(z)$ is obtained from the analytic model of intracellular potential derived by Rosenfalk which is

$$V_m(z) = 96\, z^3\, e^{-z} - 90$$

where d = diameter of the fiber, σ_i & σ_r are the intercellular and radial conductivities of the muscle

8. Volume conductor calculation: transfer function of volume conductor depends on the distances between the action potential source location and electrode positions. Transfer function of the volume conductor is

$$h = \frac{1}{\sqrt{\frac{\sigma_r}{\sigma_z}\{(x_s - x_e)^2 + (y_s - y_e)^2 \pm (z_s - z_e)^2}}$$

Action potential recorded at point (x_e, y_e, z_e) is due to two currents flowing from the endplate towards the tendons in ±z direction. Thus Transfer function for both side of the endplate needs to be calculated separately.

9. The extracellular potential V_1 is calculated as the convolution of the transmembrane current and the volume conductor transfer function h. The number of discrete values in h is Npt. The length of discrete convolution is (Npt + N_{ev} -1). Another way of simulating extra cellular action potential is to take product of Fast Fourier transform of i_m (z) & h (x,y,z,t) and taking the inverse FFT gives the generated extra cellular potential due to the propagation of action potential.

10. Compensation of endplate and tendon effect: generations of action potential at endplate and extinction at tendons have effects on recorded potential at electrode. To eliminate these effects, i_m (z) at each step (from 1 to *Npt*) are multiplied by *h(x, y, z)* and h(x, y, z0 +,Npt Δ z) to get compensation at endplate V_2 and at tendon V_3 respectively so the final single fiber action potential (SFAP) is:

$$V_{sfap} = V_2 + V_3 - V_1$$

3.4 Results and Discussion

In this section, a single fiber action potential model has been described using the finite length and radially-infinite volume conductor. A single fiber action potential has been simulated using the techniques described above. The volume conductor is assumed only conductive and any capacitive or inductive effects of the volume conductor are neglected. The simulation parameters used for the generation of the single fiber action potential is shown in Table 3.1. A single fiber action potential and its spectrum are shown in Figure 3.3 for the electrode position at $x_e = 0$, $y_e = 10$mm and $z_e = 20$mm. A 3-D figure of the action potential is also shown in Figure 3.4. The surface action potential (SFAP) can be biphasic or triphasic and it depends on the position of the recording electrode as will be discussed next. The magnitude of a single fiber action potential is in the range of microvolt and has power signal component not more than 500 Hz. It is of practical as well as simulation concerns to consider the distance of the source fiber and the recording electrode and also the effect of the volume conductor on the shape and behavior of the

Table 3-1: Simulation parameters used for modeling single fiber action potential

Simulation Parameters	Values Used
Sampling frequency	25 KHz
Fiber length	150mm
Fiber diameter (d)	Variable, mainly from 50-80 μm
Endplate location and distribution	At the middle of the fiber with a radius of 5mm
Tendon location and distribution	At the end of the fiber with a radius of 5mm
σ_z	0.33 Sm^{-1}
σ_r	0.063 Sm^{-1}
σ_i	1.01 Sm^{-1}
Conduction velocity	$v_c = 2.2 + 0.05(d - 25)$

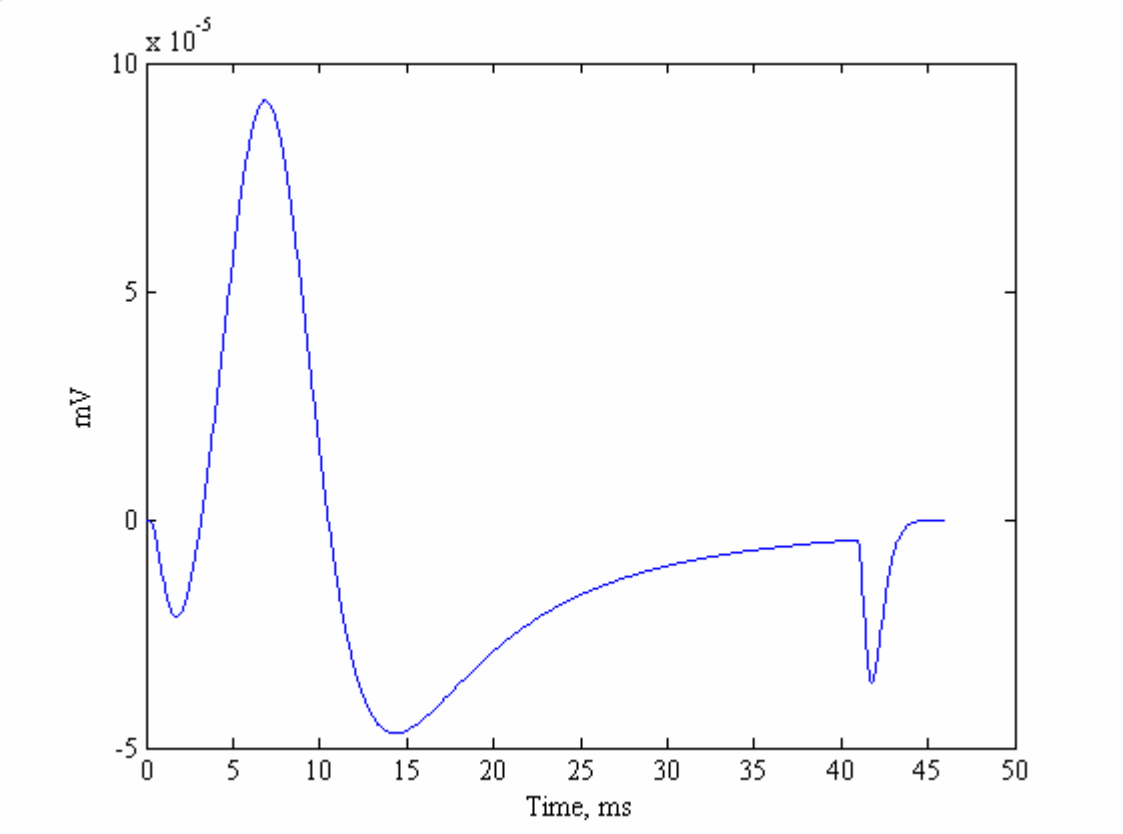

Figure 3.3: An extracellular action potential

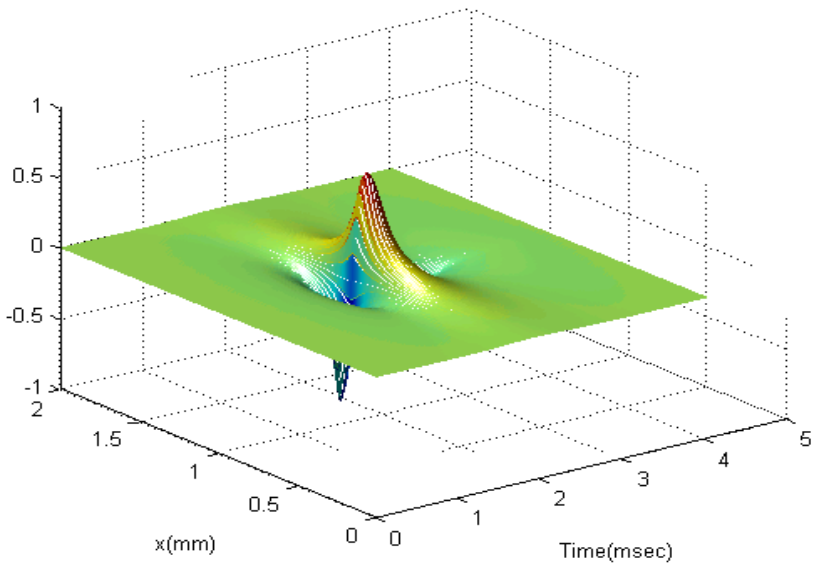

Figure 3.4: A 3-D representation of the extracellular action potential

recorded action potential. Both needle electrode and surface (either monopole or differential or grid electrode) electrode can be simulated using the model. Distances close to the muscle fibers can only be accomplished through the use of needle and fine wire electrodes. To see the effect of depth of fiber from the surface, the action potential is generated for fibers at different depth from the surface where the electrode is placed at $(x_e,z_e) = (0,10mm)$ ie, a monopolar electrode 10mm away from the origin which is also the intersecting point of the endplate zone. At large distances from the muscle fibers, the effects of the neuromuscular endplate and the fiber endings alter the shape of the simulated action potential generated at the surface of the muscle fiber. At closer distances from the muscle fiber, the effects of the volume conductor are minimized since the filter function of the volume conductor approximates the impulse function. Figure 3.5 shows the impulse response of the volume conductor. Figure 3.6 and Figure 3.7 show respectively the volume conductor effect on the shape of recorded potential very close to the fiber located at a distance from 4mm to 10mm and further away from the fiber such as from 15mm to 30mm from the muscle surface. It is visible that the closer the recording electrode is, the bigger the amplitude of the action potential and the amplitude diminishes as the electrode moves further away from the source fiber. Also it is noticeable that the shape changes from triphasic to biphasic when the fiber-electrode distance increases. Thus, the recording electrode cannot detect signals after a certain fiber-electrode distance where the detected signal amplitudes are close to the system noise level. Figure 3.8 shows the diminishing peak to peak amplitude as fiber electrode distance increases. At this point of discussion, the model is described without fat and

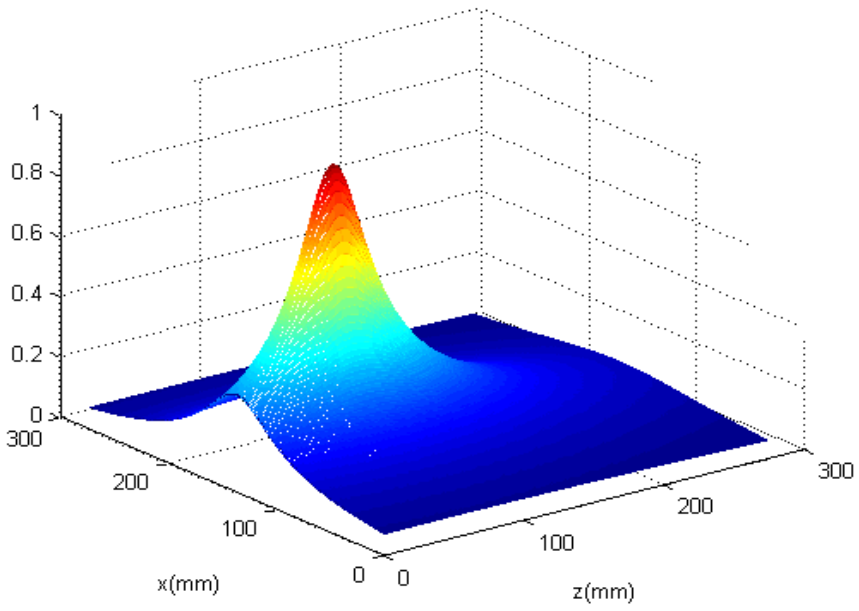

Figure 3.5: Impulse response of the volume conductor

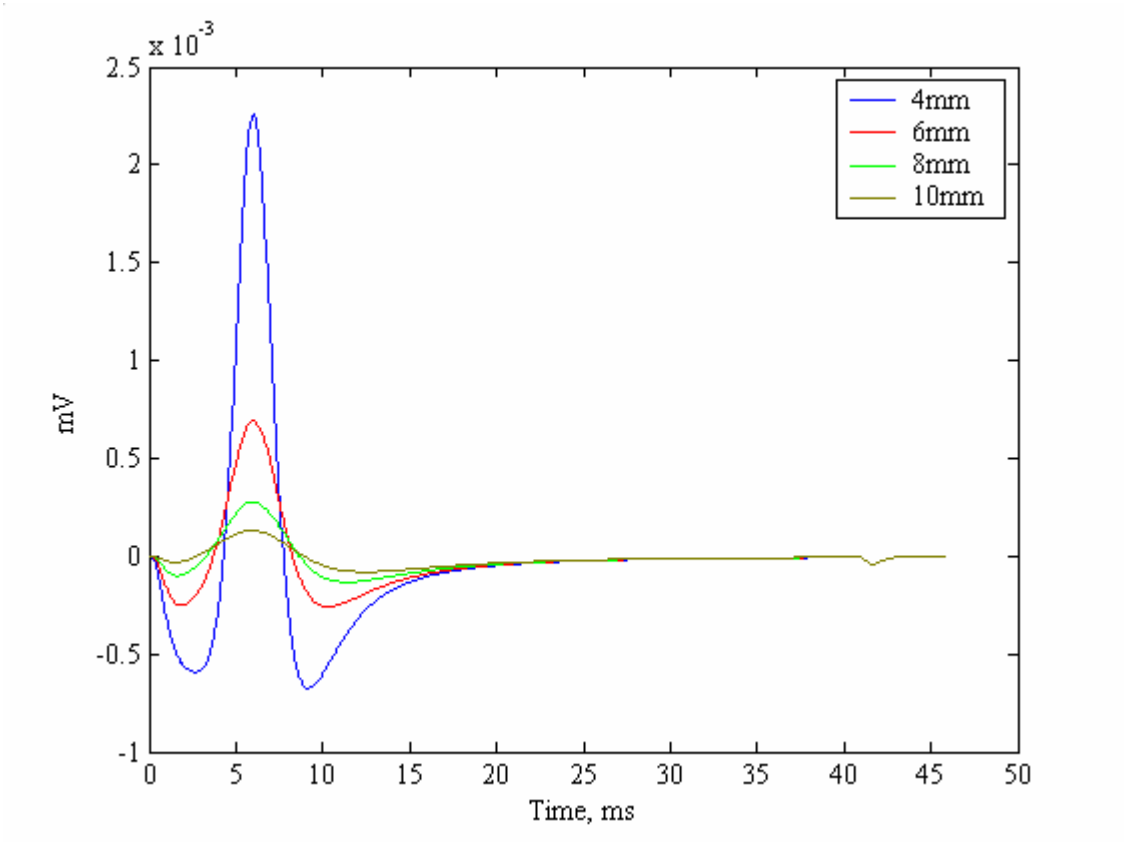

Figure 3.6: SFAPs at different depth from the recording surface

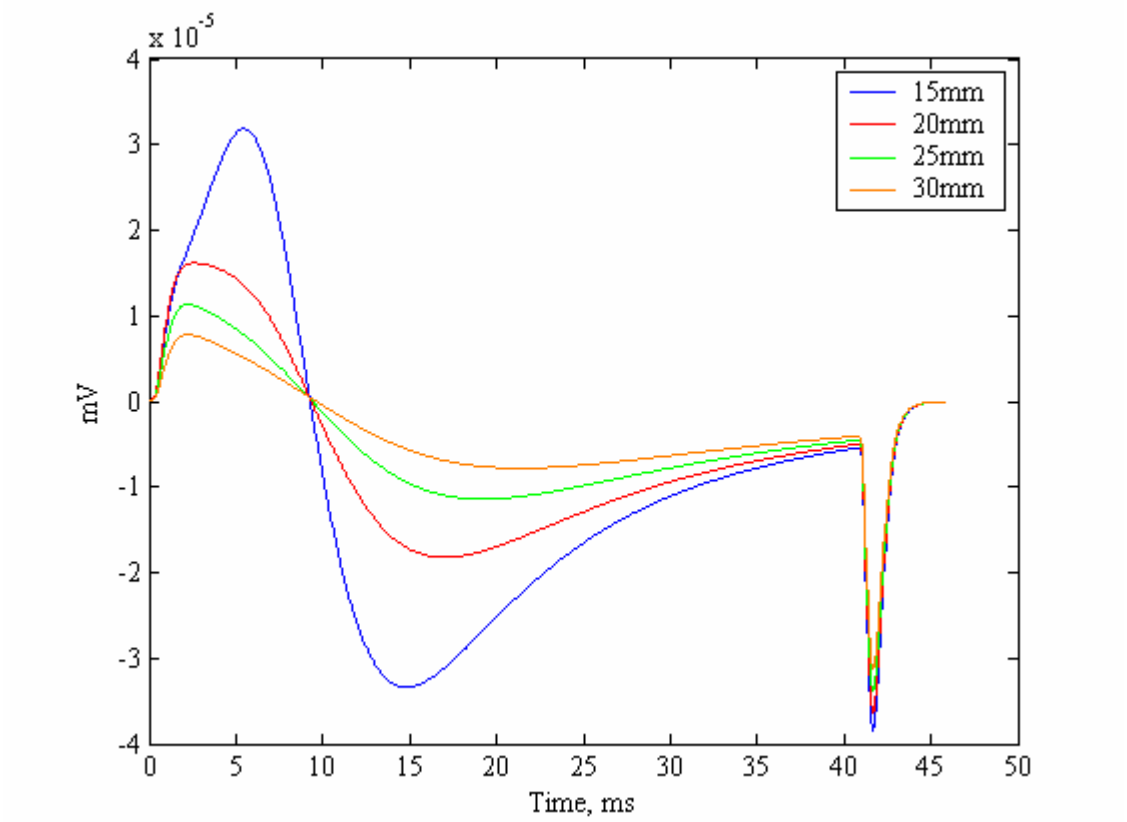

Figure 3.7: SFAPs at different depth from the recording surface. (ye=15-30mm)

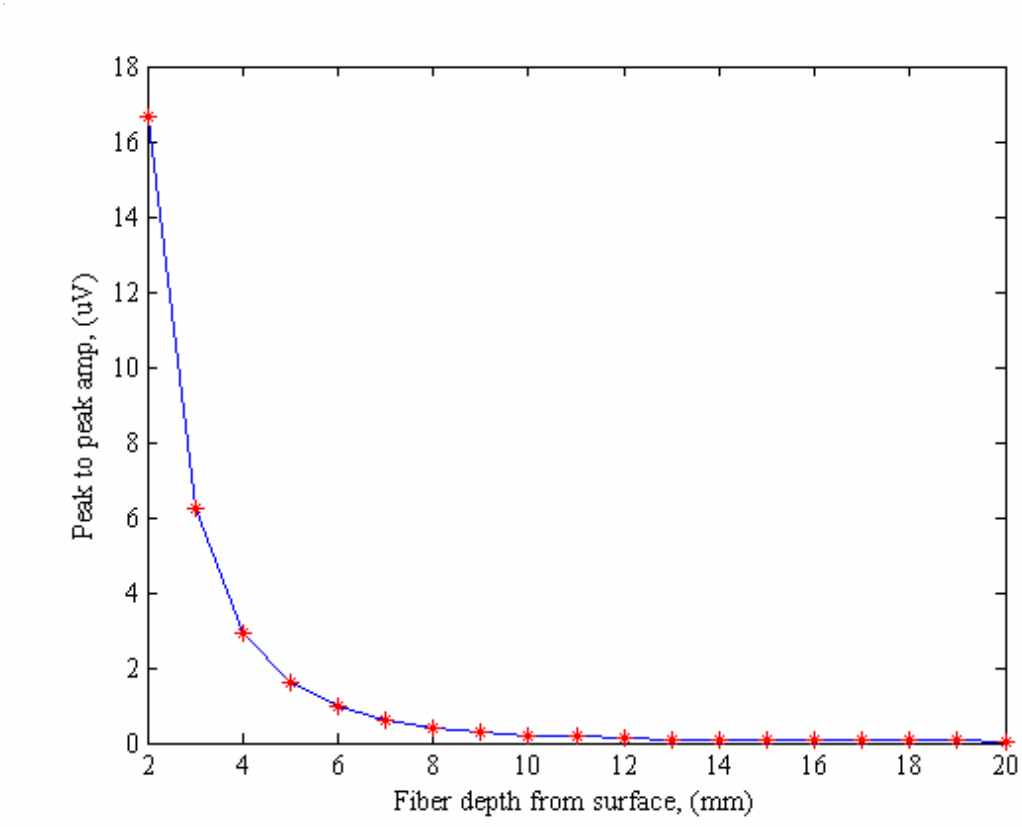

Figure 3.8: Effects of fiber to recording electrode distance on the peak to peak amplitude of SFAPs

skin and we will see later that this fat and skin will further deteriorate this signal pick up for the fiber-electrode distance.

EMG signals are not only affected by the fiber-electrode distance or the depth of the fiber from the surface, but also by the spatial position of the electrode on the surface. Simulations have been performed for electrodes in different positions along the z-direction while the fiber is at a constant depth from the surface and $x_e = 0$. Results are shown in Figure3.9. It has been found that, the further the electrode from the origin of the recording surface, the smaller the peak to peak of the action potential becomes or in other words the smaller the energy of the detected signal becomes. But not until a certain position, does the detected signal amplitude become larger again. Because, the behavior of the volume conductor transfer function is parabolic with the increasing z_e. Moreover, the switch from biphasic to triphasic in the shape of the action potential is also seen as the electrode moves away from the origin of the recording surface. Another significant phenomenon is the shift in the peak of the action potential towards right as it occurs when the electrode moves further from the origin. Another set of simulation is performed for the electrodes that are moving further out in the x-direction on the surface while keeping the depth of the fiber and the z-directional position of the electrode constant. Figure 3.10 illustrates the behavior of this action potential with the changing position of the electrode in the *x*-direction.

As expected, the magnitude of the signal diminishes when the electrode is further away from the origin of the measuring surface. One significant attribute is that the peak of the

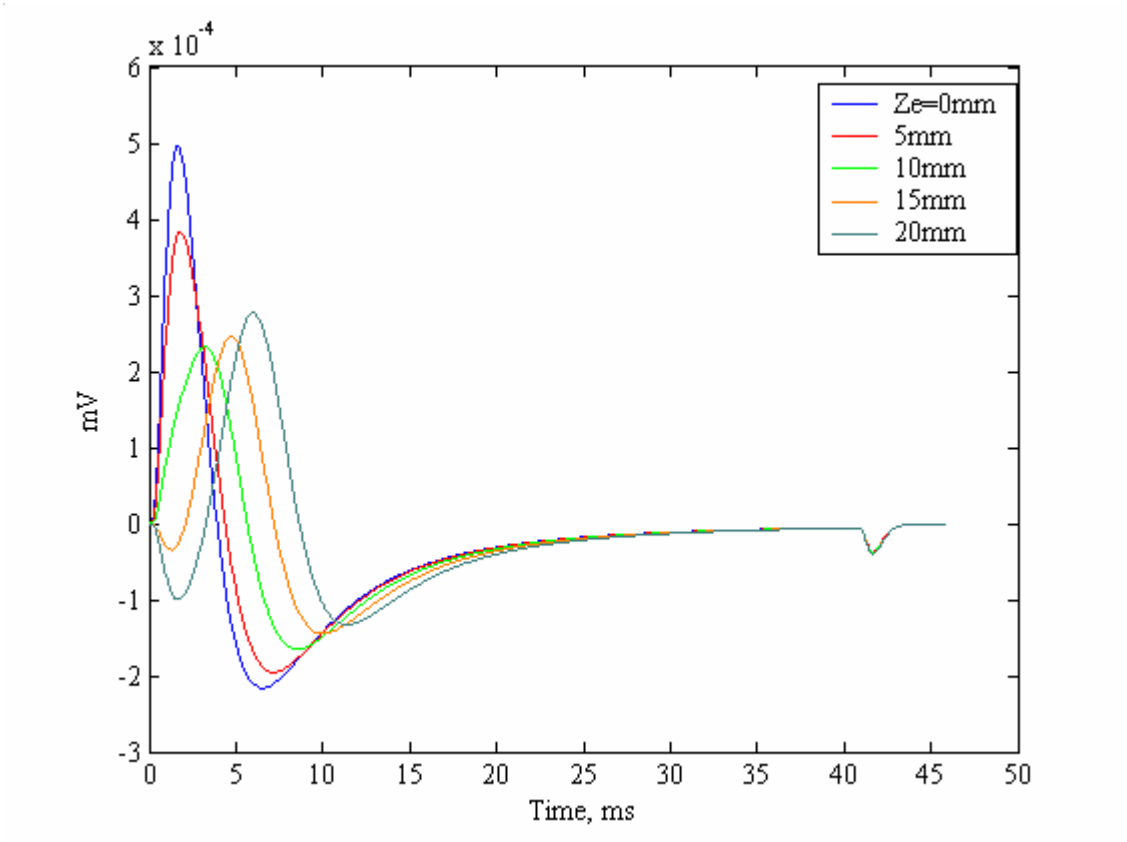

Figure 3.9: Effects of recording electrode distance in the z-direction on SFAPs

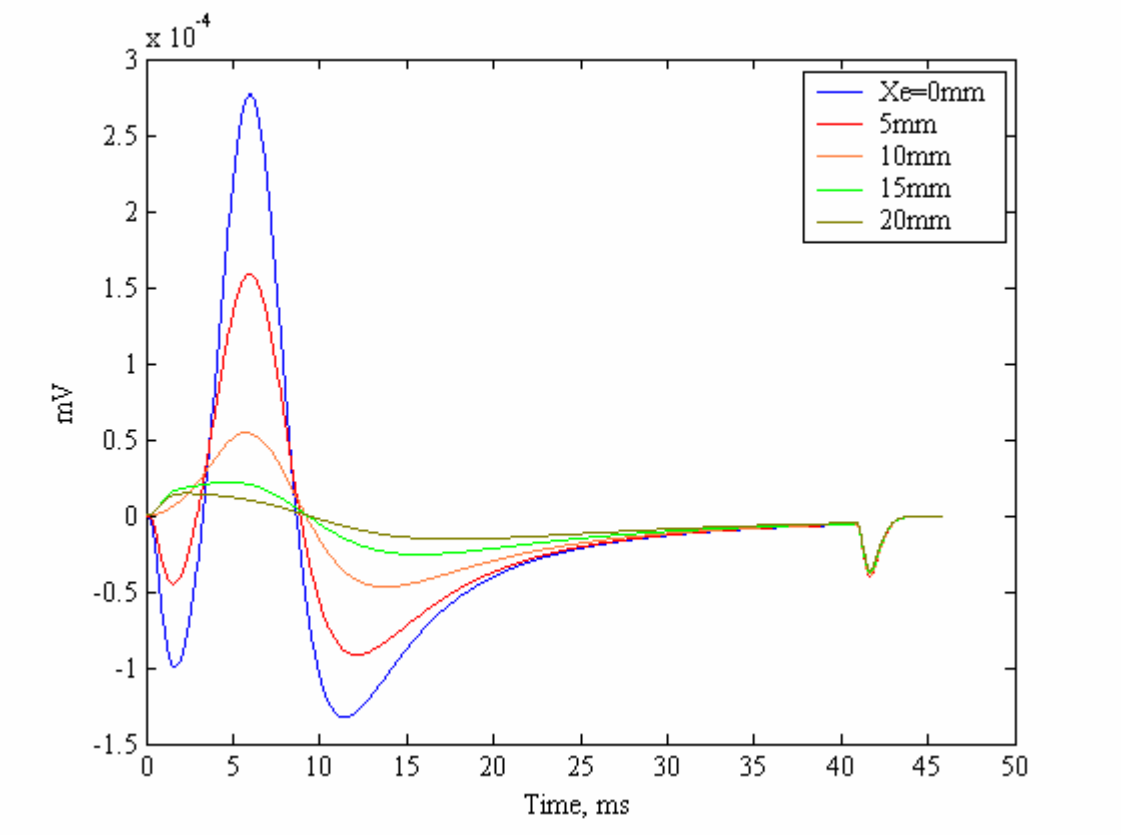

Figure 3.10: Effects of recording electrode distance in the x-direction on SFAPs

signals at different x_e does not move to the right as was seen in the z-directional change. Change in phase, that is change from tirphasic to biphasic is also seen when x_e increases.

Next phase of simulation has been done to see the effect of fiber diameter in the shape of recorded action potential. Figure 3.11 depicts the behavior of the peak to peak amplitude of the SFAP with the increase of fiber diameter. As conduction velocity is linearly proportionate to the fiber diameter and SFAP is also proportionate to the conduction velocity, it turns out that peak to peak amplitude varies linearly with the increasing fiber diameter. Figure 3.12 shows the change in shape and magnitude of the SFAP with the changing fiber diameter. As stated earlier, peak to peak amplitude increases linearly with the increase of diameter and also spatially gets tightened with the increase in diameter. No change in phase is observed due to the change in diameter.

Another important aspect of the surface action potential is of the combination of electrodes that are used for the EMG recording. As described in chapter one, differential electrodes are widely used for surface EMG recording. In Figure 3.13, a differential SFAP is recorded for two electrodes situated at z_e = 10 and z_e = 20mm with other parameters kept constant. As shown in Figure 3.14, the differential SFAP is the difference between the signals recorded at the two electrodes. Interesting feature of this simulation is that, although the signal in each electrode is biphasic, the differential signal has turned out to be triphasic or it could be vice versa as well.

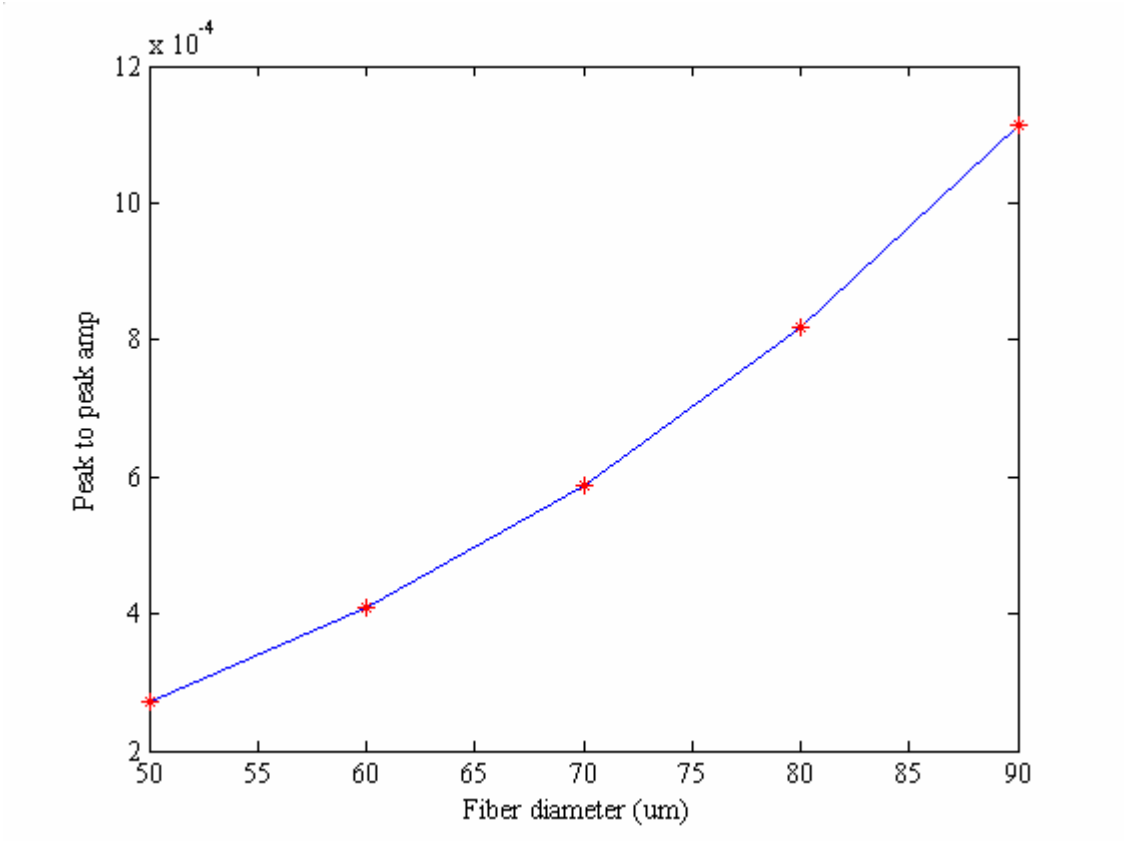

Figure 3.11: Relationship between peak to peak amplitude of SFAPs with the fiber diameter

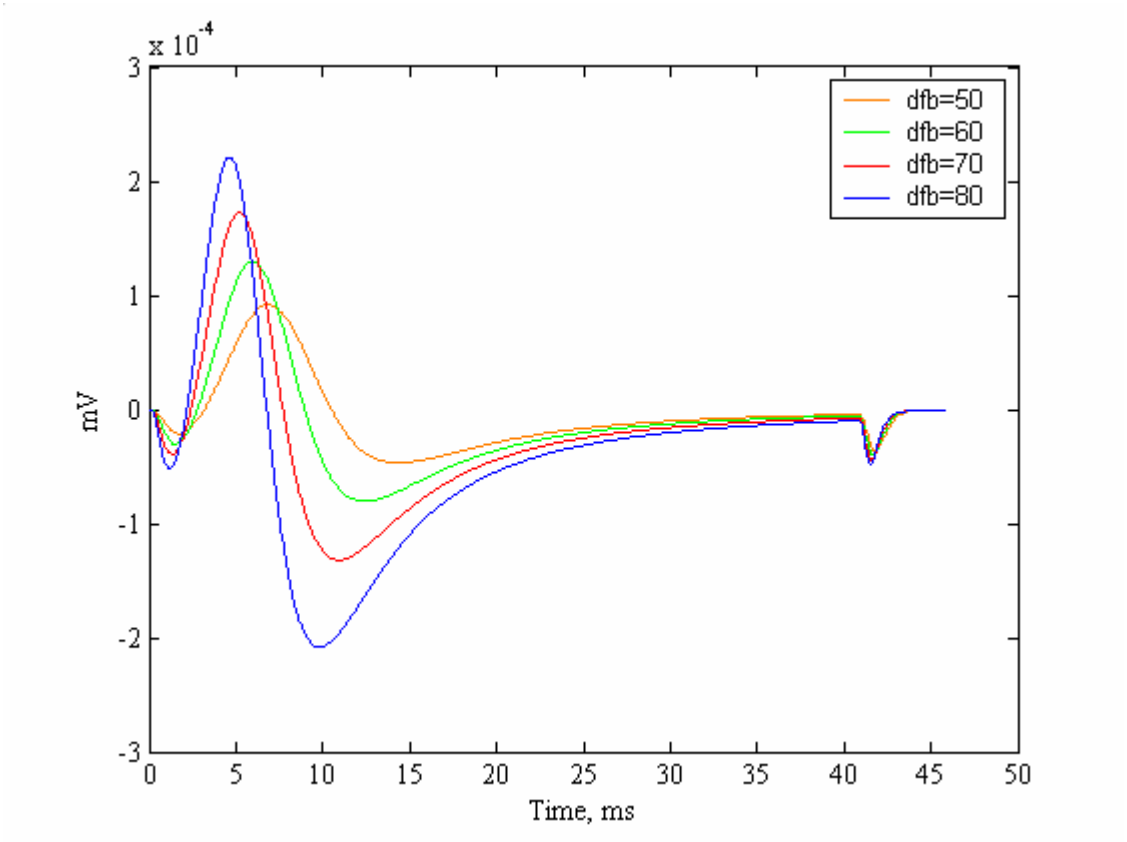

Figure 3.12: Effects of fiber diameter on SFAPs

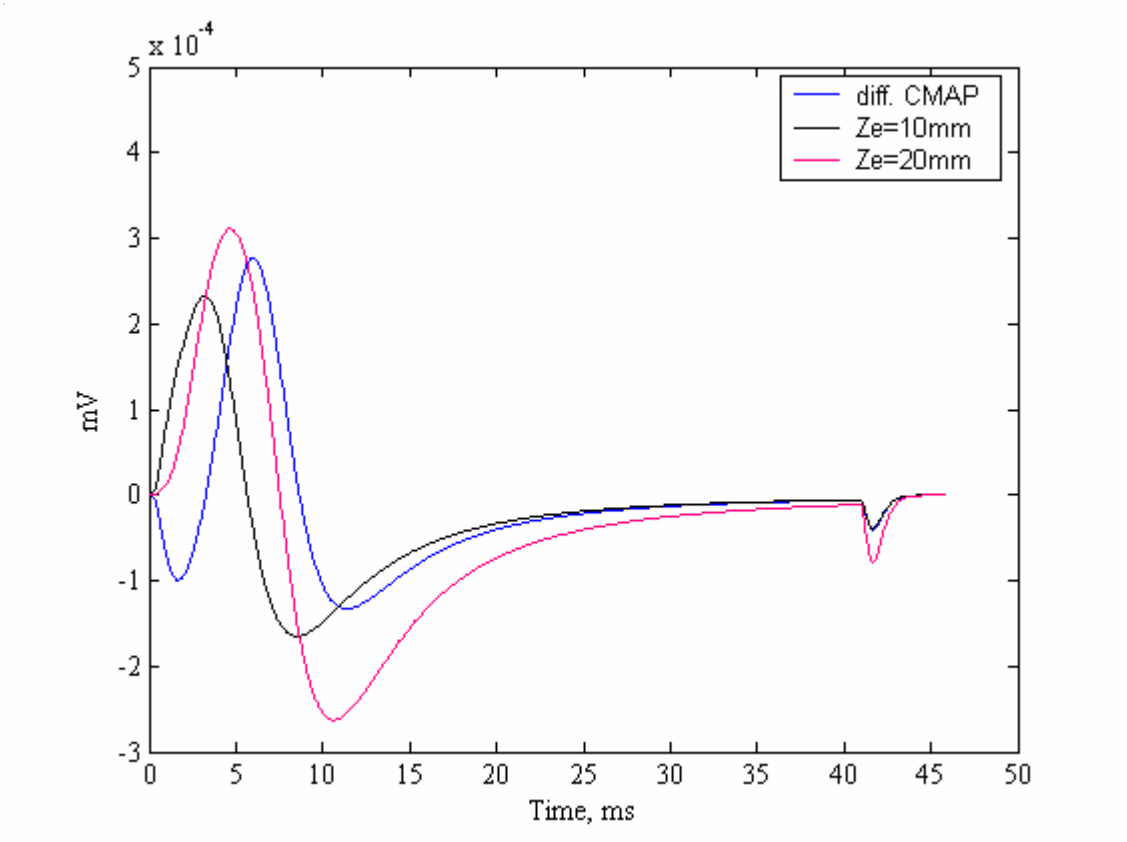

Figure 3.13: A differential SFAP derived from two monopolar SFAPs

3.5 Effect of Fat and Skin

Surface EMG is widely used because of its ease of operation and also its usefulness of acquiring global information from the surface of the muscle. In surface EMG it is essential to take consideration of the effect of fat and skin on EMG measurement and also in the modeling of EMG generation. In between muscle fibers and the surface electrodes, there are two additional tissue layers- fat and skin exist. Though the fat and skin layers are two different tissues and have different conductivity, both mediums are isotropic. The effects of highly resistive skin and adipose fat tissues can be simulated to depict the influence of each physiological parameter on the surface EMG signals. These subcutaneous tissue layers of fat and skin cause attenuation and spatial widening of the surface EMG signals. In this section, the volume conductor model that is described in the previous section will be extended to incorporate fat and skin layers at the top of muscle tissue and the potential distribution on the top of skin surface will be calculated following the procedure described in [66] and [67].

Figure 3.14 shows a Four-layer concentric cylindrical model that represents a large inner cylinder of muscular anisotropic tissue, an intermediate layer of subcutaneous fat and an outer layer of skin, both as an isotropic medium. The complete muscle structure is situated in the medium of air. It is assumed that the muscle and the fat tissue has interface at $y = 0$, fat and skin has at $y = y1$ and skin and air at $y = y2$. To develop the simulation model the position of muscle fiber is considered parallel along z-axis in the

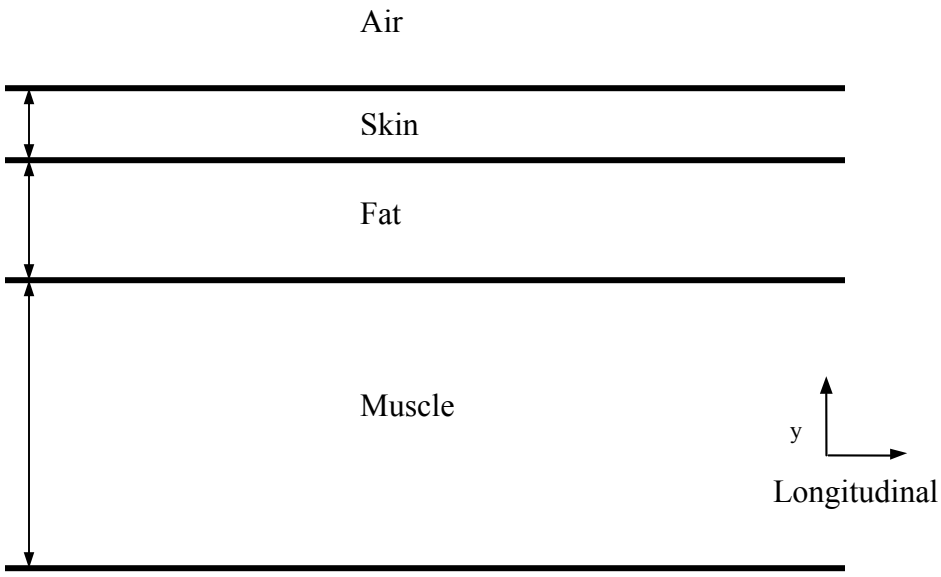

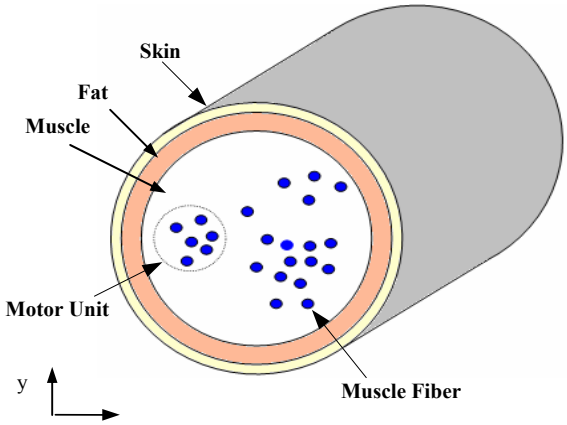

Figure 3.14: Four-layer concentric cylindrical model

superficial area of muscle. As shown earlier, the potential in the anisotropic muscle medium can be expressed using the Laplace equation as:

$$\left[\frac{\partial^2}{\partial x^2}+\frac{\partial^2}{\partial y^2}+P\frac{\partial^2}{\partial z^2}\right]\varphi_{muscle}(x,y,z)=i_m \tag{59}$$

where $P=\dfrac{\sigma_z}{\sigma_r}$

However, for the fat and skin medium, $\sigma_z=\sigma_r$. Thus Laplace equations for fat and skin layer can be written as:

$$\left[\frac{\partial^2}{\partial x^2}+\frac{\partial^2}{\partial y^2}+\frac{\partial^2}{\partial z^2}\right]\varphi_{fat}(x,y,z)=0 \tag{60}$$

$$\left[\frac{\partial^2}{\partial x^2}+\frac{\partial^2}{\partial y^2}+\frac{\partial^2}{\partial z^2}\right]\varphi_{skin}(x,y,z)=0 \tag{61}$$

In the multiple layer muscle model, current can be considered continuous along y direction and electric field can be considered continuous along x and z direction at the interface of two different layers. As shown in Figure 3.14, muscle layer and fat and skin layer has a boundary at *y = 0.* Thus at the boundaries, the following conditions hold:

$$\sigma_{fat}\left.\frac{\partial\varphi_{fat}}{\partial y}\right|_{y=0}=\sigma_{muscle(y)}\left.\frac{\partial\varphi_{muscle}}{\partial y}\right|_{y=0}$$

$$\left.\frac{\partial\varphi_{fat}}{\partial x}\right|_{y=0}=\left.\frac{\partial\varphi_{muscle}}{\partial x}\right|_{y=0}$$

$$\sigma_{skin}\left.\frac{\partial\varphi_{skin}}{\partial y}\right|_{y=y1}=\sigma_{fat}\left.\frac{\partial\varphi_{fat}}{\partial y}\right|_{y=y1}$$

$$\left.\frac{\partial \varphi_{skin}}{\partial x}\right|_{y=y1} = \left.\frac{\partial \varphi_{fat}}{\partial x}\right|_{y=y1}$$

$$\left.\frac{\partial \varphi_{skin}}{\partial y}\right|_{y=y2} = 0 \tag{62}$$

$$\left.\frac{\partial \varphi_{skin}}{\partial x}\right|_{y=y2} = \left.\frac{\partial \varphi_{air}}{\partial x}\right|_{y=y2}$$

$$\left.\frac{\partial \varphi_{fat}}{\partial z}\right|_{y=0} = \left.\frac{\partial \varphi_{muscle}}{\partial z}\right|_{y=0}$$

$$\left.\frac{\partial \varphi_{skin}}{\partial z}\right|_{y=y1} = \left.\frac{\partial \varphi_{fat}}{\partial z}\right|_{y=y1}$$

Taking the two dimensional Fourier transform of the Equations (59), (60) and (61) in x and z direction, we get:

$$\left[\frac{\partial^2}{\partial y^2} - \omega_x^2 - P\omega_z^2\right]\varphi_{muscle}(\omega_x, y, \omega_z) = I_m \tag{63}$$

$$\left[\frac{\partial^2}{\partial y^2} - \omega_x^2 - \omega_z^2\right]\varphi_{fat}(\omega_x, y, \omega_z) = 0 \tag{64}$$

$$\left[\frac{\partial^2}{\partial y^2} - \omega_x^2 - \omega_z^2\right]\varphi_{skin}(\omega_x, y, \omega_z) = 0 \tag{65}$$

Let $\omega_{ya} = \sqrt{\omega_x^2 + P\omega_z^2}$ and $\omega_{yi} = \sqrt{\omega_x^2 + \omega_z^2}$, thus the above Equations become:

$$\left[\frac{\partial^2}{\partial y^2} - \omega_{ya}^2\right]\varphi_{muscle}(\omega_x, y, \omega_z) = I_m \tag{66}$$

$$\left[\frac{\partial^2}{\partial y^2} - \omega_{yi}^2\right]\varphi_{fat}(\omega_x, y, \omega_z) = 0 \tag{67}$$

$$\left[\frac{\partial^2}{\partial y^2} - \omega_{yi}^2\right]\varphi_{skin}(\omega_x, y, \omega_z) = 0 \tag{68}$$

Solutions of the above ordinary differential equations can be given as:

$$\varphi_{muscle}(\omega_x, y, \omega_z) = A_1 e^{y\omega_{ya}} + B_1 e^{-y\omega_{ya}} \tag{69}$$

$$\varphi_{fat}(\omega_x, y, \omega_z) = A_2 e^{y\omega_{yi}} + B_2 e^{-y\omega_{yi}} \tag{70}$$

$$\varphi_{skin}(\omega_x, y, \omega_z) = A_3 e^{y\omega_{yi}} + B_3 e^{-y\omega_{yi}} \tag{71}$$

Boundary conditions in the spatial frequency domain can be expressed as:

$$\sigma_{fat}\left.\frac{\partial\varphi_{fat}(\omega_x, y, \omega_z)}{\partial y}\right|_{y=0} = \sigma_{muscle(y)}\left.\frac{\partial\varphi_{muscle}(\omega_x, y, \omega_z)}{\partial y}\right|_{y=0}$$

$$\varphi_{fat}(\omega_x, y, \omega_z)\big|_{y=0} = \varphi_{muscle}(\omega_x, y, \omega_z)\big|_{y=0}$$

$$\sigma_{skin}\left.\frac{\partial\varphi_{skin}(\omega_x, y, \omega_z)}{\partial y}\right|_{y=y1} = \sigma_{fat}\left.\frac{\partial\varphi_{fat}(\omega_x, y, \omega_z)}{\partial y}\right|_{y=y1} \tag{72}$$

$$\sigma_{skin}\left.\frac{\partial\varphi_{skin}(\omega_x, y, \omega_z)}{\partial y}\right|_{y=y2} = 0$$

$$\varphi_{skin}(\omega_x, y, \omega_z)\big|_{y=y2} = \varphi_{air}(\omega_x, y, \omega_z)\big|_{y=y2}$$

Thus the six coefficients of the above potential solutions can be evaluated from the six boundary conditions described above. Substitution of these coefficients provides the

potential distribution for each layer. At those layers, potential distribution in 2D spatial frequency domain can be expressed as:

$$\varphi(\omega_x,0,\omega_z)=\frac{I_m(\omega_z)}{\sigma_r}e^{-y0\omega_{ya}}\frac{(1+R_c)\cosh(\omega_{yi}(t_f+t_s))+(1-R_c)\cosh(\omega_{yi}(t_f-t_s))}{\alpha_1(\omega_{yi},\omega_{ya},R_c,t_f,t_s)+\alpha_2(\omega_{yi},\omega_{ya},R_c,t_f,t_s)} \quad (73)$$

$$\varphi(\omega_x,y1,\omega_z)=\frac{2I_m(\omega_z)}{\sigma_r}e^{-y0\omega_{ya}}\frac{\cosh(\omega_{yi},t_s)}{\alpha_1(\omega_{yi},\omega_{ya},R_c,t_f,t_s)+\alpha_2(\omega_{yi},\omega_{ya},R_c,t_f,t_s)} \quad (74)$$

$$\varphi(\omega_x,y2,\omega_z)=\frac{2I_m(\omega_z)}{\sigma_r}e^{-y0\omega_{ya}}\frac{1}{\alpha_1(\omega_{yi},\omega_{ya},R_c,t_f,t_s)+\alpha_2(\omega_{yi},\omega_{ya},R_c,t_f,t_s)} \quad (75)$$

where α_1 and α_2 for a specific value of frequency are,

$$\alpha_1(\omega_y,\omega_{ya},R_c,t_f,t_s)=(1+R_c)\cosh\{\omega_y(t_f+t_s)\}[\omega_{ya}+R_b\omega_y\tanh\{\omega_y(t_f+t_s)\}] \quad (76)$$

$$\alpha_2(\omega_y,\omega_{ya},R_c,t_f,t_s)=(1-R_c)\cosh\{\omega_y(t_f-t_s)\}[\omega_{ya}+R_b\omega_y\tanh\{\omega_y(t_f-t_s)\}] \quad (77)$$

$$\sigma_{muscle(y)}=\sigma_r,\quad R_b=\frac{\sigma_{fat}}{\sigma_r}\quad and\quad R_c=\frac{\sigma_{skin}}{\sigma_{fat}} \quad (78)$$

The above three potential equations will provide the potential distribution on various region of the multi-layer model. The transfer function of the isotropic layers of fat and skin can be obtained by dividing the potential at the top of skin by the potential of the muscle region. In other words, the total transfer function of the intermediate tissue layers is a cascade of transfer function of anisotropic and isotropic medium. Thus, the transfer function of the fat and skin layer can be written as:

$$H_{fat\&skin}(\omega_x,\omega_z)=\frac{\varphi(\omega_x,y2,\omega_z)}{\varphi(\omega_x,0,\omega_z)} \quad (79)$$

$$H_{fat\&skin}(w_x, w_z) = \frac{2}{(1+R_c)\cosh(w_y(t_f + t_s)) + (1-R_c)\cosh(w_y(t_f - t_s))} \quad (80)$$

Where $\omega_x = 2\pi f_x$ and $\omega_z = 2\pi f_z$ are the spatial angular frequency in x (perpendicular to the fiber) and z (parallel to the fiber) directions, $\omega_y = \sqrt{\omega_x^2 + \omega_z^2}$ in the direction of distance between muscle and electrode, R_c is the conductivity ratio between skin and fat, t_f and t_s are thickness of fat and skin respectively. The solution of potential distribution in the space domain can be obtained by taking the two dimensional inverse Fourier transform. So the final action potential equation will be the inverse Fourier transforms of the product of $H_{fat\&skin}$ and $\Phi(r, \omega)$.

$$\varphi_{total} = F^{-1}(\Phi(r, \omega).H_{fat\&skiin}) \quad (81)$$

3.6 Results

The existence of these subcutaneous layers substantially effect the potential profile generated by an excited muscle fiber. So while using surface electrodes, it is essential to take consideration of the effect of fat and skin. The effects of subcutaneous fat and skin on the recorded surface action potential can be analyzed by simulating the potential distribution at different layers. Figure 3.15 shows the two-dimensional potential distribution in spatial domain at muscle and at the skin surface from a fiber parallel to skin at a depth of 2 mm in the muscle. Thickness of fat and skin are assumed to be 3mm and 1mm respectively. From the comparison of Figure 3.15a and Figure3.15b it can be stated that the isotropic layers cause attenuation and spatial widening of the signal. Figure 3.16 shows the characteristics of simulated potential in two-dimensional spatial

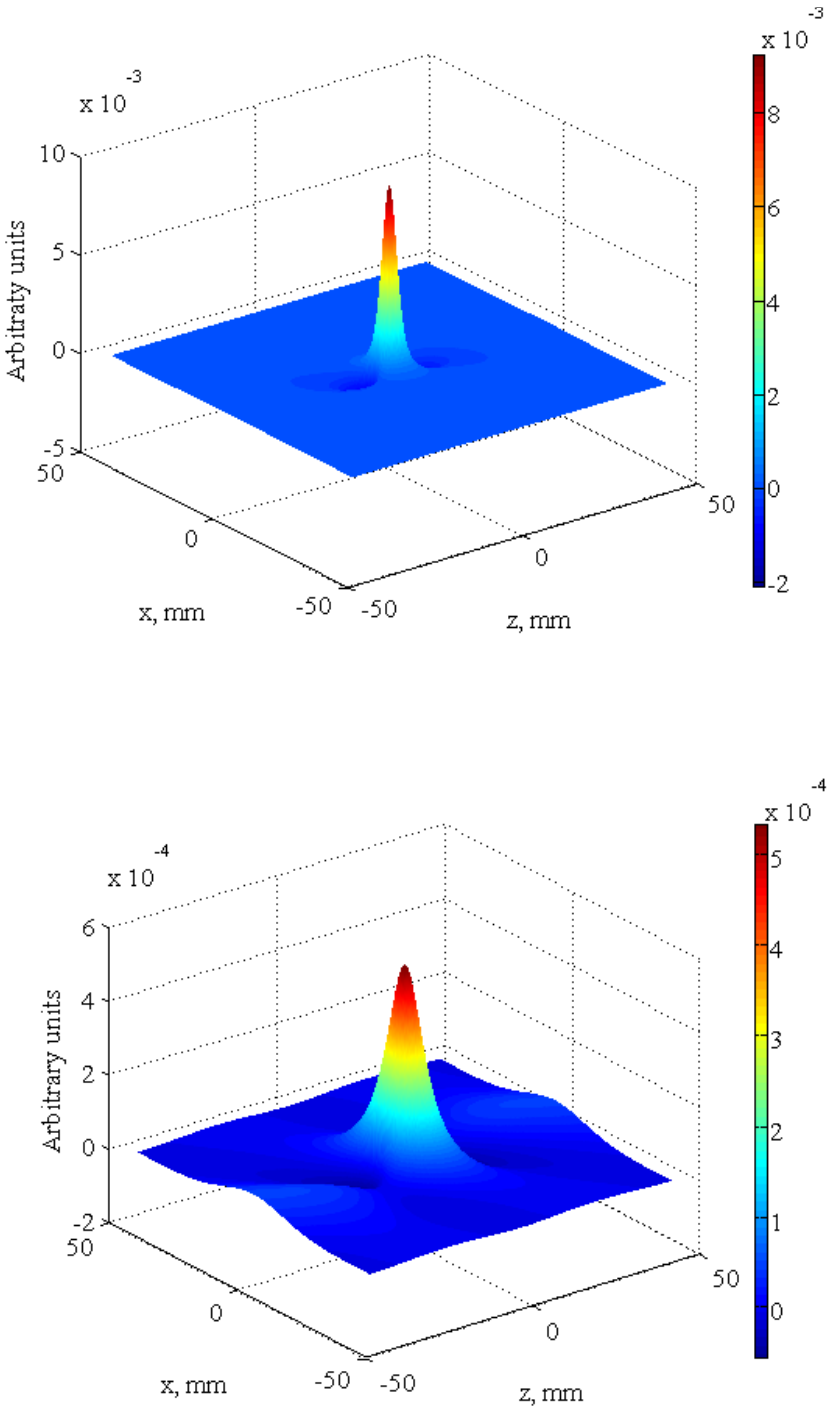

Figure 3.15: Two dimensional potential distribution in spatial domain at a) muscle and b) at skin

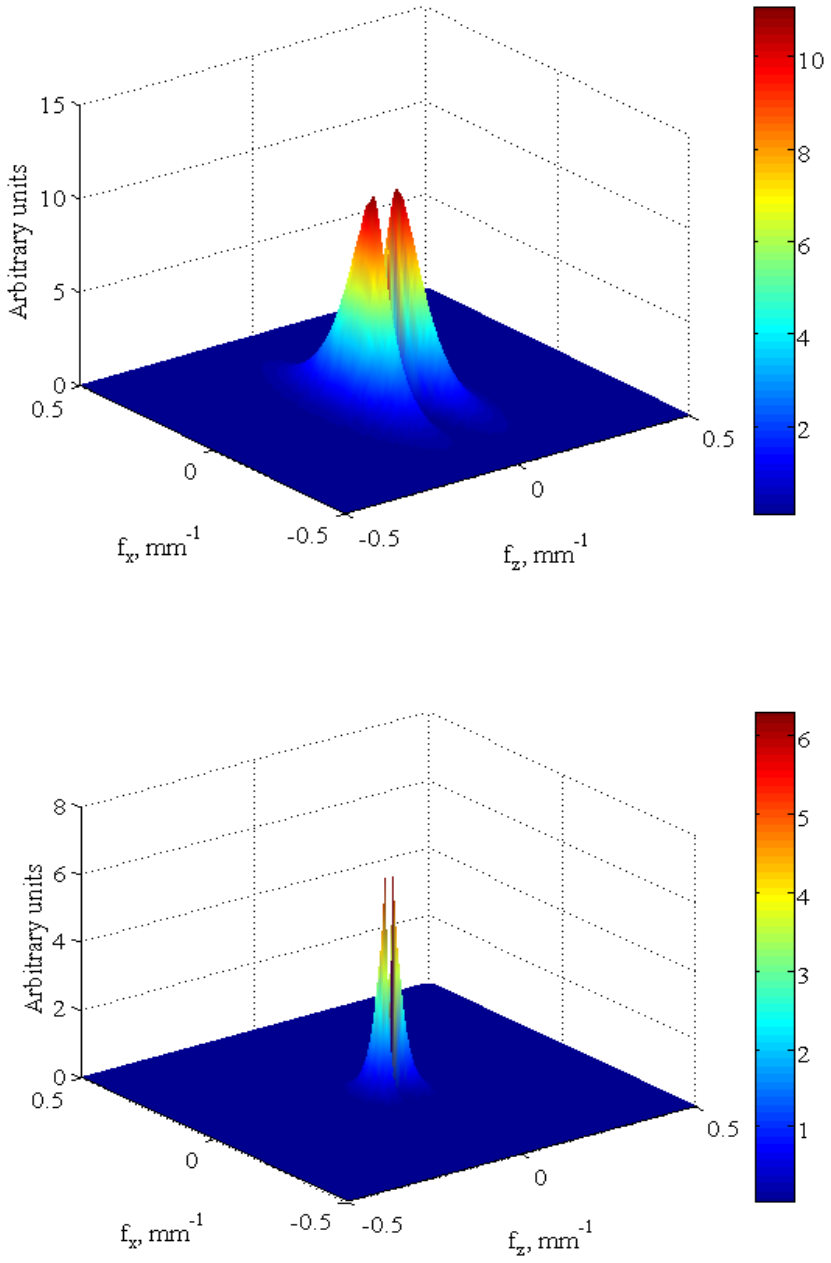

Figure 3.16: Two dimensional potential distribution in spatial frequency domain at a) muscle and b) at skin

frequency domain. Isotropic fat and skin layer behaves as a low pass filter obstructing to pass any high frequency component that might be with the generated action potential. Figure 3.17 shows the comparison of the simulated action potential at muscle and at skin, which shows clearly the reduction in signal amplitude. The variation in thickness of fat and skin layer, which is expected among different people, also has effect on the surface action potential. Figure 3.18 shows the spatial characteristics of the fat and skin layer transfer function along z direction with the variation of fat thickness, t_f form 3 mm to 9 mm while skin thickness is 1mm. The location of the source and other electrophysiological parameters are kept unchanged. Increase in fat thickness decreases the cutoff frequency of the low pass volume conductor of the fat and skin layer. Also seen from the figure is the attenuation that is increased when the fat thickness increased.

3.7 Conclusion

In this section, first a single fiber action potential model is described and its analytical solution for calculating the potential due to the propagating action potential in the fiber is given. The solution is based on line source model representation of the transmembrane current. The fiber is assumed parallel to the skin surface although in reality the fiber might be curve shape. An algorithm to simulate SFAP is given and the effects of electrode to fiber distance and electrode orientation on the SFAP measurement have been discussed. In the second part of this chapter, a multi-layer muscle model is described which includes muscle as well as fat and skin tissues as concentric cylinder. Effect of these two isotropic mediums on SFAP has been illustrated by generating the potential

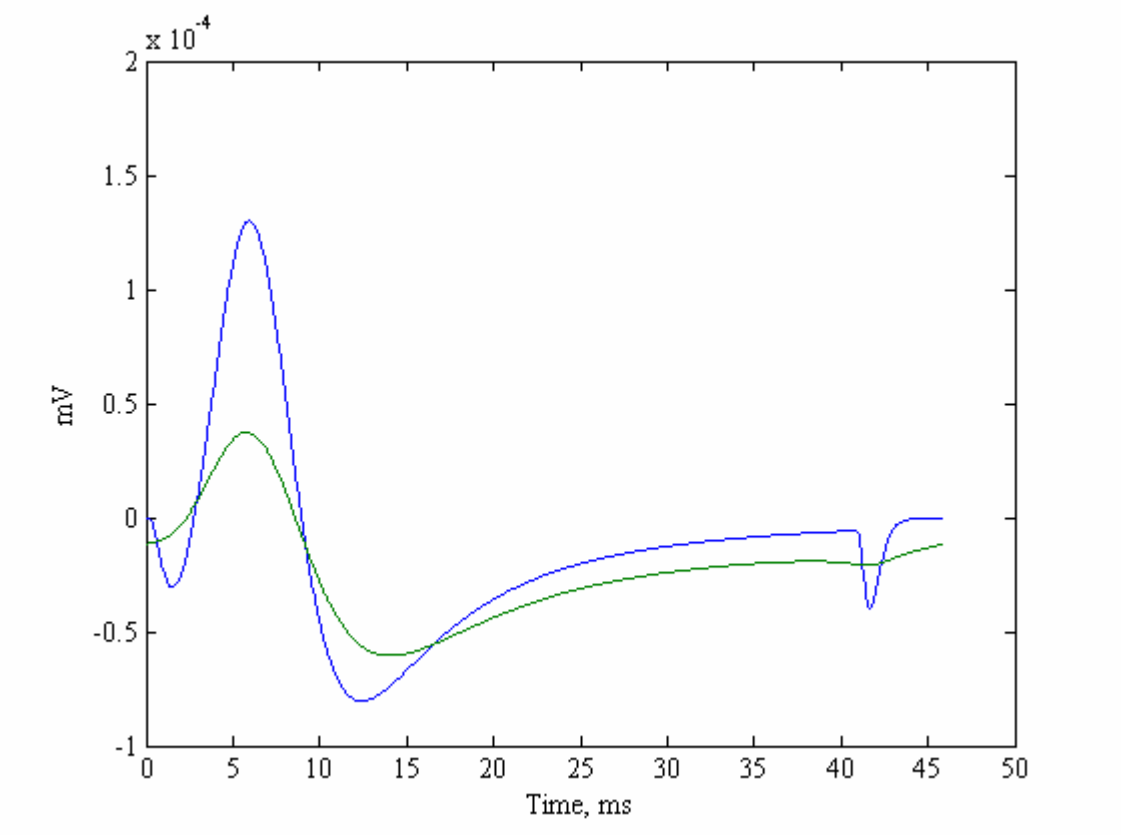

Figure 3.17: Two-dimensional potential distribution in spatial domain at a) muscle and b) at skin

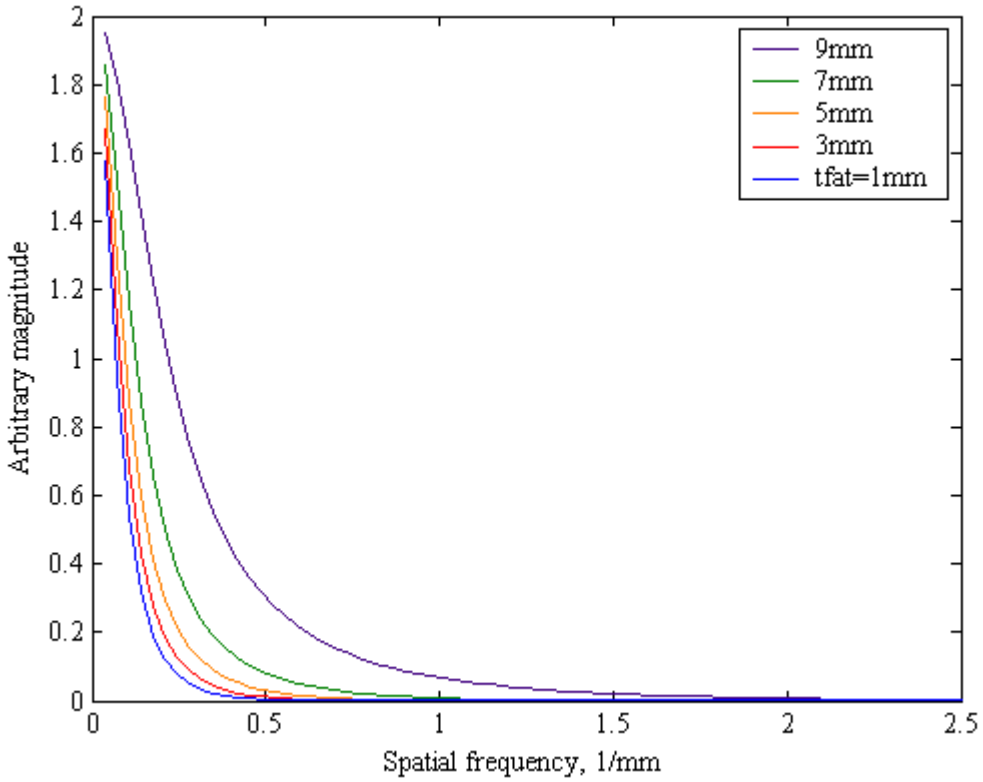

Figure 3.18: Effects of different depth of fat on volume conductor

distribution on each medium. Spatial widening and signal attenuation of the SFAP are the two distinct effects that took place while fat and skin layers are incorporated to the single fiber action potential model.

CHAPTER 4

4. The Motor Neuron Pool Model

4.1 Introduction

There is a huge collection of literature on motor unit physiology and its behavior, which underscores the variability of motor unit functions during voluntary contraction. Nonetheless, some principles have emerged that have enabled us to reduce the observed variability and to examine the mechanisms used by the nervous system in the control of movement. The central nervous system (CNS) can increase the strength of muscle contraction by the following:

- Increasing the number of active motor units (i.e., spatial recruitment)
- Increasing the firing rate at which individual motor units fire to optimize the summated tension generated (i.e., temporal recruitment or rate coding)

The nervous system acts in a complex fashion to control the force generated by our skeletal muscle by using intricate and systematic procedure of recruiting a number of motor units and controlling their corresponding firing frequencies. Functionally, the critical point in the modulation of motor-neuron recruitment and discharge is whether a given synaptic input generates sufficient current at the soma to recruit the cell. This has been called the effective synaptic current. During muscle contraction, these effective

synaptic current inputs from various sources of nervous system activate the required motor units. Firing frequency or the frequency of activation of the motor units depends on the amount of force needed to produce and also dependent on the type of contractions. The behavior of the motor unit recruitment and the firing frequency is not yet well understood among the physiologists for various muscle activities. Nevertheless, this chapter tries to use the current available published rules of motor unit behavior during constant voluntary contraction. Using these experimental results, a motor unit pool model has been developed here. A motor neuron pool model predicts the number of motor units that is recruited from a pool of motor units in a muscle as a function of force and recruitment threshold and also the pattern of recruiting as the force increases and remains constant at certain amount of maximum voluntary contraction. The model also incorporates a firing frequency for each of the motor unit as a function of force as well. It also limits each of motor unit's minimum and maximum firing frequency and the variation in the steady state firing frequency. This model does not predict the recruitment and firing frequency for fatiguing contraction or the transient behavior of the contraction.

4.2 Motor Unit Distribution

As described in Chapter two, motor units are distributed randomly inside the muscle. In this chapter, a generic motor unit pool model is developed. If muscle radius, number of motor units, number of fibers per motor unit, different fiber concentration and fiber diameter is known, then muscle cross sectional surface is divided into number of small square areas whose one side is equal to the maximum fiber diameter and total number of

areas are equal to total number of fibers in that muscle. Each square area is numbered as '1' or '2' as type-I and type-II fiber respectively. Motor unit center point is randomly selected inside this cross sectional surface and each motor unit is filled with the required number of fibers using the equation described in Chapter Two (Equation 4). Figure 4.1 shows the random distribution of the motor units inside a muscle. To analyze the effect of random distribution of the motor units, compound muscle action potential (CMAP, discussed in detail in Chapter Six), which is the summation of all the single fiber action potential in a muscle, is simulated for 50 trials for tibialis anterior muscle. Results show that, different metrics of CMAP such as peak to peak amplitude, area under the curve and rise time are differently affected [68]. Table 4.1 shows these metrics as mean and standard deviation.

As muscle in a motor unit is comprised of many motor units with different diameters, conduction velocities differ among the muscle fibers in a motor unit. A Gaussian distribution of the fiber diameter is assumed within a motor unit [44]. The last two variations factor will not be used in the simulation of the single fiber action potential. They will be used while motor unit pool as well as motor unit action potential model is developed.

4.3 Motor Unit Recruitment

Recruitment is defined as the successive activation of the motor units with increasing strength of voluntary muscle contraction. It is a complex process that is under central

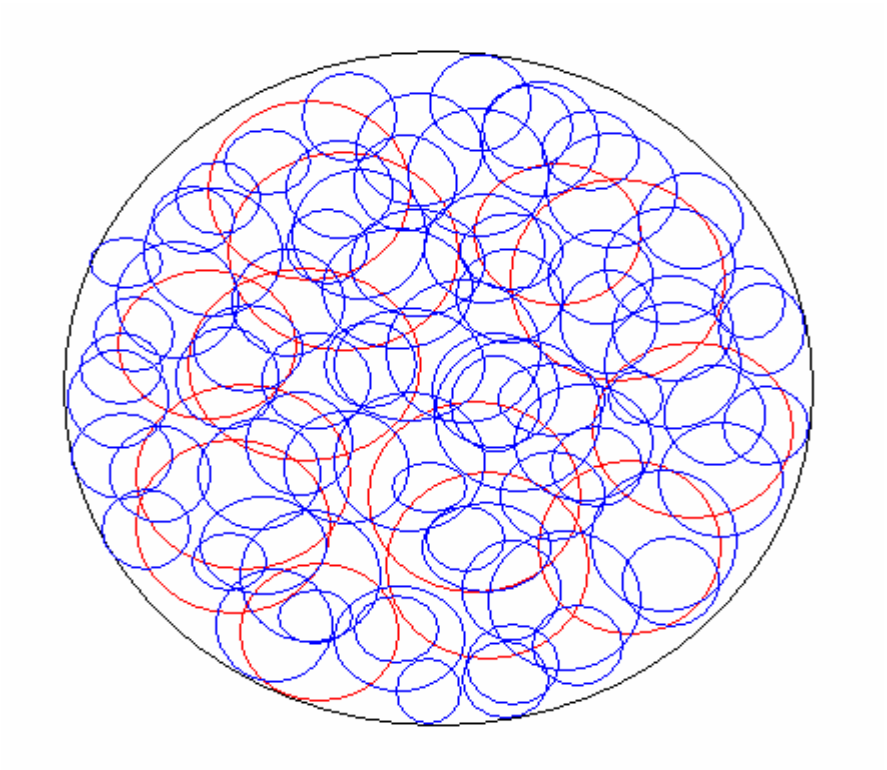

Figure 4.1: Motor unit distribution inside a muscle with 100 motor units. Type-I are blue and Type-II are red

Table 4-1: Simulated CMAP metrics in 50 trials for anterior tibialis muscle

Muscle	Peak to peak (mV)	Area under the curve (mV.ms)	Rise time
Tibialis Anterior	16.19 (SD = 0.72)	1.23 (SD = 0.14)	1.39 (SD = 0.03)

nervous system control. Motor unit recruitment results in a strong efficient muscle contraction. Patterns of recruitment may differ between various types of motor activation. But for most of the cases, the recruitment order follows the 'size principle', which states that, smaller motor units will be recruited earlier than the larger motor units [69, 70, 71]. The size principle refers to alpha motoneuron size relative to its order of recruitment in a population of motor units that comprises the fundamental organizational units of a muscle. The soma of alpha motoneurons varies in size, accounting for some of the differences between type-I and type-II motor unit. Dendritic volume (i.e. number of excitatory synapses on the neuronal soma) is constant in the two types of alpha motoneurons. Therefore, smaller type-I motoneurons have relatively greater excitatory input given their smaller membrane size. In contrast, type-II alpha motoneurons have a larger membrane, but given the same number of excitatory inputs, they have a lower excitatory potential. When the muscle is activated initially, the first motor units to be recruited are small in size and weak in the degree of tension they can generate. Starting with the smallest motor units, progressively larger units are recruited with increasing strength of muscle contraction. The result is an orderly addition of sequentially larger and stronger motor units resulting in a smooth increase in muscle strength. The recruitment sequence is thus to begin with slow type I motor units, to progress to type II units that first include moderate type IIA and to end with fast type IIB, which are active only at relatively high force output.

4.3.1 Relative Threshold of the Motor Units

An individual motor unit is not active until the level of muscle contraction or the excitatory input current to the motoneurons is above some minimal level, which is termed its recruitment threshold. Once a motor unit is active it remains active throughout a contraction as long as the force created remains above its recruitment threshold. In accordance with the 'size principle', the earlier recruited motor units will have smaller recruitment threshold and later recruited motor units will have larger threshold. In other words, smaller motor units need smaller excitatory synaptic input currents than the larger ones. As suggested by Fuglevand [31], a Poisson distribution of recruitment thresholds similar to the distribution of motor unit territories adequately reflects the distribution of thresholds of the motor units and the size principle suggested by Henneman [72]. For ease of simulation procedure if the recruitment thresholds are assigned in the unit of percentage of maximal voluntary contraction (MVC), then the exponential equation that describes the Poisson distribution of recruitment thresholds is as follows [32]:

$$\eta_i = \eta_{\min} e^{\frac{\ln(R)}{n} \cdot i} \tag{82}$$

where,

η_i is the recruitment threshold of the i^{th} motor unit in units of %MVC

η_{min} is the minimum recruitment threshold

R is the ratio of the maximum to minimum recruitment threshold

n is the total number of motor units in the muscle

This equation will result in many motor units having a relatively smaller recruitment threshold and fewer motor units having larger recruitment thresholds. η_{min} is arbitrarily set at 1. Thus any voluntary contraction that produces a total synaptic excitatory current of I_i, the motor units, which have thresholds greater that I_i will not be activated. The range or the ratio (R) of recruitment threshold is chosen from published physiological condition of the muscle and the desired level of voluntary contractions. Figure 4.2 shows the relative recruitment thresholds for 200 motor units in an arbitrary muscle where the recruitment threshold range is 60.

4.4 Motor Unit Firing

The rate at which motor units produce action potentials during contraction is called the firing frequency. Motor unit firing or the rate coding is one of the two neural methods that the nervous system adopts during contraction of the muscle. Motor units have been found to modulate their firing rates in unison and simultaneously. The firing rate of motor units is not constant, even during constant force contractions rather it fluctuates. The firing rates of earlier recruited motor units are greater than those of later recruited motor units at any given force value [31, 32]. At a force reversal, the firing rates of high threshold motor units reduce their firing rates before the low threshold motor units. The fluctuations in a force output of a muscle during a constant-force contraction are caused by the fluctuations in the firing rates of the motor units. The firing rates of the motor units decrease during a constant-force isometric contraction. These phenomena suggest

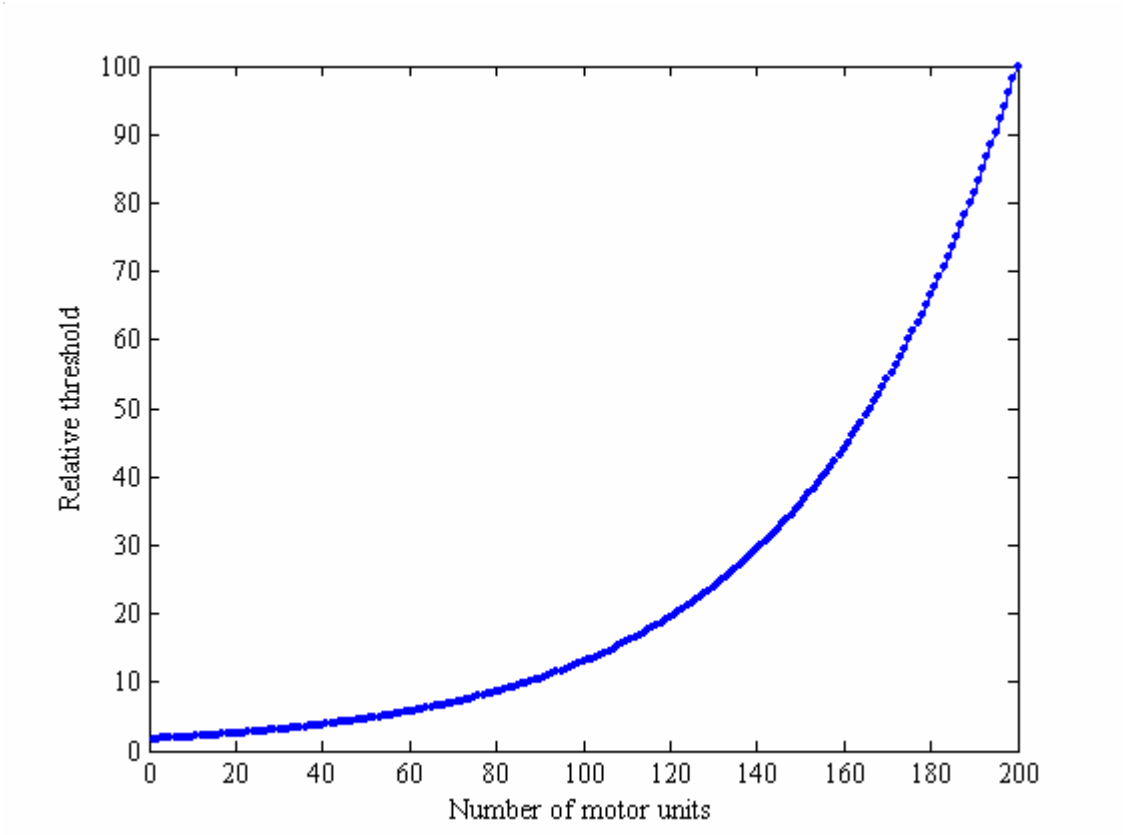

Figure 4.2: Relative recruitment thresholds for 200 motor units in an arbitrary muscle

that the motor units have a net excitation, which acts through a common input. The most likely location of this common input is the anterior horn cell. The control to the muscle is not designed to generate constant-force contractions. Motor unit firing frequency is characterized by four parameters, namely, minimum firing frequency, peak firing frequency, force and firing frequency relationship and interpulse interval of the firing action potentials. In the human body, smaller muscles are generally involved in performing accurate movements. Such movements require small incremental changes in force. In contrast, large muscles are generally involved in either producing large forces or in controlling posture. Large muscles generally do not require finer force gradation to accomplish their task. Thus, the firing rates of such muscles do not require continual regulation and do not possess the highly dynamic characteristics seen in smaller muscles.

4.4.1 Minimum Frequency

The motor units with a low threshold in sustained contraction had a low minimum frequency. The higher the threshold of the unit in sustained contraction, the higher was its minimum frequency. However, when excited simultaneously, all motor units will have the same minimum firing frequency irrespective of their threshold excitation. When the exerted force remains at the threshold level for any motor unit, then that motor unit will fire in the minimum frequency. For most of the human skeletal muscle the minimum frequency is found in between 7 to12 Hz.

4.4.3 Force-Firing Frequency Relationship

The steady state injected current to the motoneurons and its firing frequency shows a linear relationship. The gain of this linear relationship is constant for all motor units in a muscle and independent of motor unit recruitment threshold. Therefore, if the excitation current exceeds the motor unit threshold, the motor unit firing will be linearly proportionate to the applied current. However, this frequency for a particular motor unit does have saturation at its peak frequency (which will be discussed next) from where the firing frequency does not increase with the increase of the input excitation. The firing rate can be modeled to increase linearly with the increased force above the recruitment threshold for a particular motor unit. The equation can be written as follows [31]:

$$FF_i = mff + m(VC - \eta_i) \tag{83}$$

where, mff = minimum firing frequency

VC = voluntary contraction level in %MVC

η_i is the recruitment threshold of the i^{th} motor unit in units of %MVC

m is the rate at which the firing rate changes with changes in simulated level of contraction

The value of m can be chosen from the experimental result. Usually the value of m of 0.75 is used to simulate the firing behavior of smaller muscles while a value of 0.25 is typically used to simulate larger muscles [32].

4.4.4 Peak frequency

In voluntary contraction, it was found that, after a certain force exerted to a muscle, the firing frequency does not increase [73]. This saturation in firing frequency is called the peak or maximum firing frequency. It was also found that earlier recruited motor units have higher peak frequency than the later recruited motor units. However there are contradictory findings too where higher threshold units had higher peak frequency than that of the lower threshold motor units. In the literature, the reported peak frequency is 20-50 Hz, although some researchers even found 100 Hz of peak frequency [74]. The peak firing rate has been modeled as an inversely proportionate to the recruitment thresholds [31]:

$$FF_{\max} = FF_{i(\max)} - R\frac{\eta_i}{\eta_{\max}}, \tag{84}$$

where, FF_{max} = maximum or peak firing frequency

$FF_{i(max)}$ = peak firing frequency of the first motor unit

R = Difference in peak firing rates between the first and last units recruited

η_i = recruitment threshold for the i^{th} unit

η_{max} = recruitment threshold of the highest or the last motor unit

4.4.5 Variation of Inter-pulse-interval (IPI)

Interpulse interval (IPI) is the time difference between two successive action potentials. IPI variation expresses the pulse-to-pulse variation. At constant force, the firing frequency of a motor unit varies around a mean value with a fixed covariance. This

variation varies with age and muscle although for a muscle, this value is constant for all the motor units in that muscle. Analysis of motor unit discharge trains has indicated that IPIs resemble a random process with a Gaussian probability distribution function where the mean and the standard deviation of IPI distributions are related in such a way that the coefficient of variation remains relatively constant with changes in mean IPI [25, 71, 75, 76, 77, 78, 79]. For a given motor unit, the variation of IPIs was observed to increase with decreasing firing rate. Equation (83) can be written as:

$$IPI = t_{i,j} - t_{i,j-1} = \frac{1}{FF_i} = \frac{1}{mff + m(VC - \eta_i)} \tag{85}$$

To simulate the stochastic nature of motoneuron discharge, the IPI predicted by the above equation can be assumed equivalent to the mean IPI (IPI_{mean}). In a normally distributed population, the deviation from the mean can be expressed as:

$$X = \frac{\overline{X} - IPI_{mean}}{\sigma} \tag{86}$$

where, $\overline{X}$ can be represented as the value of IPI in a train of action potentials with a standard deviation of σ. Equation (86) can be written as:

$$\overline{X} = IPI_{mean} + \sigma.X = IPI \tag{87}$$

So the equation (87) becomes:

$$IPI = t_{i,j} - t_{i,j-1} = IPI_{mean} + \sigma.X \tag{88}$$

$$\text{i.e,} \quad t_{i,j} = t_{i,j-1} + IPI_{mean} + \sigma.X \tag{89}$$

As the coefficient of variation (*cv*) remains constant and

$cv = \frac{\sigma}{\mu}$ or $\sigma = \mu.cv$, where μ is the mean. Equation (89) becomes

$$t_{i,j} = t_{i,j-1} + IPI_{mean} + IPI_{mean}.cv.X \tag{90}$$

For each discharge, *X* has randomly selected from a Gaussian distribution with known mean and standard deviation using Box-Muller transformation method. It allows us to transform uniformly distributed random variables, to a new set of random variables with a Gaussian (or Normal) distribution. The most basic form of the transformation looks like:

$$y1 = \sqrt{(-2\ln(x1)}\cos(2\pi x2) \tag{91}$$

$$y2 = \sqrt{(-2\ln(x1)}\sin(2\pi x2) \tag{92}$$

where *x1* and *x2* are derived from a uniform distribution of [0 1]. The polar form of the Box-Muller transformation is both faster and more robust numerically. The algorithmic description of it is:

1. Generate two uniformly distributed random numbers *x1* and *x2*.
2. Add the square of each of the random numbers until the sum *w*, is less than or equal to 1.
3. $w = \sqrt{((-2.\ln(w))/w)}$.
4. The new Gaussian distributed number is $y1 = x1 * w$.

where random numbers are uniformly distributed in [0,1]. Substituting the value of y1 for X in equation (90) will give the interpulse interval between two successive action potentials. The equation can be solved recursively to get all the interpulse intervals in a train of action potentials. Figure 4.3 shows the IPI variation for five different motor units in a motor unit pool of 200 for a force of 30%MVC.

4.5 Recruitment and Firing Frequency Interaction

Considerable anatomical and functional coupling exists among the motor units within a muscle. This behavior has been studied extensively in animals as well as in humans by providing external electrical and mechanical stimuli to sensory receptors in the muscle. The force produced by a muscle during a voluntary contraction depends on the number of active motor units and the rate at which those units discharge action potentials. This interaction between recruitment and firing rate provides an apparently simple strategy for providing smooth force output. Upon recruitment of a new motor unit it may be desirable to produce an increase in muscle force, which is less than the minimal incremental contribution of the new motor unit. One way to achieve this goal is to decrease the firing rates of the motor units, which are already active, so as to diminish their contribution to the total force output when the new motor unit is recruited. Thus, compensatory decreases of the firing rates of previously activated motor units will enable the muscle to produce a smoother force output during recruitment. This effect becomes more important as the newly recruited motor units provide an increasingly stronger twitch contribution.

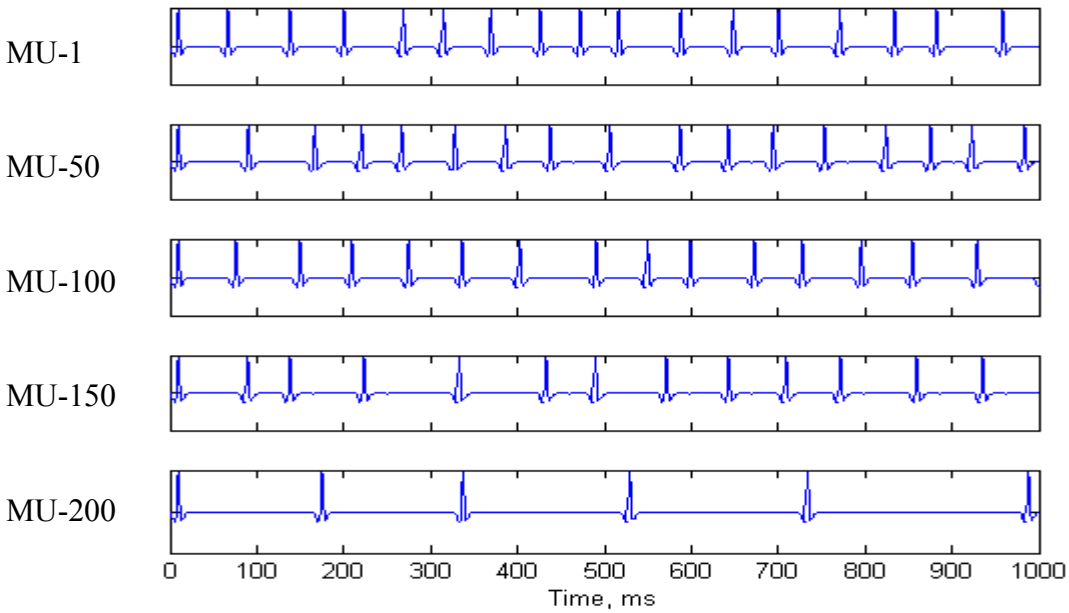

Figure 4.3: IPI variation for five different motor units in a motor unit pool of 200 for a force of 30%MVC

Thus, in general, motor units recruited later should have a stronger effect on the firing rates of previously-activated motor units.

The distribution of net synaptic input currents on a motor neuron pool varies as a function of task. Thus it means that the nervous system determines a priori whether a contraction will involve shortening or lengthening of a muscle and develops appropriate commands by varying the pattern of synaptic inputs [24]. The relative contribution of motor unit recruitment and firing frequency to increase force varies across the working range of the muscle. Recruitment dominates at low forces, whereas rate coding is more significant at high forces. For most muscles, the recruitment of motor units continues up to forces of around 80% of maximum contraction, which means that the remaining 20% is achieved solely by variation of discharge rate of the motor unit action potential [24, 80, 81, 82, 83]. Thus in the initial force build up, recruitment is the primary process that a muscle undertakes, whereas, when the force reaches its maximum, discharge rate becomes important to maintain the force.

CHAPTER 5

5. EMG Generation

5.1 Introduction

Electromyography (EMG) signal is the summation of all activated motor unit action potential trains for a given force applied to the muscle. Both single fiber action potential model and motor neuron pool model are required to be utilized to develop EMG signal for any type of contraction and force level. Figure 5.1 shows a block diagram of the EMG generation using the developed models. Motor unit activation and firing pattern depends on the applied task on the muscle. The tasks can be voluntary isometric (when tension develops but load does not move and muscle does not shorten), voluntary isotonic (when muscle shortens and load moves) or electrically elicited contraction when all the motor units in a muscle are activated synchronously. In this study, only the voluntary isometric contraction has been considered with a ramp contraction. A motor unit pool model will predict the number and timing of the motor unit recruitment. A single fiber action potential model will be utilized to find each activated motor unit action potential, which, is the summation of all the single fiber action potentials belonging to that motor unit. Finally the motor unit pool model will predict the firing frequency and the variation of that frequency for each activated motor unit. Table 5.1 shows the comparison of the distinct features of this EMG generation model with that of Fuglevand's model.

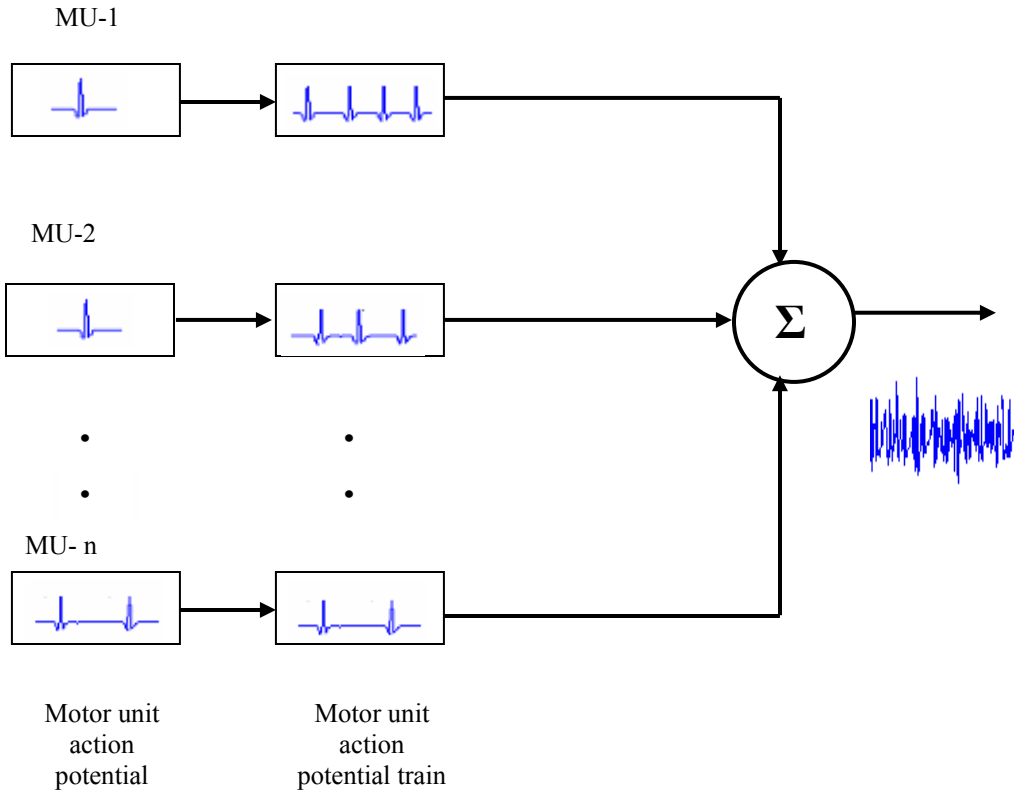

Figure 5.1: A block diagram of the EMG generation

Table 5-1: Comparison of different model parameters of Fuglevand's model and the model developed in this study.

Modeling Parameters	Fuglevand's Model	New Model
Modeling of current source	Dipole representation	Line source current representation
Multilayer volume conductor model	No	Yes
Motor unit type distribution	All same type	Distributed as Type-I and Type-II motor units
Muscle excitation	Excitation synaptic currents	Force as a voluntary contraction
Recruitment range	Narrow range (< 50%) and Broad range (>70%) of excitation	At 60% MVC
Minimum firing rate	Constant for all motor units	Increased linearly with force
ISI variability	Constant for all motor units	Decreased linearly with force

5.2 Methods

Using the single fiber action potential model and the motor unit pool model, any human skeletal muscle can be simulated for EMG generation. In this study, tibialis anterior muscle will be used for simulation. The size and length of this muscle for average young person have been collected from [84]. Fiber diameter range and distribution for different types of fiber and fiber type concentration have been shown in Table 5.2. Number of motor unit and average number of fiber per motor unit are shown in Table 2.2. All other required parameters have been adopted from the published journals and applied to the models that have been developed in this work for EMG generation. As stated earlier, a ramp voluntary contraction has been applied as a force or excitation for the motor neuron pool model, which increases to the level of simulated %MVC in one second and stays at that level for another three seconds without getting fatigued. As it is not the intent to analyze the effect of fatigue in this dissertation, it is assumed that maximum voluntary contraction for the simulated period of time will not cause any fatigue in the muscle. Figure 5.2 shows the ramp force and its constant stay at contraction level. Thus the developed EMG signal is constant force EMG without consideration of fatigue. The muscle is simulated for 5%, 10% and for every 10% increment until the maximum voluntary contraction or 100%MVC. Recruitment level is set at 60%MVC, which means that all motor units in the muscle will be activated when the contraction reach at 60% of MVC. In other words, at 60% of MVC the highest threshold motor unit will be recruited. Thus the range for the recruitment threshold has been set from 1 to 60. The first or the lowest threshold motor unit will have threshold limit of 1%MVC and the last or the

Table 5-2: Different types of fiber and fiber type concentration for both young and old

Muscle Type	Young subjects				Old subjects			
	Type-I		Type-IIA		Type-I		Type-IIA	
	%	*d* μm	*%*	*d* μm	*%*	*d* μm	*%*	*d* μm
Bicep Brachii	45.0 ±3.0	65.4 ±7.0	31.0 ±3.4	71.5 ±7.0	48.0 ±5.0	58.4 ±5.0	29.0 ±7.0	60.9 ±5.0
Tibialis Anterior	76.0 ±7.0	70.9 ±6.5	22.7 ±7.0	98.9 ±7.8	84.1 ±5.0	71.8 ±6.6	15.2 ±3.0	80.0 ±4.0

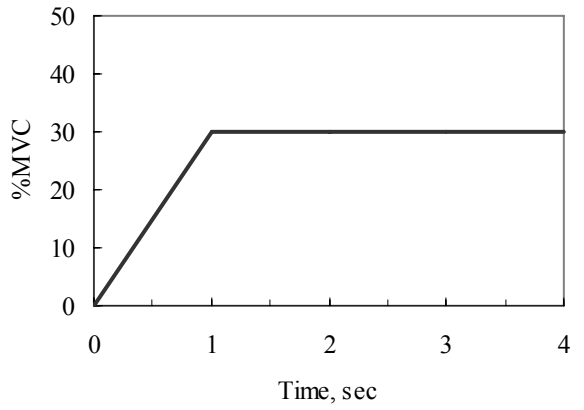

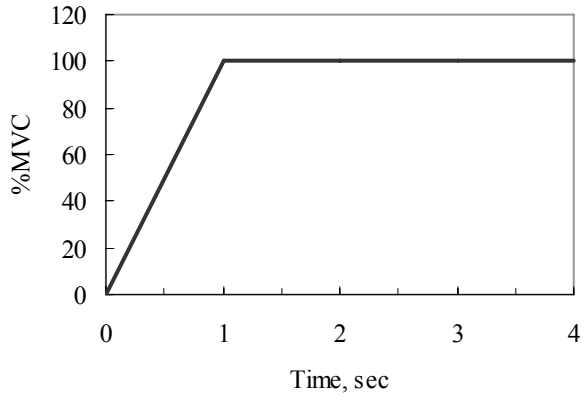

Figure 5.2: Simulated applied force to the muscle in %MVC

highest threshold motor unit will have threshold limit of 60%MVC. Thus at 50%MVC, for example, the number of recruited motor units can be found using the Equation (80), which is calculated as 411 or more than 95% of the total motor units. Figure 5.3 shows the distribution of the recruited motor units for various input force levels. Both unipolar and bipolar differential electrode has been simulated. The unipolar electrode is situated 10mm away from the center of neuromuscular endplate of the muscle in the z-direction on the surface whereas two electrodes 10mm and 20mm away from the endplate were simulated for differential setting. EMG signal will be simulated and analyzed for the case when there are no subcutaneous tissues in the model (mimicking needle electrode EMG) and also when fat and skin layer lies above the muscle tissue (surface EMG).

EMG signals are random in nature. A raw EMG burst cannot be reproduced a second time by its precise shape. Four parameters of the EMG signal and its spectrum are usually used to describe the content of EMG signals. These are root mean square value (*RMS*) and average rectified value (*ARV*) for the time varying signal and mean and median frequency for the power spectrum of the EMG signal. The mean value of the rectified EMG over a time interval *T* is defined as average rectified value (ARV) and is computed as the integral of the rectified EMG over the time interval *T* divided by *T*. ARV relates to information about the area under the selected signal epoch. RMS reflects the mean power of the signal. The equations used for the calculation of *RMS* and *ARV* are described below:

$$RMS = \sqrt{\frac{1}{T}\int_0^T x^2(t)dt} \tag{93}$$

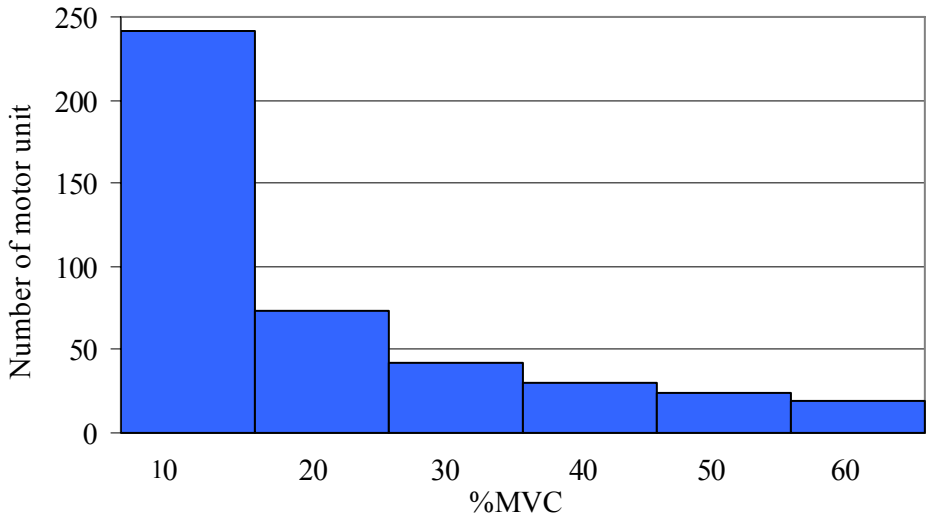

Figure 5.3: Distribution of the recruited motor units for various input force levels

$$ARV = \frac{1}{T}\int_0^T |x(t)|.dt \tag{94}$$

where *x(t)* is the time varying EMG signal for a time *T*. The mean frequency estimates the mean of frequencies in the frequency spectrum of the EMG signal. Median frequency is defined as the frequency that divides the power spectrum in two regions having the same amount of power or area under the power spectrum. Following are the equations used to calculate the mean and median frequency:

$$f_{mean} = \frac{\int_0^\infty P(f).f.df}{\int_0^\infty P(f).df} \tag{95}$$

$$\text{Median frequency, } f_{med} \text{ when } \int_0^{f_{med}} P(f)df = \int_{f_{med}}^\infty P(f)df \tag{96}$$

where *P(f)* is the spectral density function which is the Fast Fourier Transform (*FFT*) of a epoch of the EMG signal *x*:

$$P(f) = [FFT(x)]^2 \tag{97}$$

In this study, EMG signals are generated and analyzed for the muscle model considering 1) muscle in the absence of fat and skin layer and 2) muscle with subcutaneous fat and skin layer.

5.3 Results and Discussion

EMG signal is the result of many physiological, anatomical and technical factors. To use the signal effectively, it is first necessary to understand as much as possible the sources

of, and the influences on, the signal, which have somewhat been discussed in part in the previous chapters. Figure 5.4 and Figure 5.5 show respectively the EMG signal for 2 seconds recorded in the monopolar electrode at 20 %MVC when there are no external fat or skin tissues and when the subcutaneous fat and skin layer exists on the top of the muscle. These figures show the initial build up of the EMG amplitude as the force in ramp builds up in one second. Figure 5.6 and Figure 5.7 show the frequency spectrum of the EMG signal at 20% MVC for the above two cases.

5.3.1 EMG Force Relationship

Figure 5.8 illustrates the behavior of the RMS values of the EMG signal generated for various levels of voluntary contraction. In both cases of the model, the relationship is curvilinear although until 60% of MVC, EMG RMS magnitude increases linearly with the increase in input contraction with a slope higher than the slope by which the RMS amplitude increase from 60% to 100% of MVC. Behavior of average rectified value (ARV) with force is also similar to that of the RMS of the EMG, which is shown in Figure 5.9. For first linear increment (0-60%MVC) of the EMG force curve, the explanation could be as follows: When a motor unit is recruited, it contributes quanta of force to the muscle contraction. However, the contribution to the EMG signal amplitude is dependent on the proximity of the detection surfaces of the electrode to the nearest fibers of the recruited motor unit - the nearer the fibers, the greater the contribution [85]. Thus, the vector representing the incremental increase may increase or decrease the instantaneous slope of the force-EMG signal relationship**.** For the second part of the linearity (60-100%MVC), the EMG amplitude is increased slightly as at 60% MVC all

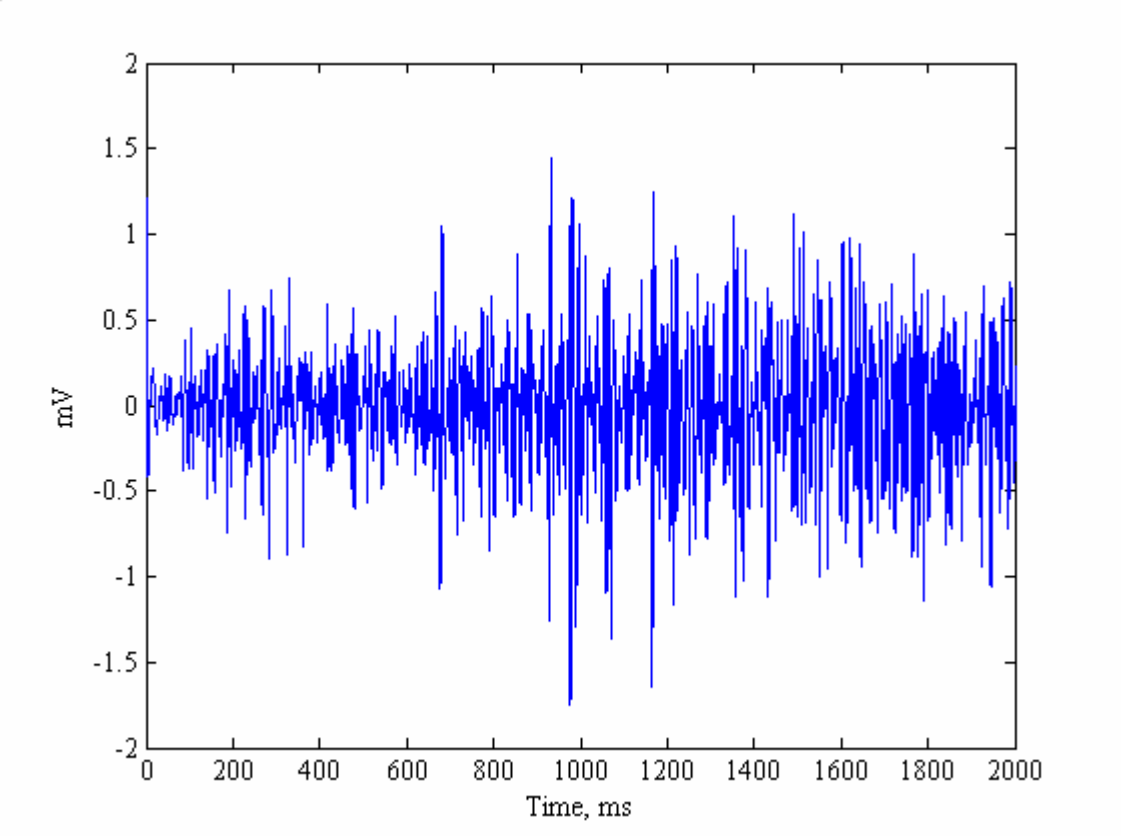

Figure 5.4: EMG signal for 2 seconds recorded in the monopolar electrode at 20 %MVC when there are no external fat or skin tissues

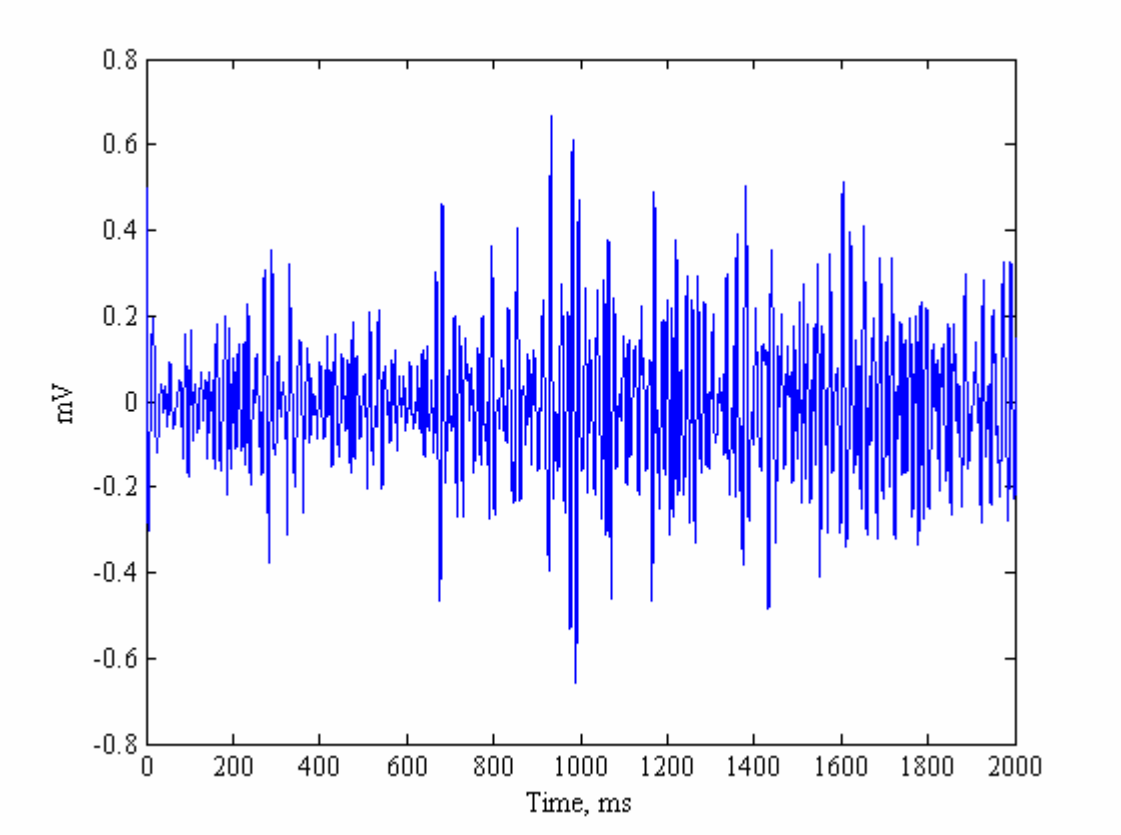

Figure 5.5: EMG signal for 2 seconds recorded in the monopolar electrode at 20 %MVC when there are external fat or skin tissues

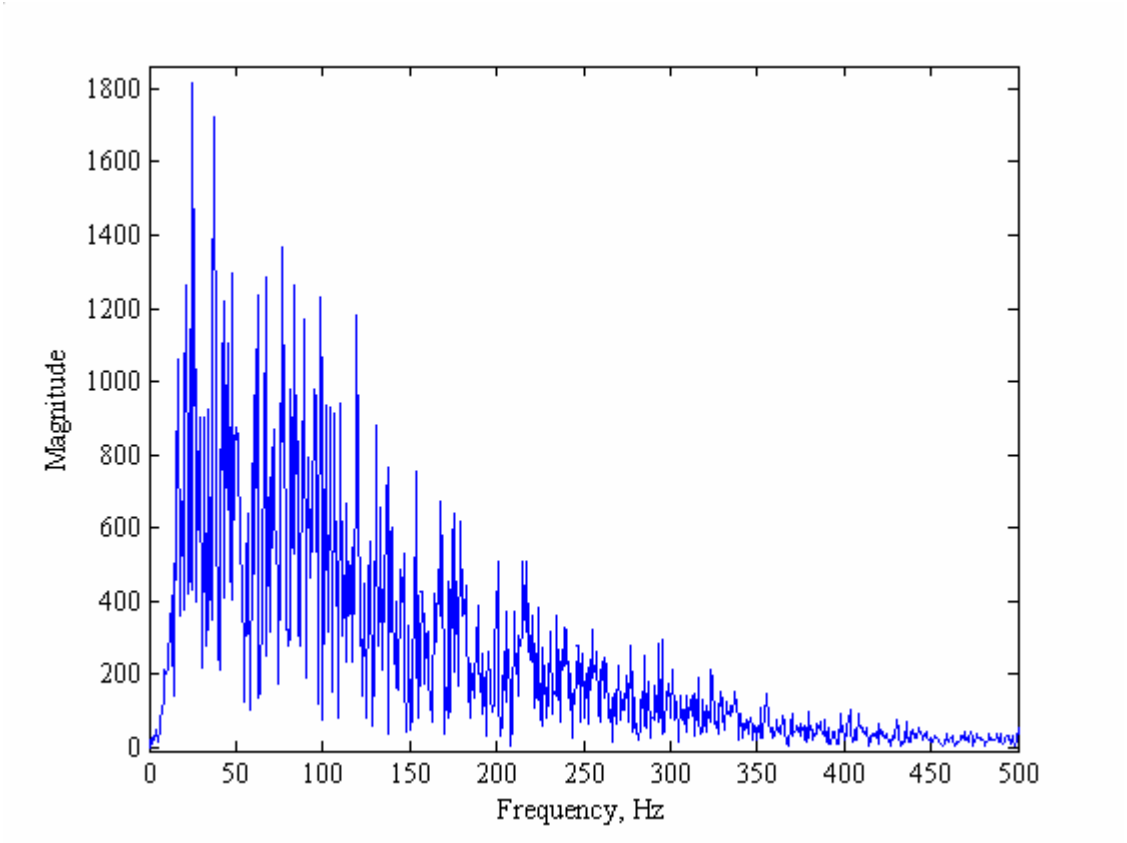

Figure 5.6: EMG signal spectrum recorded in the monopolar electrode at 20 %MVC when there are no external fat or skin tissues

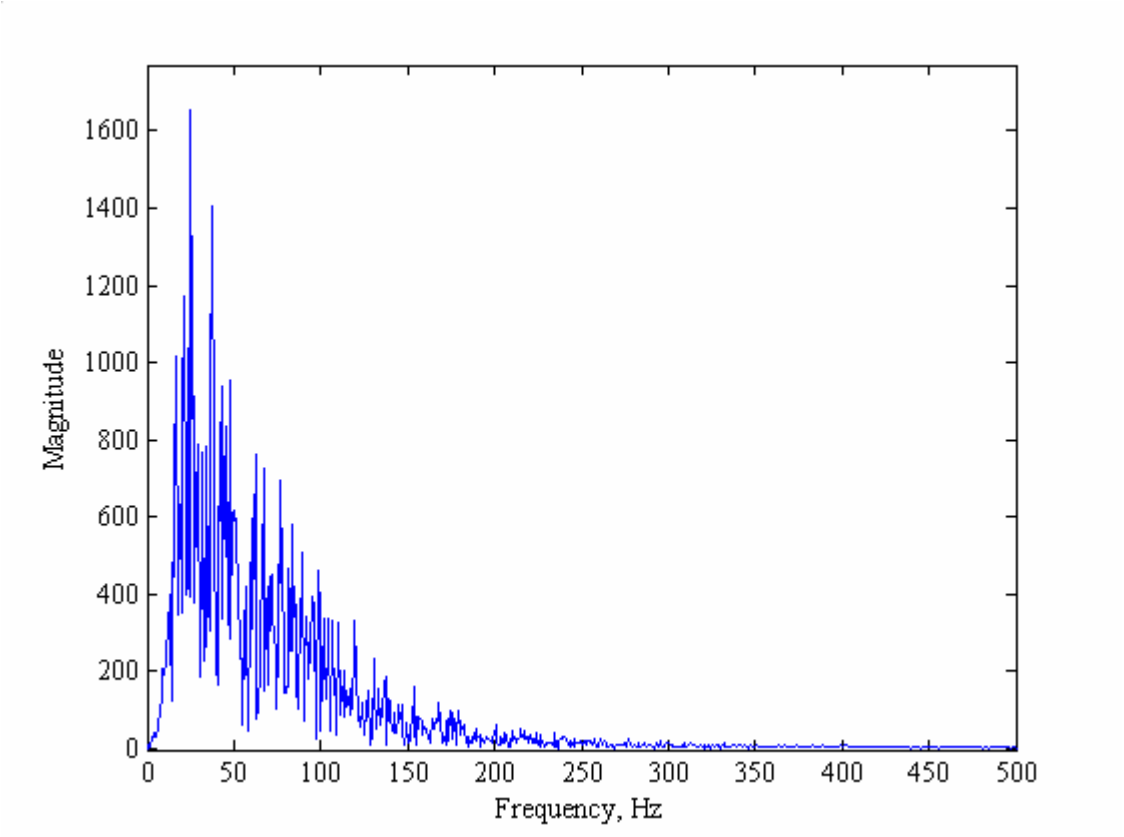

Figure 5.7: EMG signal spectrum recorded in the monopolar electrode at 20 %MVC when there are external fat or skin tissues

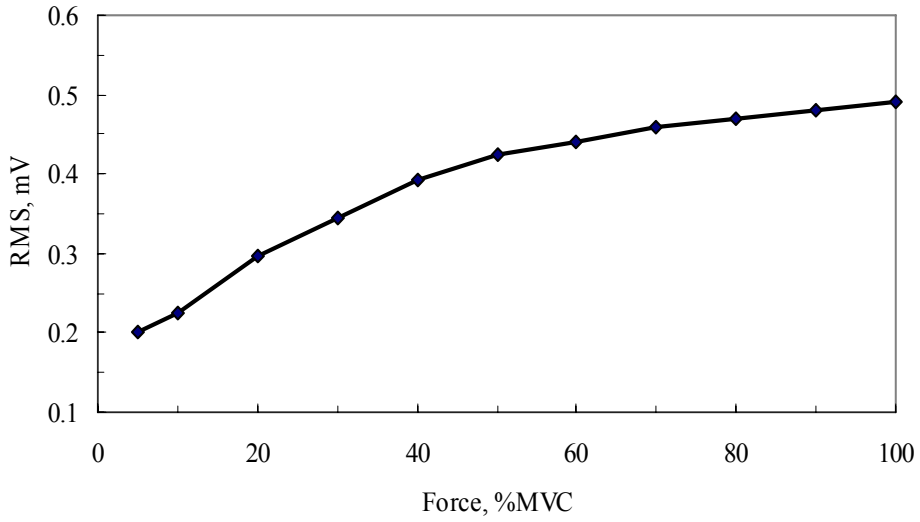

(a)

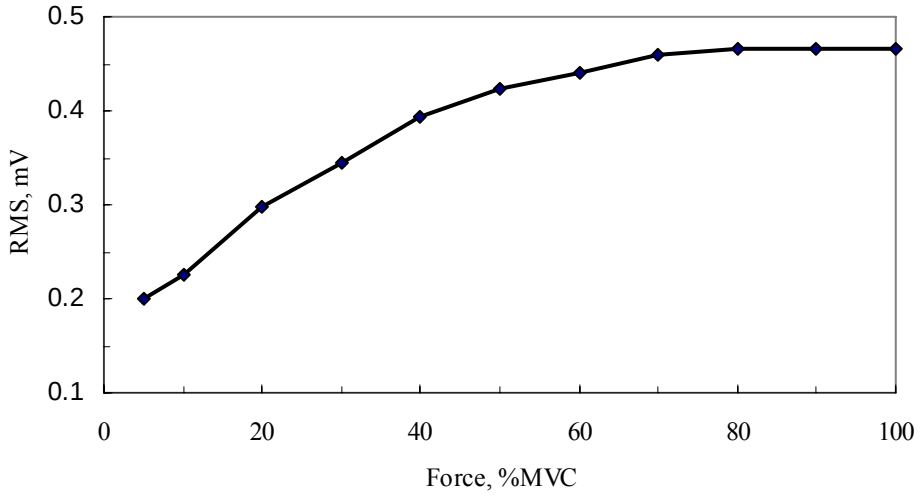

(b)

Figure 5.8: Relationship between EMG RMS value with the level of force generated. a) in muscle b) on skin

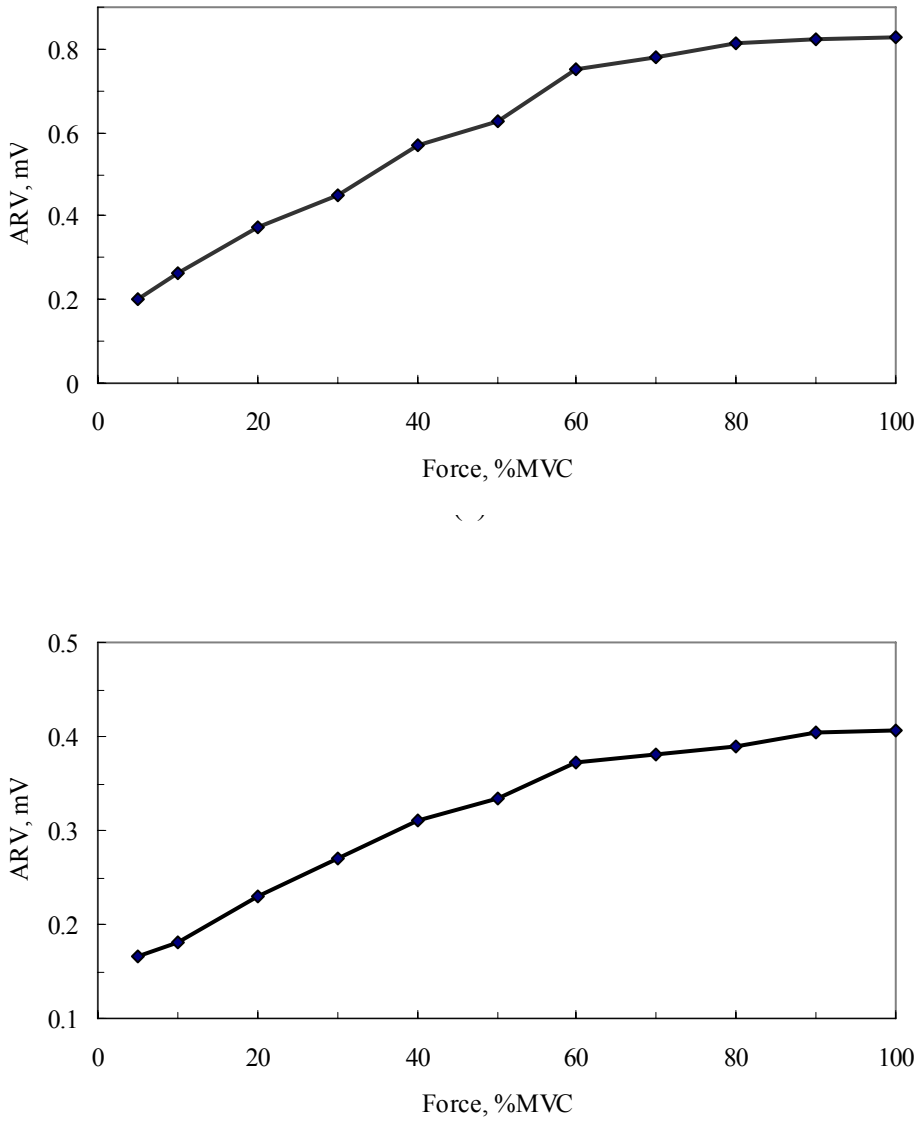

(b)

Figure 5.9: Relationship between EMG ARV with the level of force generated. a) in muscle b) on skin

of the motor unit in the muscle were recruited and no other motor units are recruited after that. Thus the muscle maintains that EMG amplitude and increases by the increased firing frequency of the recruited motor units due to the increased level of contraction (motor unit firing frequency increases linearly with the applied force).

Most of the practical observation is that the amplitude of the EMG signal generally increases as the force and/or contraction velocity of the muscle increases [85]. Figure 5.10 illustrates the experimental result of the RMS-force relationship of first dorsal interosseous muscle. In fact this relationship is not rigid for all muscles and there are many factors that cause the relationship to be nonrigid. As the amplitude of the surface EMG signal is a random variable, the instantaneous value of the amplitude is not monotonic with respect to the force value. Furthermore, the estimate of the signal amplitude will vary as a function of force due to intrinsic anatomical and physiological factors. The detection electrode size and placement plays an important role on the amplitude of the EMG signal. If the newly recruited motor unit is located close to the electrode, then the relative increase of the EMG signal will be greater than the corresponding increase of the force because the new MUAP will contribute more than an average unit of energy to the EMG signal. However that is not the case when newly recruited motor unit is located far away from the electrode. The control strategy, described in terms of firing rate dynamics and recruitment range used by the central nervous system (CNS) to control different muscles can also affect the EMG-force relationship. In the case of surface electromyography, cross talk, which is unwanted signal from the neighboring muscles can contaminate the recorded signal for a specific muscle and thus affect the force EMG amplitude relationship.

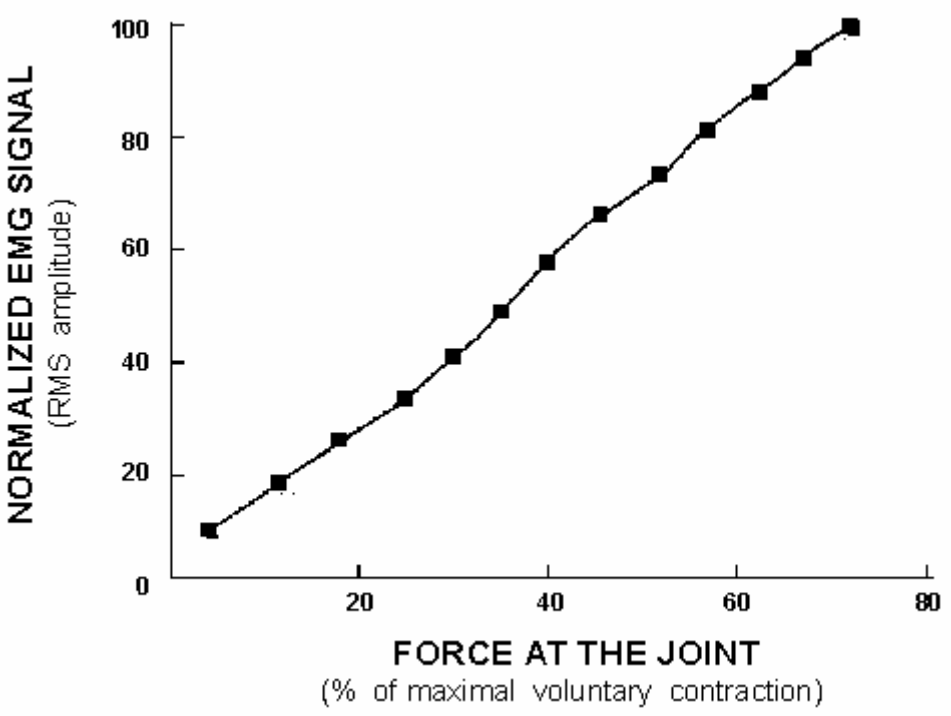

Figure 5.10: Experimental result of the RMS-force relationship of first dorsal interosseous muscle [85]

4.3.2 Force EMG-Spectral Relationship

Figure 5.11 and Figure 5.12 depict the relationship between the contraction force and mean and median frequency respectively for muscle in the absence of fat and skin. Figure 5.13 and Figure 5.14 show the relationship between the force and mean and median frequency respectively when a subcutaneous layer of fat and skin exists. Mean and median frequency increase linearly until 60%MVC of voluntary contraction. After that level both mean and median frequency of the simulated EMG fluctuates from the value at 60%MVC. In practical situations, it is also found that, mean and median frequency increase with the increase of force.

There are two main properties of the EMG signal that can affect the frequency spectrum: 1) the firing behavior of the motor units, and 2) the shape of the motor unit action potential (MUAP). The dominant effect of the firing rate of the motor unit is limited to the frequency neighborhood of the value of the average firing rate (15 to 25 Hz). The second harmonics of the firing rates are considerably smaller than the first harmonics and they occur at double the frequency of the first harmonics, where they are overwhelmed by the energy of the MUAP shapes [85]. The variance of the firing rates will determine the broadness of the frequency peak representing the firing rate, therefore, any influence will be limited to the same region. However, the shape of the MUAP is the determining factor of any change in frequency spectrum of the EMG signal. In chapter three, different parameters involving the change in MUAP are described. If the isometric contraction is maintained at constant force, recruitment of the motor units is unlikely to occur and the average size of the active muscle fibers remains constant. Thus, for a

constant-force isometric contraction, the only factors that affect the MUAP are the conduction velocity and the depolarization zone of the muscle fibers. The conduction velocity of the muscle fiber is proportional to its diameter. Therefore, muscles with larger diameter fibers, such as those generally belonging to higher threshold motor units, will have greater average conduction velocities which, in turn, will shift the frequency spectrum towards the high frequency range and consequently increase the value of the median frequency. Both mean and median frequency increases linearly until 60% of MVC due to the increase in higher threshold motor units and consequently Type-II motor units recruitment.

The amount of subcutaneous (fatty) tissue between the electrode and the active fibers determines the amount of spatial filtering to which the signal is subjected. The greater the thickness of the tissue, the greater is the low-pass filtering. Thus, additional subcutaneous tissue reduces the value of the median frequency. Simulated results justify this statement, as the subcutaneous layer reduces the mean and median frequency (some %) from that of the muscle without fat and skin.

Moreover it is important to note that, electrode location and orientation, electrode configuration are also important factors influencing the EMG spectrum. The distance between the electrodes determines the bandwidth of the filtering characteristics of the differential electrode configuration. Therefore, when the frequency spectrum parameters are compared among contractions, the same electrode configuration and dimensions must be used.

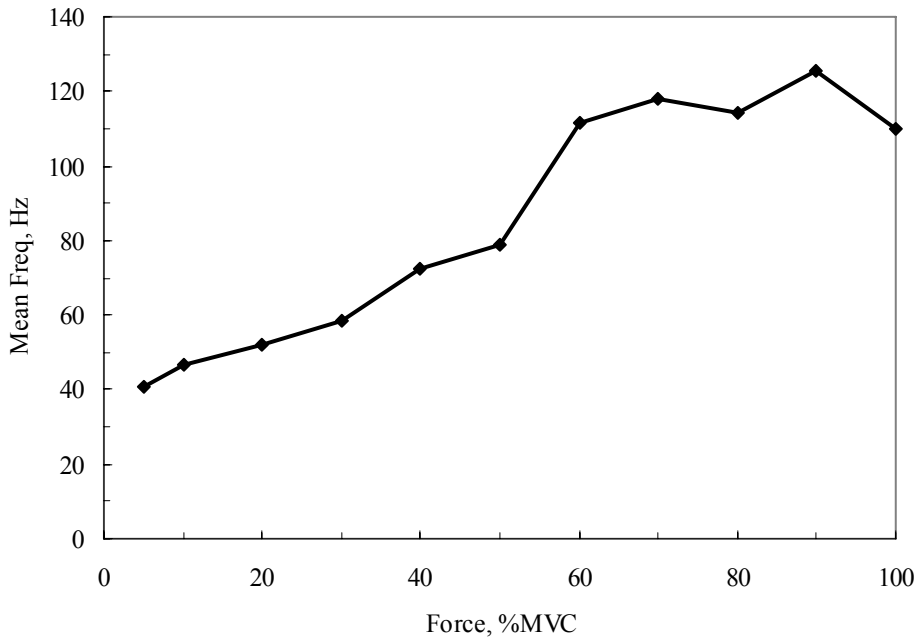

Figure 5.11: Relationship between the contraction force and mean and frequency when no fat and skin lies above the muscle

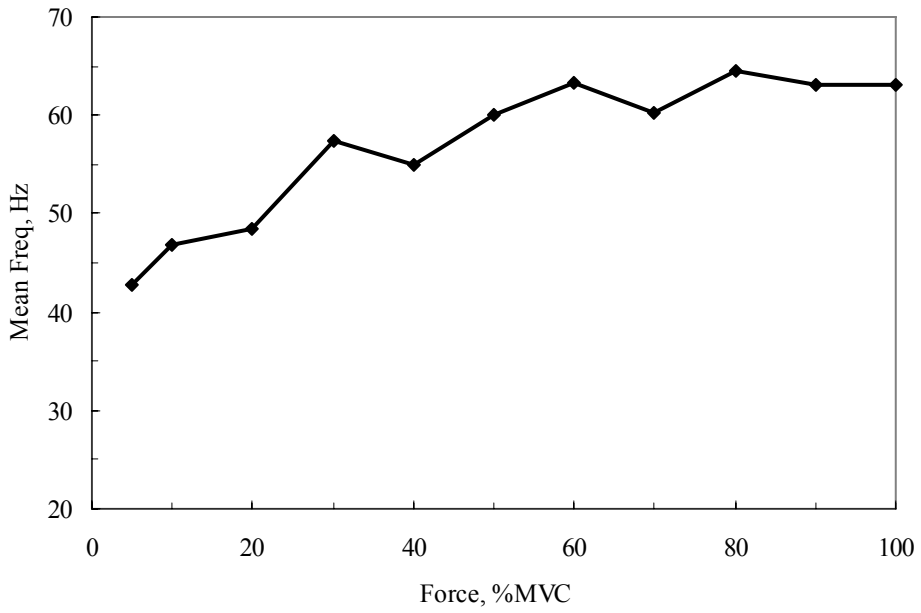

Figure 5.12: Relationship between the contraction force and median frequency when no fat and skin lies above the muscle

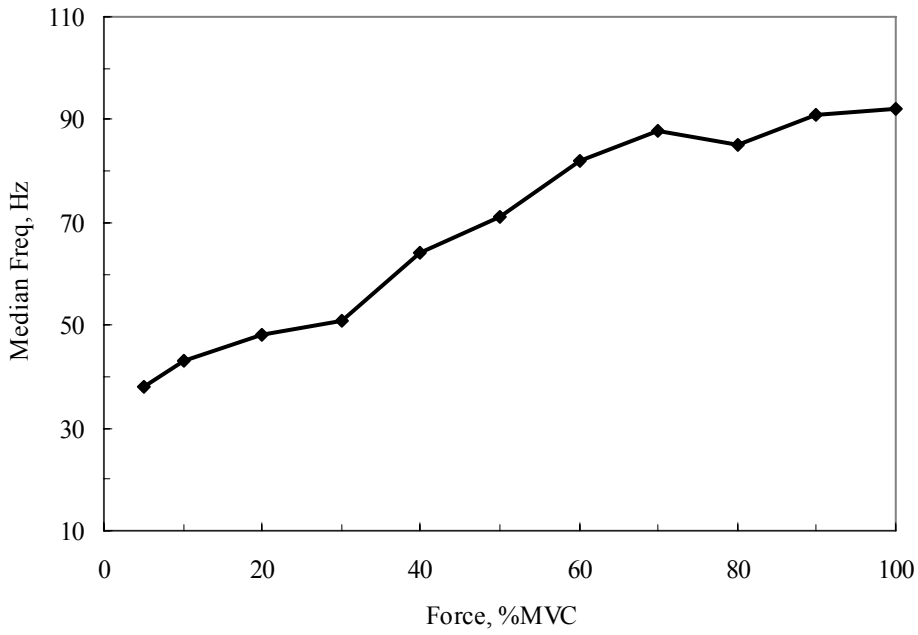

Figure 5.13: : Relationship between the contraction force and mean frequency when fat and skin lies above the muscle

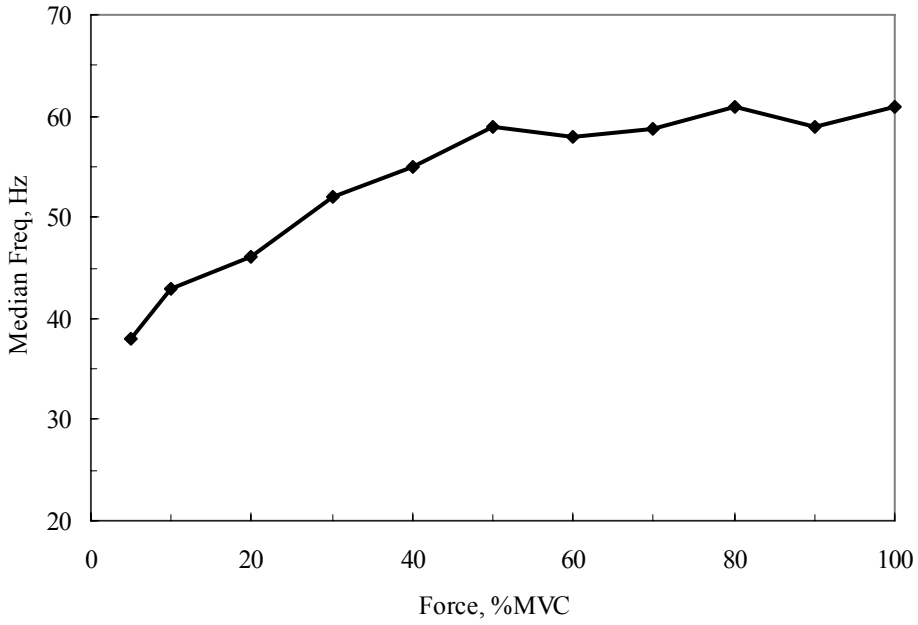

Figure 5.14: Relationship between the contraction force and median frequency when fat and skin lies above the muscle

CHAPTER 6

6. Age Related Muscle Remodeling

6.1 Introduction

Since impairment of skeletal muscle function leads to disability and loss of independence, it is important to understand the basic cellular mechanism underlying muscle dysfunction in the elderly. This knowledge is essential to optimize rehabilitation and preventive strategies for this population, which by the year of 2030 will increase by 107% for the age group of 65 years and 133% for the age group of 85 years as predicted by the US Census Bureau [86]. In addition, the percentages of older people with disabilities in activities of daily living and of older people requiring institutionalization for disabilities are expected to remain similar to current levels over the next 30 years, although these statistics vary by ethnicity. This means that the number of people requiring institutionalization for disabilities will increase substantially. As humans grow older, their skeletal muscles loose the strength and the capacity to generate force due to skeletal muscle mass reductions. This is known as sarcopenia [87, 88]. Some investigators have suggested that the loss of muscle mass is primarily due to the loss in the number of muscle fibers and to a lesser extent, a reduction in muscle fiber size [89, 90]. Most researchers, however, reported that age related muscle atrophy results from fiber atrophy rather than a loss of muscle fibers [91,92,93,94,95]. In addition to the decrease in skeletal muscle mass due to the atrophy of the muscle fibers, the muscles of

elderly subjects (65-83 years of age) contain less contractile tissues (Type-II) and more noncontractile tissues (Type-I) when compared with the skeletal muscle of younger subjects (26-44 years of age). Consequently, elderly people may lack strength and force production. In recent reviews, it is also found that the size of Type-I fibers does not change substantially with age, but Type-II fibers undergo selective atrophy [86,87,96].

In attempt to understand the aging skeletal muscle, this section investigates the effects of the physiologic changes that occur during aging on computer generated compound muscle action potentials (CMAPs) of Bicep Brachii muscle group. CMAP are used in the motor conduction studies. Figure 6.1 shows different parameters of the CMAP wave shape. These parameters are:

(a) Latency: Latency is the time delay for the CMAP to rise to its peak. Latency can also be expressed as rise time, which indicates the rise of the CMAP from 5% to 95% of its peak amplitude.

(b) Amplitude: The amplitude of the evoked motor response carries important information. Amplitude is dependent on the number of axons that conduct impulses from the stimulus point to the muscle, the number of functioning motor endplates and muscle volume. Peak to peak amplitude is often calculated which is the summation of the positive and negative peaks.

(c) Area under the curve: Area represents a combination of amplitude and duration. It reflects the number and synchrony of the muscle fibers activated. A prolongation of the duration can cause a decrease in the amplitude and may be misinterpreted as a conduction block. Area under the curve is calculated as total area of the CMAP on the time scale.

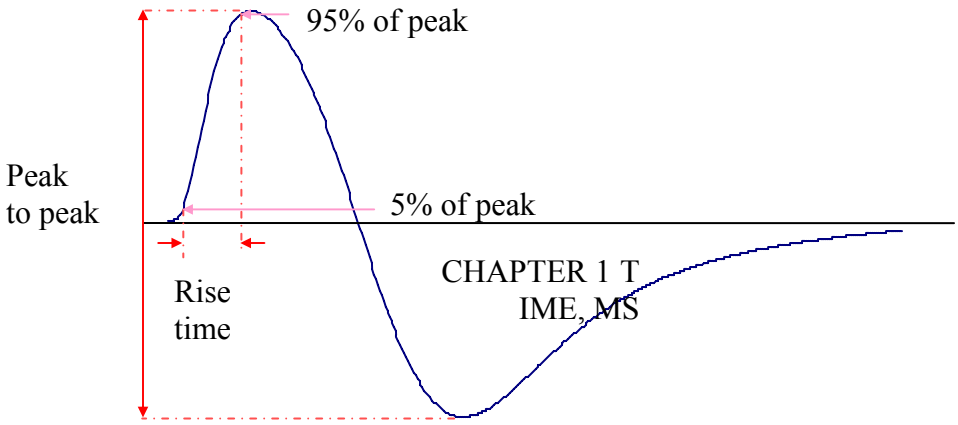

Figure 6.1: Different parameters of the CMAP wave shape

(d) Duration: The duration reflects the synchrony of individual muscle fiber discharges. If there is a significant difference in the conduction velocity among nerve fibers, the duration will be prolonged. Mean frequency is also used as a CMAP parameter instead of duration, which describes the mean of the frequency content in the CMAP spectrum.

6.1.1 Clinical Importance of CMAP Parameters

Amplitude: Some neuromuscular disease such as axonal neuropathies, which affect repiratory function may cause a reduction in the amplitude of the CMAP. Therefore quantification of amplitude of the CMAP is sometimes more relevant than measuring the phrenic nerve conduction. Area under the action potential will also be used instead of amplitude only.

Duration and latency: Duration in the measured CMAP can indicate the muscle slowing or nerve conduction block. In the nerve conduction of thener muscle, it is found that thener muscle with degenerative joint disease (DJD) in the hand of elderly people shows larger duration in the CMAP than those of healthy hand of the elderly.

The nonlinear behavior of the physiologic changes during aging is adapted from the work of Robert Schwartz on Sarcopenia and physical performance in old age [97] which is shown if Figure 6.2. Behavior of CMAPs and its metrics such as peak to peak amplitude, area under the curve, rise time and mean frequency during aging have been computed and analyzed. The physiologic data such as the number of motor units in a muscle group,

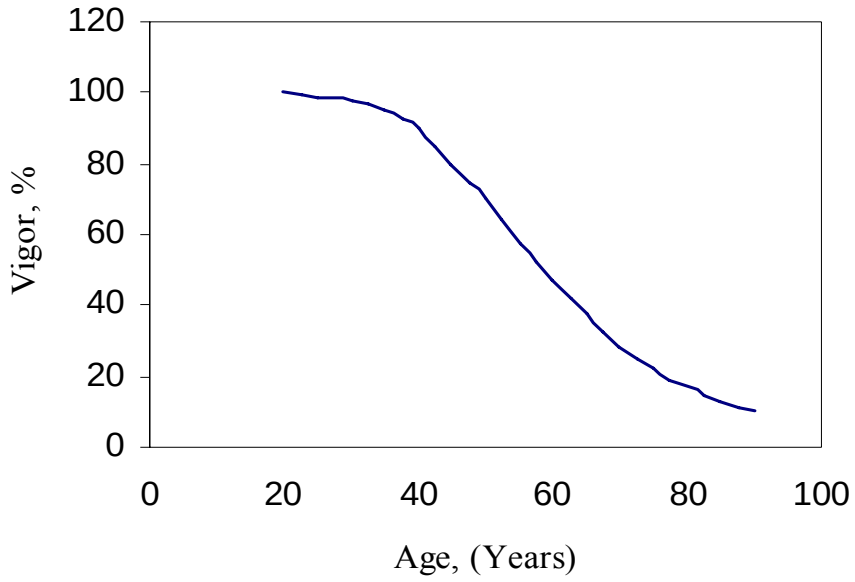

Figure 6.2: Behavior of change in strength during aging process

number of fibers per motor unit, diameter, length and percentile concentration of different types of fiber in a motor unit were adapted from the published clinical data [98, 99].

Hypothesis:

1. Most of the researchers said that type-I fiber diameter does not change substantially.
2. Almost every researcher agreed that type-II fiber diameter decreases substantially during aging.
3. Almost every researcher agreed that type-II fiber concentration decreases in old people.
4. Some researchers said type-I concentration remains same whereas some said it increases during aging.
5. Some researchers said number of fibers does not change substantially during aging whereas some said it decreases during aging

6.2 Muscle Simulation and Data Analysis

Muscle fiber action potentials and surface electrodes were simulated to describe the physiological changes that occur during aging. The characteristics of simulated composite action potentials (CMAPs) metrics for Bicep Brachii muscle group were investigated. Table 6.1 shows the documented percentile concentration of Type-I and Type-II fibers and their corresponding diameters for this muscle group for both young (age 22-44) and old (age 65-83) population for bicep brachii and also for tibialis anterior.

Table 6-1: Diameter and fiber type concentration for Bicep Brachii for both young and old

Young subjects				Old subjects			
Type-I		**Type-IIA**		**Type-I**		**Type-IIA**	
%	*d* μm	*%*	*d* μm	*%*	*d* μm	*%*	*d* μm
45.0±3	65.4±7	31.0±3.4	71.5±7	48.0±5	58.4±5	29.0±7	60.9±5

The muscle model consisted of Type-I, Type-IIA and Type-IIB fibers, which were distributed randomly inside the muscle model. We assumed that Type-IIA and Type-IIB had same percentile concentration. Fiber diameters were generated randomly using their corresponding mean and standard deviation values. A linear relationship described in Equation (57) was used to calculate the conduction velocity for each fiber. Two surface electrodes, 10 and 20 mm away from the muscle motor point, were simulated to record the monopolar as well as differential CMAPs at a sampling frequency of 25 KHz. Simulations for bicep brachii muscle group in young subjects were performed in 50 trials to investigate the effects of uniform random distribution of the fibers within the cross section of the muscle model. To observe the effects of physiological changes on the CMAPs during aging, simulations were also performed when fiber diameter, Type-I and Type-II fiber concentration and total number of fibers in bicep brachii muscle changed from the values of young subjects (20 years) to that of elderly subjects (80 years) using the nonlinear curve of physiological changes described in [97]. In attempt to simulate this aging behavior, it is required that the aging curve is described by an empirical equation. For this, the aging curve is fitted using MATLAB (Figure 6.3). First of all, the aging curve behaves as a sigmoid function as follows:

$$y = \frac{1}{1 + e^{-x}} \tag{98}$$

The shape of the sigmoid function is shown in Figure 6.3. The coefficients of this sigmoid function are derived while fitting the curve exactly. The equation that describes the aging curve is as follows:

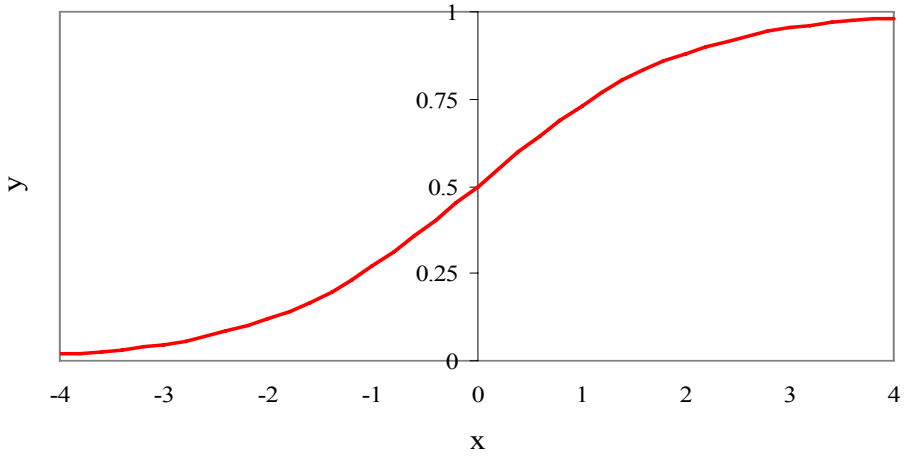

(a)

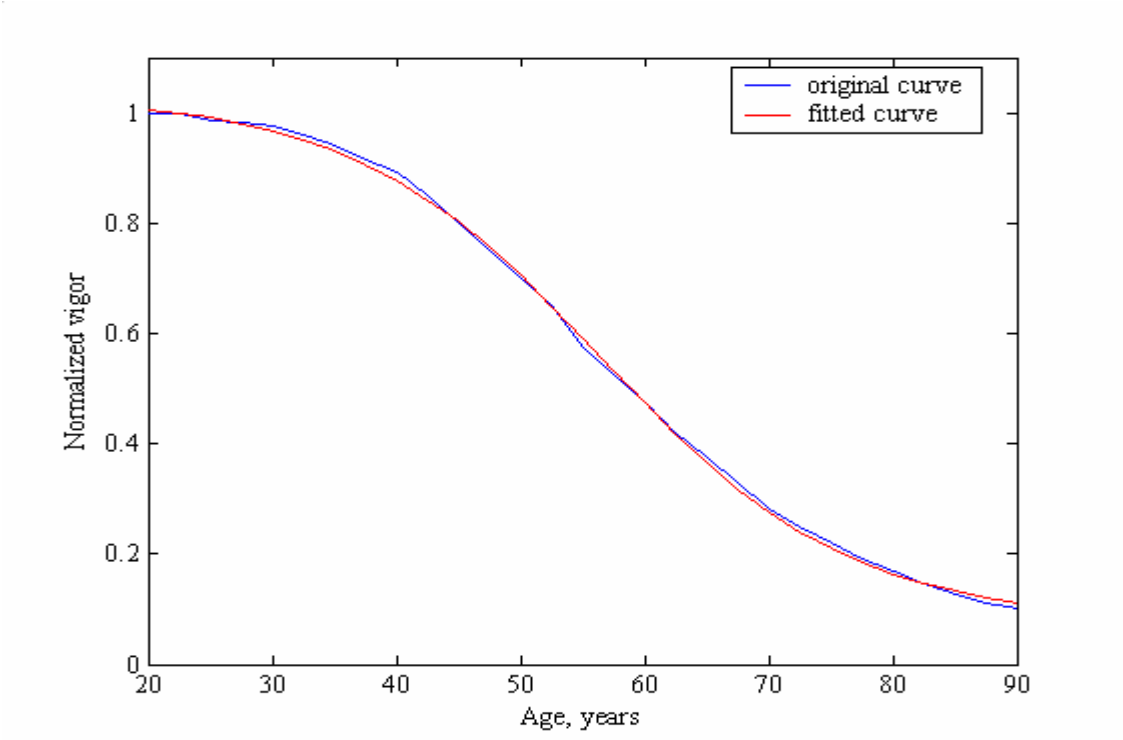

(b)

Figure 6.3: a) A sigmoid function, b) Curve fitting of the aging process

$$y = k\frac{1+ae^{-bx+c}}{1+de^{-bx+c}} \tag{99}$$

where, the coefficients are:

$a = 27.4$
$b = 10.33$
$c = 5.18$
$d = 2.0$
$k = 0.075$

6.3 Results

CMAPs were simulated for both young and elderly subjects using physiologic data for Bicep Brachii muscle group. Peak to peak amplitude, area under the curve, rise time, and mean frequency of these CMAPs have been calculated. Table 6.1 shows the mean and standard deviation values of these CMAP metrics, which were calculated from 100 trials for the three different muscles of young subjects for single electrode position.

Figure 6.4 shows the CMAP plots of bicep muscle during aging. The CMAP wave shapes for young and elderly subjects are shown in this figure for visual comparison. Figure 6.5 illustrates the changes in the CMAP peak to peak amplitude during simulated aging. Peak to peak amplitude of the CMAP decreased in the same fashion as the nonlinear aging curve. Figure 6.6 and figure 6.7 shows the area under the curve and mean frequency of the CMAP of bicep, which also decreased in the same fashion. Rise time was calculated as the time for CMAP to increase from 5% to 95% of its positive

Table 6-2: CMAP metrics simulated for 50 trials for three different muscles

CGAP Metrics	Bicep Brachii	Vastus Leteralis	Tibialis Anterior
Peak to Peak Amp (mV)	23.85±0.21	31±0.41	18±0.16
Area under the Curve (mVms)	2.12±0.04	3.24±0.02	1.68±0.02
Rise Time (ms)	1.1±0.01	1.03±0.01	0.93±0.01
Mean Frequency (Hz)	91.80±0.08	84.88±0.07	59.36±0.04

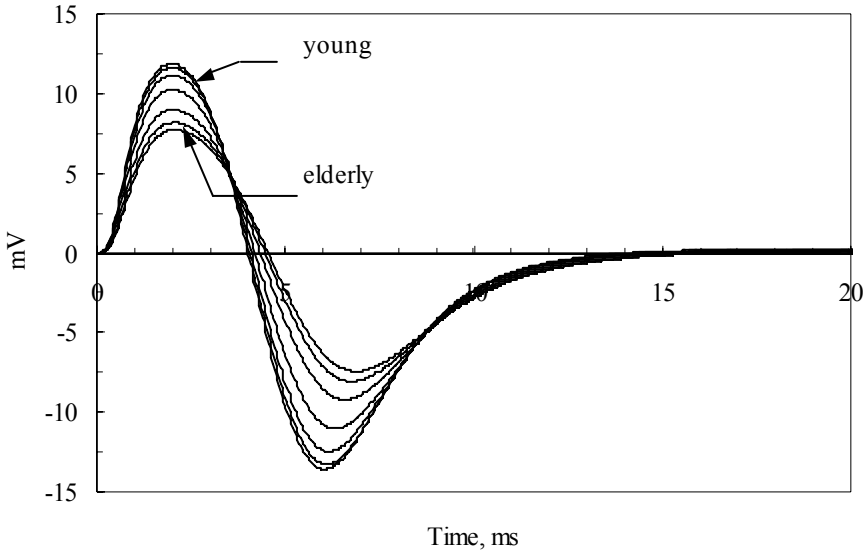

Figure 6.4: CMAP wave shapes during aging

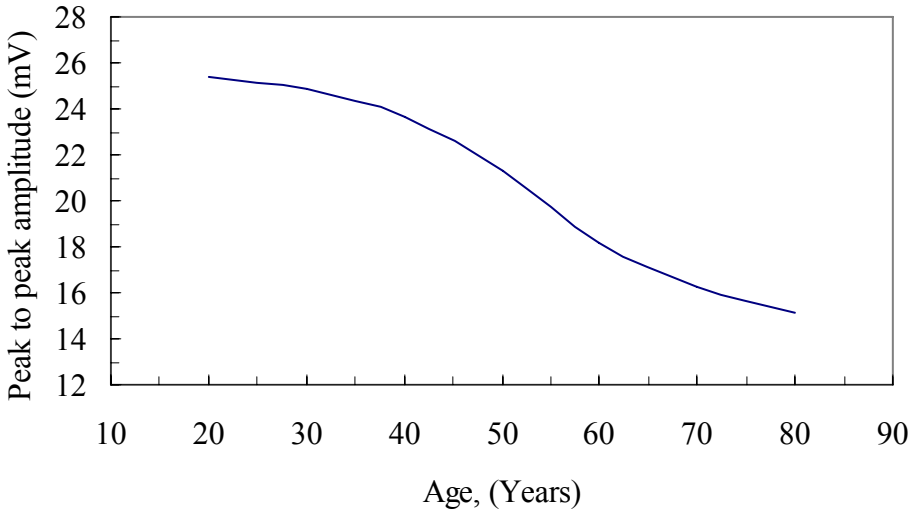

Figure 6.5: CMAP peak to peak amplitude during aging

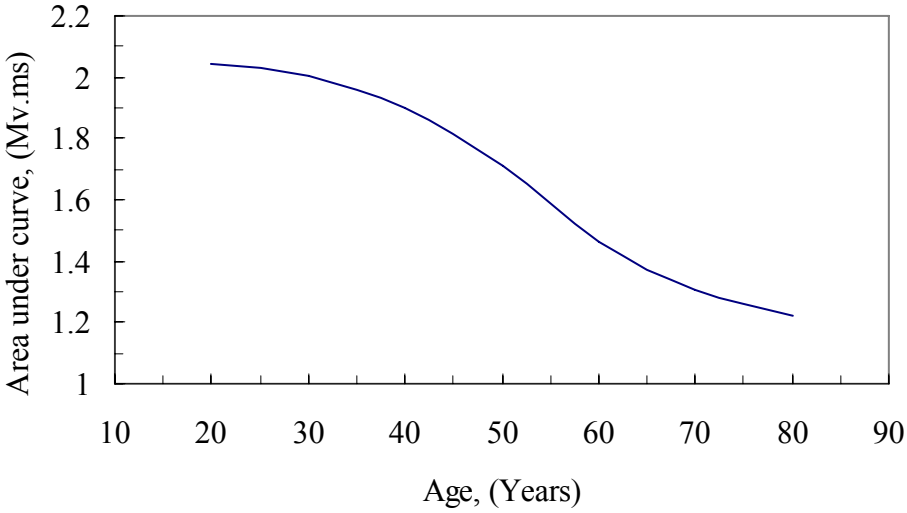

Figure 6.6: CMAP area under curve during aging

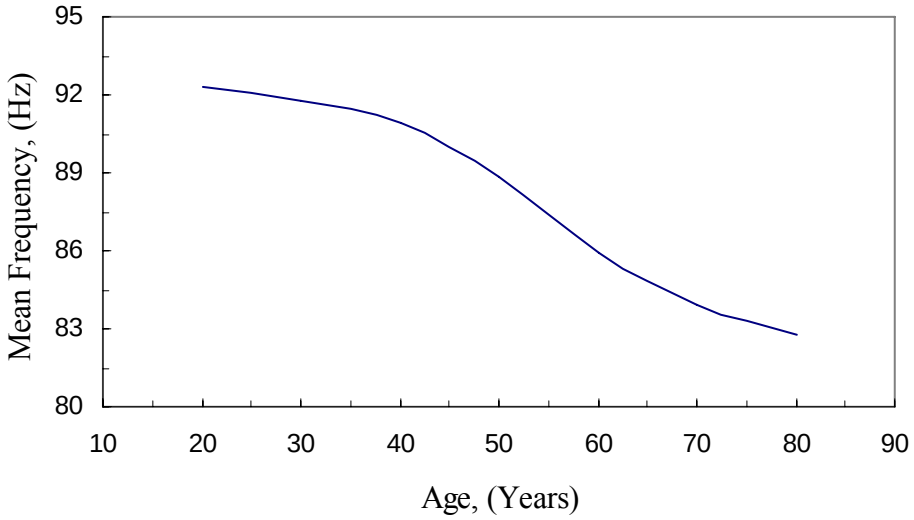

Figure 6.7: CMAP mean frequency during aging

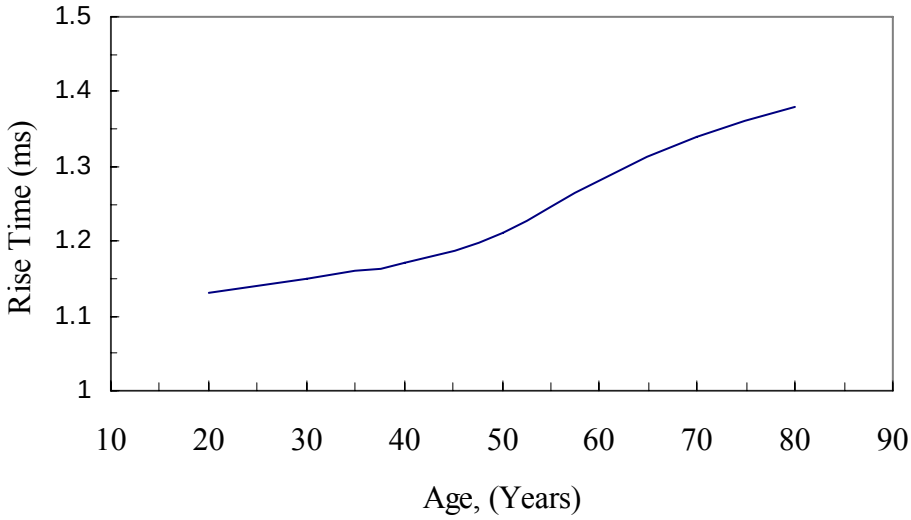

Figure 6.8: CMAP rise time during aging

peak amplitude. Figure 6.9 shows the rise time of CMAP, which increases, in the opposite pattern of the nonlinear aging curve during aging.

In the elderly subjects, the simulated CMAPs had reduced amplitude, area under curve and mean frequency as compared to that of young subjects, whereas rise time, of the compound action potential were higher in elderly than those of the young population. These CMAP metrics were investigated when the number of Type-I muscle fiber increased from the corresponding values of young subjects to those in elderly subjects.

It was found that, peak to peak amplitude decreased with aging. This was expected as amplitude of CMAP depends on the fiber diameter. With age both Type-I and Type-II fiber suffer atrophy, which lead to reduction in diameter and size of the fibers. As we assumed linear conversion of Type-II fiber to Type-I during the aging process, amplitude decline of CMAP followed the same pattern of the nonlinear aging curve. Area under the curve is the area under the CMAP plot and therefore it also decreased in the same fashion.

For the investigated muscle group, rise time increased with age. This result is consistent with the pathological changes that occur during aging as Type-II fiber, known as fast twitch fiber, concentration decreases during aging. Mean frequency varies linearly with the conduction velocity. During aging process, Type-II fiber, which has bigger diameter than that of Type-I fiber, decreased. As fiber diameter is proportional to conduction velocity, the mean frequency decreased during the aging process.

Figure 6.9: Tibialis Anterior muscle

6.3 Conclusion

The objectives of this study were to investigate the effects of physiological changes on the computer generated composite action potentials in the aging skeletal muscles. The aging process was simulated as the change of fiber diameter, total number of fibers and Type-I and Type-II fiber concentration changes from the values of young subjects to that of elderly subjects using the nonlinear physiological changes described by Robert Schwartz**.** The computer muscle model designed in this study allowed to simulate this aging process successfully. CGAPs of elderly subjects produced smaller peak to peak amplitude, area under the CGAP curve and mean frequency and substantially higher rise time of the CGAPs than those of young subjects. The results found in this study illustrate the implications of the physiological changes that occur in the aging skeletal muscles.

6.4 Effects of Aging on EMG Signal Generation

In the previous section, the pathological changes that occurred during aging of human muscles have been described. As CMAP is the summation of all the muscle fiber action potentials in a muscle group at one sudden instance of muscle excitation, the simulation for the aging process above did not consider the motor unit function such as recruitment and firing frequency during aging. However, in voluntary contraction, it is necessary to consider motor unit remodeling during aging process. The vast bulk of research in this area has been done on identifying the changes in the morphological [100], physiological [101], and histochemical [102] properties of the motor unit (MU) with age. Zeynep Erim

et al [103] described three novel observations regarding the firing behavior of aged motor units.

1) Among elderly subjects, there is a decrease in the common fluctuations of firing frequency i.e. IPI variation that are observed among the firing rates of motor units in the young.

2) The linear relationship observed between the firing rate and recruitment threshold of young subjects is also seen in the elderly. In young subjects, at any point in a given submaximal contraction, earlier recruited motor units have higher firing rates than later-recruited units. But in aged subjects this dependency of firing rate on recruitment rank is compromised.

3) The progressive decrease observed in the firing rates of concurrently active motor units in constant-force contractions in the young is not seen in the aged.

In addition to these findings, EMG of the muscle of elderly people has

- decreased average firing rates probably reflecting the slowing of the muscle,
- decreased number of motor units or α-motoneurons
- a shift in recruitment thresholds toward lower force levels in line with the shift toward type I fibers, and
- multiphasic action potential shapes which indicates the reinnervation process that takes place during aging.

Taken as a whole, these findings indicate significant age-related modifications in the control properties of human motor units. Although the number of α-motoneurons decrease and as a result number of motor units decrease, the muscle fibers belonging to the deceased motor unit are often reinnervated by one of the existing motor units [86,

104]. Therefore, although there is a reduction in the number of motor units, some motor units specially the low force type-I units become larger. This reorganization probably impairs the ability of elderly persons to perform finely controlled tasks, including maintaining steady submaximal forces [24, 105, 106]. The reinervation of denervated type-II muscle fibers by neighboring type-I motor units has also been implicated in the increase co-expression of type-I and type-II myosin heavy chain iso-forms observed in the skeletal muscle of older individuals [86]. In the light of the significant changes in the properties of the elements of a motor unit, it can be hypothesized that the control aspects of the motor unit would be modified as an adaptive or compensatory mechanism to preserve force production. EMG signals from young and elderly are expected to be significantly different due to pathological changes and changes in motor unit functioning strategy. In this section, EMG signals will be generated for both young and elderly using the model described in Chapter Four. The purposes of these simulations are to utilize the developed EMG model on describing aging effect on the EMG signals and verify the result with the published data on EMG for both young and old people.

6.5 Methods

Tibialis Anterior muscle group has been selected for the simulation of EMG generation for both the young and the elderly. Figure 6.9 shows the tibialis anterior muscle group located at the right below the knee and thus an important muscle group for posture and balance control. Aging people are vulnerable to falling due to the lack of balance control. Thus Tibialis Anterior muscle has always been an object of interest for the clinicians and

gerontologists. The physiological data, such as number of motor units, number of fibers per motor unit, percentage of fiber types and their diameter for both the young and the elderly are collected from the published data [47, 84, 107]. Motor unit firing and recruitment properties for young and old have been adopted from the work of Connelly D.M et al [108]. The average age group for the young is 20 years and for the elderly it is 80 years. It has been found that, even in aging muscle, recruitment order follows the size principle during voluntary contractions [47, 109, 110]. The force-firing rate curve is redrawn from [108] which is shown in Figure 6.10. Minimum firing rate in the elderly decreased from 8.14 Hz of young to 4.18 Hz. The slope of the linear curve for the young is 0.3 and for the elderly is 0.27. As stated earlier, variation in the inter pulse interval (IPI) of the firing frequencies is less in the old than in the young. The covariance of the IPI variation is estimated as 0.25 for young and 0.20 for elderly [108]. It is estimated in [111] that about 60% motor neuron die out at the age 80 years and older. Out of these neurons, type-II motor units are vastly affected. All these physiological changes are incorporated in the model developed in Chapter Four and applied in Chapter Five. In this section, simulation has been performed for both young and elderly for 5% to 100% of the maximum voluntary contraction. Only a monopolar electrode, which is situated 10mm away from the center of the endplate zone, has been simulated for EMG generation for both populations. Also in simulation, only muscle with fat and skin has been considered.

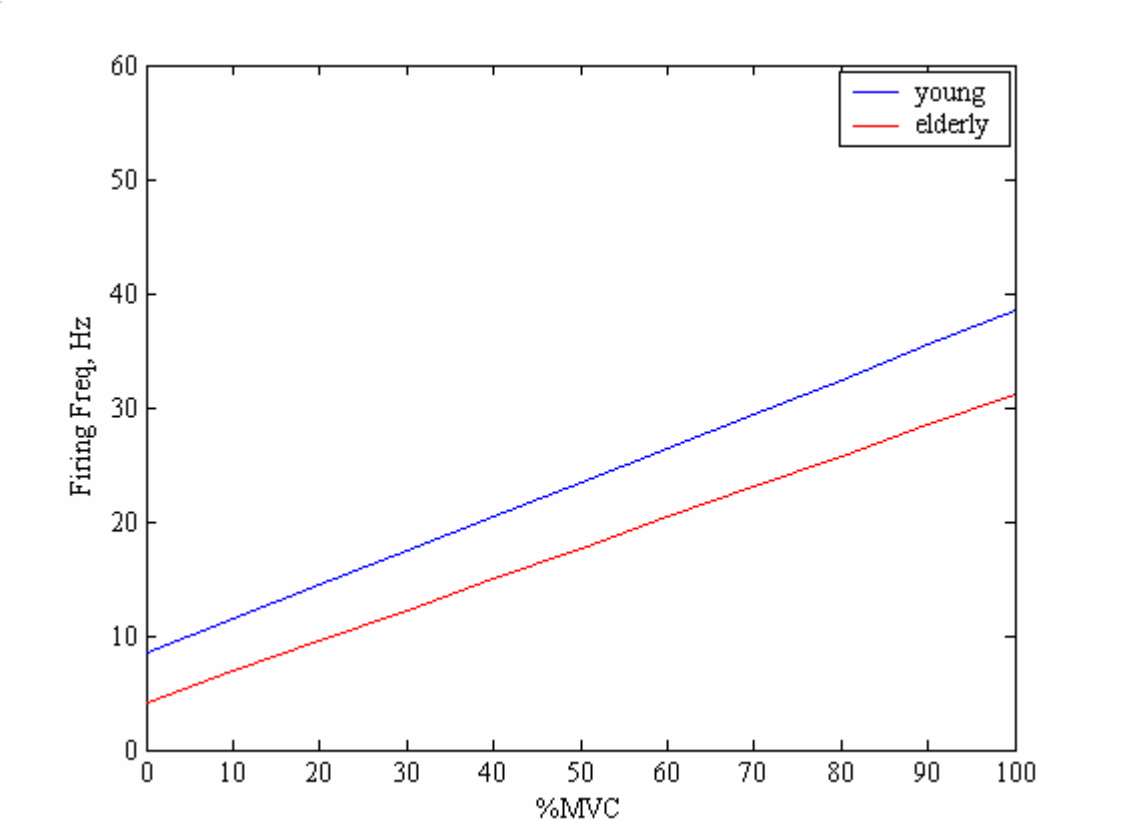

Figure 6.10: Force firing frequency relationship in both young and elderly, redrawn from [25]

6.6 Results and Discussion

The purpose of these simulations is to verify the proposed model with the published experimental data and also describe the effect of aging on the EMG signals. Because of the motor unit distribution effects described in Chapter Five, all simulations have been performed 10 times. Figure 6.11 shows the generated EMG signal for the elderly along with the signal for the young at 100% MVC. The frequency spectrum for both these signals are shown in Figure 6.12 for visual comparison. These figures show that, for elderly, the EMG signal has less high frequency contents than that of young, mainly because elderly has fewer fast type-II fibers, which has smaller duration of the action potential than the type-I. On the other hand, in the EMG of elderly, the magnitude of the lower frequency contents in the range of 30-40Hz is larger than that of the young. The muscles of elderly has more type-I motor units of bigger size due to the re-enervation of the muscle fibers, which fires more frequently than the type-II motor units that is seen in larger amount in the muscle of young. Thus the magnitude of the frequency content in the range of 30-40 Hz, which is the average peak firing frequency of type-I motor units, is higher in the tibialis anterior muscle of elderly.

Force-EMG relationship of the anterior tibialis muscle of elderly is also similar to that of young, although the slope of this linear force EMG behavior is bigger in the muscles of young than that of elderly. Figure 6.13 depicts this behavior. This behavior is expected as during aging, muscle fibers are lost mostly of type-II, which are bigger size than that of type-I and which produces larger force. Figure 6.14 shows the comparison of different

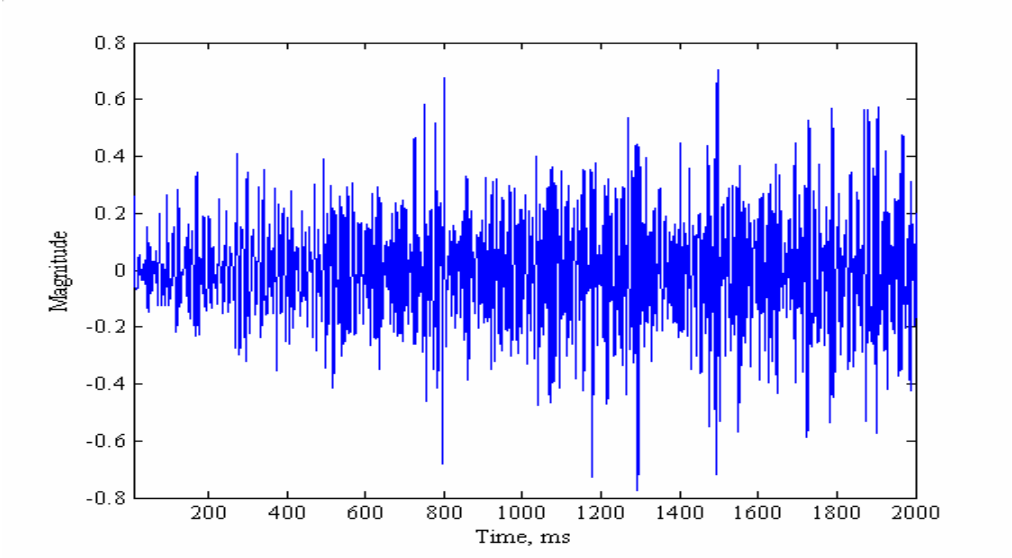

(a)

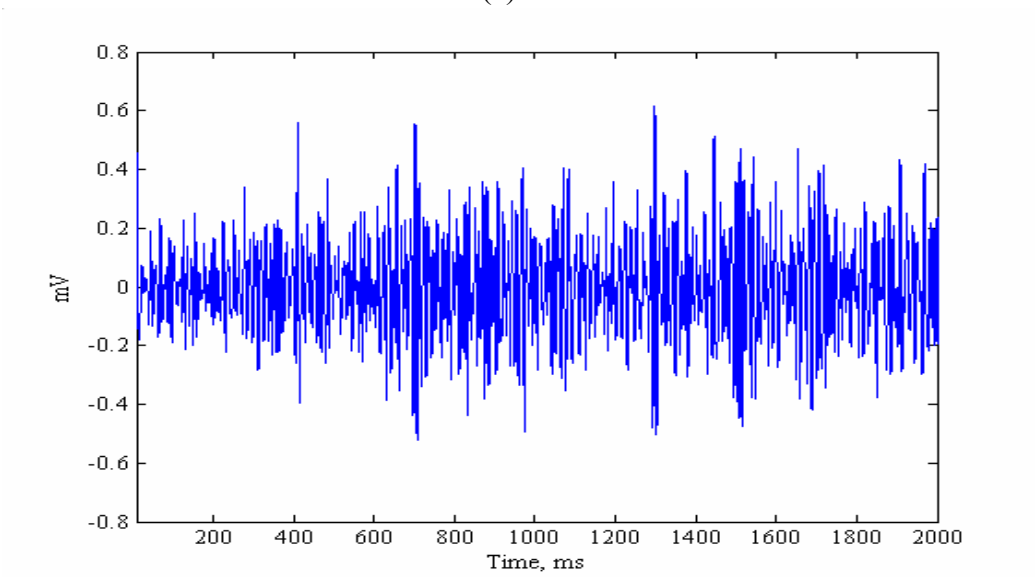

(b)

Figure 6.11: Generated EMG signals for a) young and b) elderly at 100% MVC

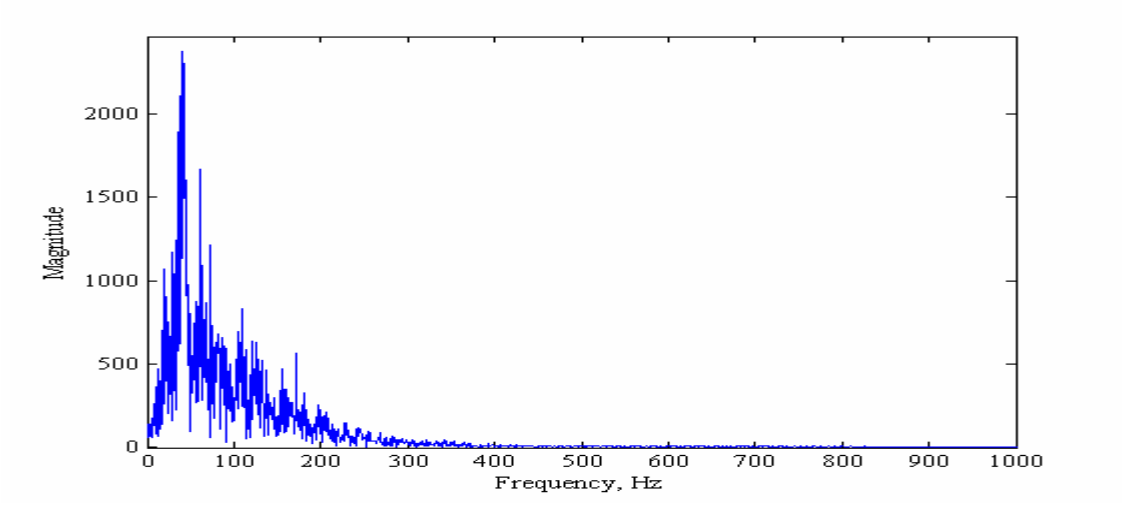

(a)

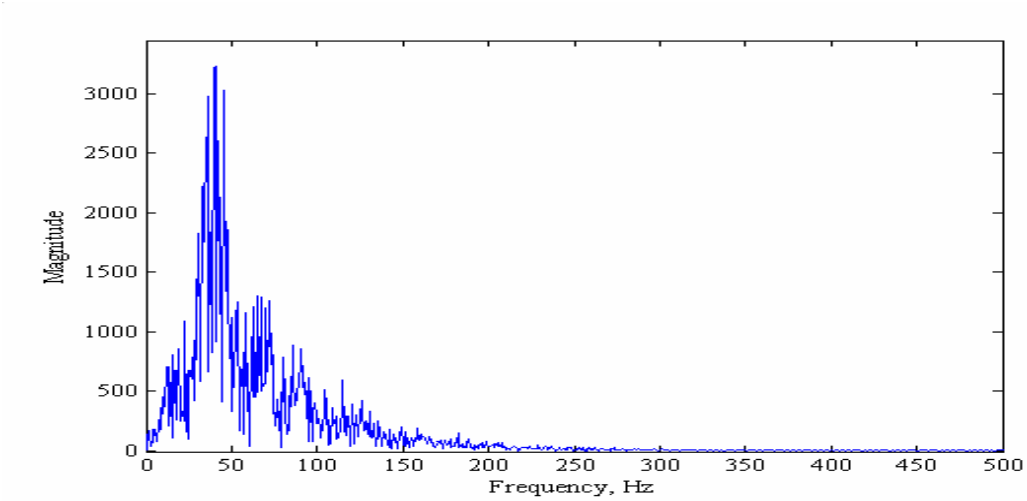

(b)

Figure 6.12: Generated EMG signal spectrum for a) young and b) elderly at 100% MVC

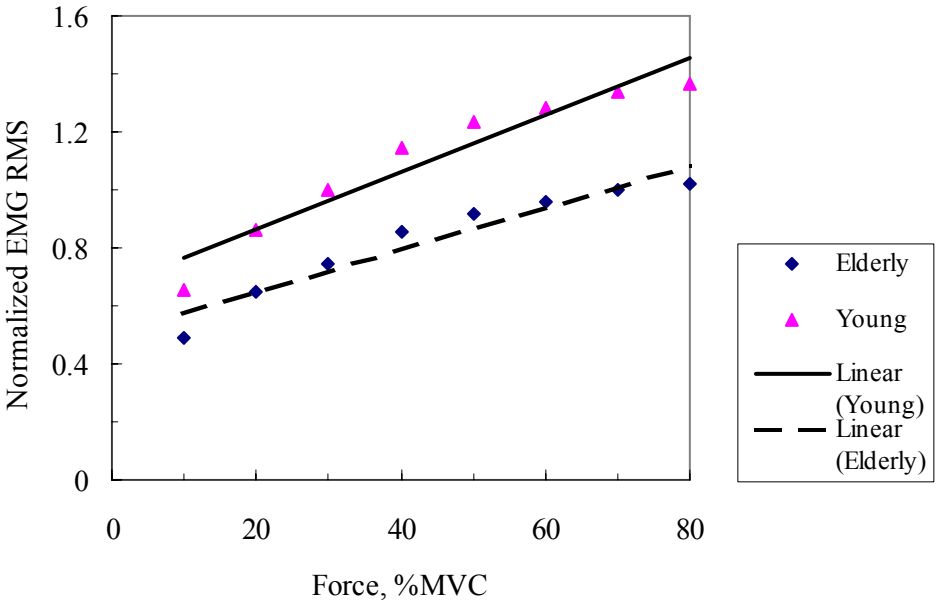

Figure 6.13: Normalized EMG-force relationship for both young and elderly in tibialis anterior muscle

time variable parameters of EMG between young and elderly tibialis muscle. Mean and median frequency of the EMG signals for both young and elderly are compared in Figure 6.15.

To verify the simulation results, experimental work of Yamada et al [112] on young and elderly is adopted. Although the exact experimental parameters were not known, the different physiological parameters for young (20 year old) and elderly (80 year old) are for the average young and old subjects that were adopted from the published data described in this chapter and the earlier chapters. Figure 6.16 illustrates the simulated average rectified value (ARV) and the experimental value for young and elderly subjects respectively at the maximum voluntary contraction. Comparison and statistical analysis shows that simulated and experimental results are not significantly different ($p < 0.05$, two tailed, paired). Similarly, median frequency for both young and elderly are compared in Figure 6.17 for simulated and experimental results. These results also show that there is no significant difference ($p < 0.05$) between simulated and the experimental results.

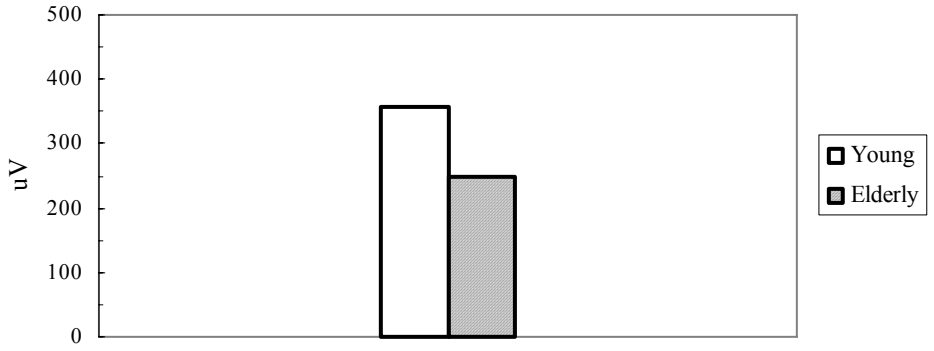

(a)

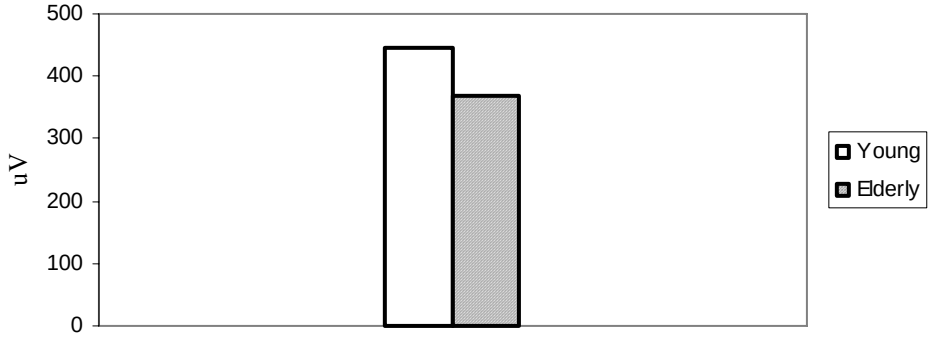

(b)

Figure 6.14: Comparison of a) ARV and b) RMS of the EMG for young and elderly at 50% MVC

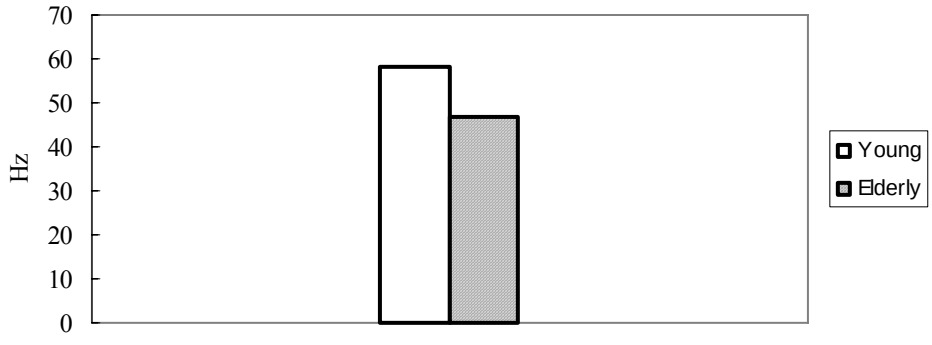

(a)

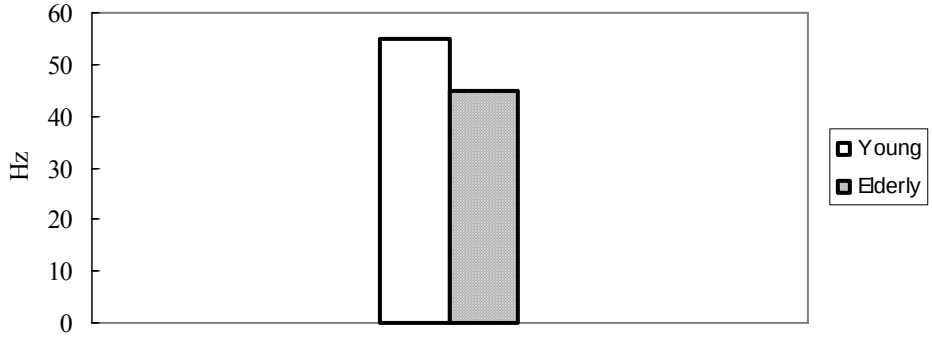

(b)

Figure 6.15: Comparison of a) mean and b) median frequency of the EMG for young and elderly at 50% MVC

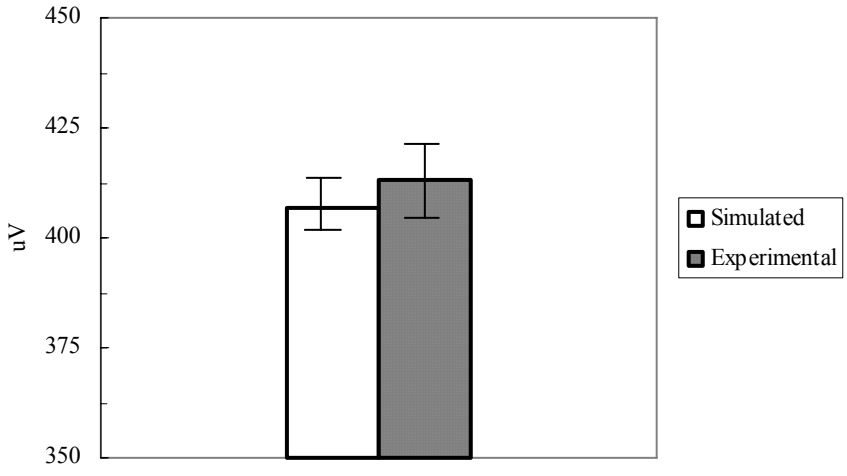

(a)

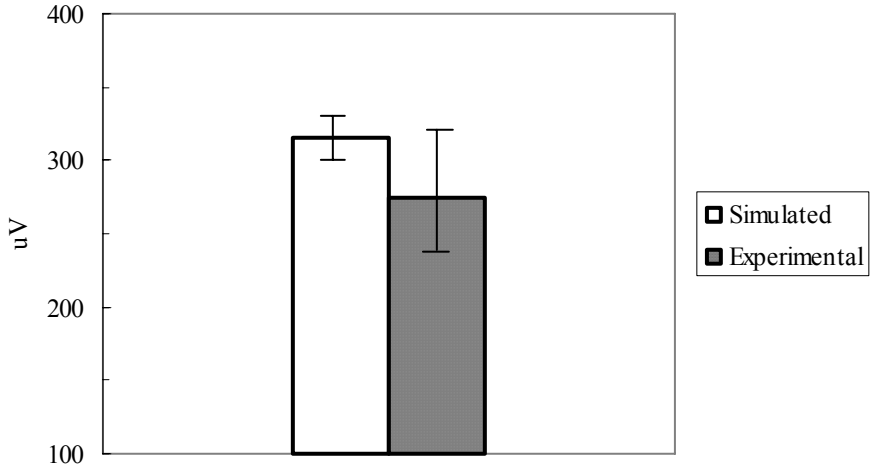

(b)

Figure 6.16: Comparison of ARV of the simulated and experimental EMG of a) young and b) elderly at 100% MVC

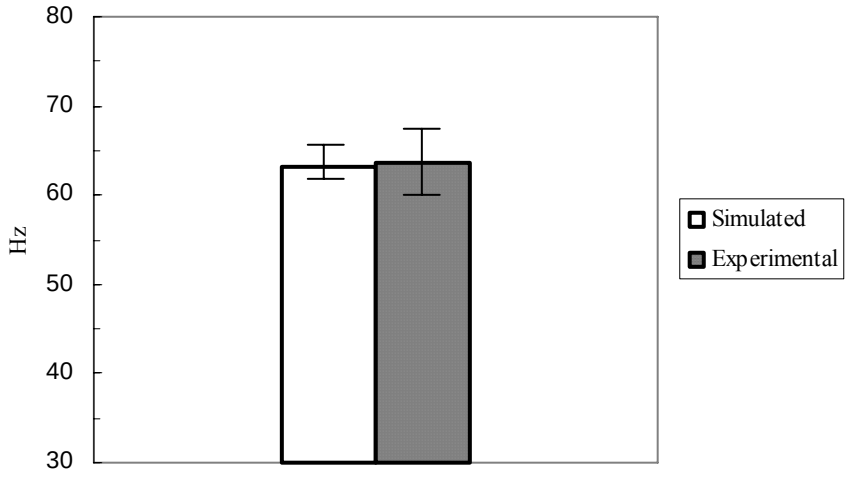

(a)

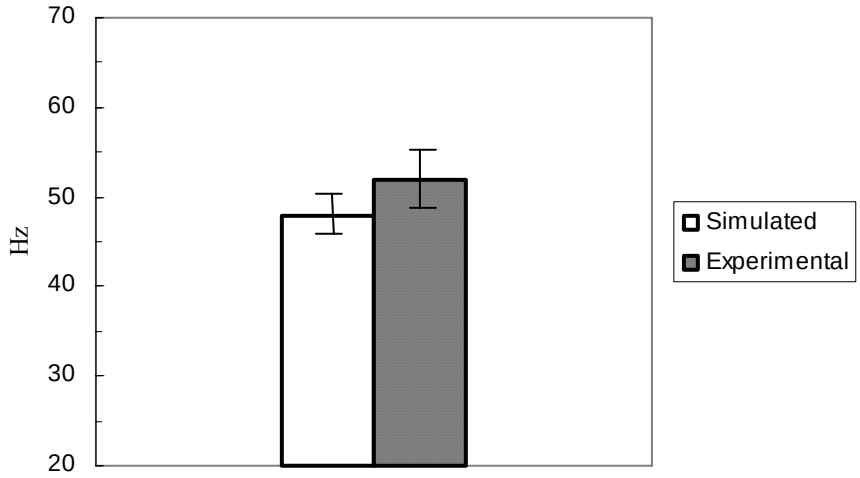

(b)

Figure 6.17: Figure 6.17: Comparison of a) median frequency of the simulated and experimental EMG of a) young and b) elderly at 100% MVC

CHAPTER 7

7. Conclusion and Recommendations For Future Work

7.1 Conclusion

An EMG generation algorithm has been developed in this study using two separate models. The first model describes an extracellular single fiber action potential calculation and thus motor unit action potential, which is the summation of all the single fiber action potential in a motor unit. The second model is a motor neuron pool model which is a mathemetical description of brain muscle interaction. This model describes the nature of motor unit recruitment and their discharge rate during contraction. Although these two models were not necessarily original in design, the techniques followed to develop the motor neuron pool model algorithm using the accurate and most up to date motor unit physiology will facilitate the application of this model in several areas of biomedical research. One of the application of this EMG generation model has been shown in remodeling of human muscle during aging.

Difference between most of the single fiber action potential generation technique lie in the representation of the membrane current in different mathemetical forms. In this study, line source model which considers the transmembrane current as discrete point sources along the axis of the muscle fiber for a finite fiber was utilized to derive the

analytical solution of extracellular action potential. The effects of anisotropic muscle volume conductor were investigated for fibers located in different distances from the recording surface. These findings show that, muscle volume conductor attenuate and can also shift the phase of the recorded potential. Moreover different electrode orientations have been simulated to analyze their effects on extracellular action potentials. A multilayer model, which includes fat and skin at the top of the muscle, described by Farina [66], was also incorporated in the model of single fiber action potential. These isotropic mediums act as low pass filter and cause further attenuation of the signal that was recorded at the muscle with the increasing fat and skin layer. This single fiber model readily provides the motor unit action potential, which is the summation of all the muscle fiber action potentials innervated by the motor unit.

Motor units are mostly two types: type-I and type-II and they have structural and functional differences. In the motor unit pool model, these two types of motor units are distributed randomly inside a hypothetical muscle and each of them were assigned a motor unit diameter and total number of fibers innervated, based on some rules from the published experimental findings. The percentage of different types of motor units in a muscle differ from muscle to muscle and this difference depends on the functionality of a specific muscle. Some rules have been reported in the earlier work about the recruitment order of motor units and the discharge behavior and pattern of the recruited motor units. Recent experimental findings validate some of the earlier concept and at the same time invalidate some of the hypothesis regarding motor unit physiology that were used in the EMG simulation by some researchers. In this study, a unique algorithm has been

presented which incorporates motor units as two different types of motor units rather than assigning the same diameter for all the motor unit fibers that was used in the earlier EMG simulation. Excitation input currents to the population of motoneurons are simulated in the form of voluntary isometric contraction to the muscle, and all the muscle input output relationships are described in the form of voluntary contraction as input and generated EMG signals as output. Simulation was performed for the tibialis anterior muscle to generate EMG signal when the input contraction is increased linearly until the simulated level of contraction in one second and stayed in that contraction level for remaining three seconds without fatigue. Temporal and spectral behavior of simulated EMG signals for various input forces were investigated. The experimental finding of the force-EMG magnitude (RMS and ARV) relation is linear for most of the muscle atleast until 80% of maximum voluntary contraction (MVC). Similar results were also found in the simulation results which showed the linear force-EMG relation until the highest recruitment threshold level that was set 60% MVC for this simulation. Thus this simulation supports the agreement between the researchers that recruitment thresholds are spread in a broader range of muscle contraction. Mean and median frequency were also found increasing with the increasing force although there is not unique relationship between them. These results are also in agreement with the experimental findings. All these simulation results suggest that overall, the model produces simulated EMG signals which closely resemble the real signals.

The utility of an EMG signal model is dependent on the degree of rigor and detail it possesses. As the model developed in this study is based on recently found physiological

behavior, it will be useful to address many neuropathological situations that undergo subtle pathological changes. One of the major pathological changes is seen in the muscle of elderly people. Thus the developed model was utilized to address these changes and their effects on the EMG signals. Tibialis anterior muscle was selected for the simulation of both young and elderly muscle using the published pathological data for both groups. Simulation showed significant changes between temporal and spectral parameters of the EMG signal of young and elderly. The results were verified with the published experimental data for both population. An aging process model was also developed in this study, which describes the pattern of changes in the compound muscle action potential (CMAP) wave shape and different metrics of CMAP during aging.

7.2 Future Recommendations

EMG signal in this study was developed for isometric voluntary contraction in which, muscle length does not change with the contraction. There are not enough data available about the physiological behavior of the muscle when the length of the muscle changes. Moreover, very little is known about the motor unit recruitment and firing rate in the high level of tension to the muscle. These information are necessary to model the EMG generation technique for its general use.

Recorded EMG signals are decomposed in its constituent parts to analyze the signals. Many researches are underway to develop techniques to decompose the EMG signals. The EMG model developed in this study provides the expected output signal for various

input force to the muscle thus can be easily employed to assess the qualitative and quantitative reliability of the decomposition techniques.

In this study only one application has been shown of this EMG model. Several other neuromuscular conditions such as muscle fatigue, Parkinson desease, Cerebral Palsy and many others can easily be modeled using the model described in this dissertation.

The EMG model described here can also be improved by modeling the single fiber action potential for actual shape of the muscle rather than considering all fibers parallel to the surface of the muscle.

REFERENCES

[1] G. A. Bekey, C Chang, J Perry, M.M. Hoffer,"Pattern recognition of multiple EMG signals applied to the description of human gait," Proceedings of IEEE, 65: 674-689, 1977.

[2] Boisset S, Matson MS, "Quantitative Relationship Between Surface EMG and Intramuscular Electromyographic Activity in Voluntary Movement," Amer J Phys Med, 51: 285-295, 1972.

[3] S. Boisset, F Goubel, "Integrated electromygraphy activity and muscle work," J Applied Physiol, 35:695-702, 1972.

[4] R. Plonsey, "The active fiber in a volume conductor," IEEE Trans Biomed Eng, 21:371-381, 1974

[5] DiFabio PP, "Reliability of Computerized Surface Electromyography for Determining the Onset of Muscular Activity," Physical Therapy, 67:43-48, 1987.

[6] Lorente de No, "A Study of Nerve Physiology," Studies from the Rockefeller Institute for Medical Research, 132:384-477, 1947.

[7] Binder M.D and Mendell L.M., 'The Segmental Motor System", Oxford, UK: Oxford Univ. Press, 1990.

[8] Burke R.E., "Motor units: anatomy, physiology and functional organization. In: Handbook of Physiology. The Nervous System, Motor Control. Bethesda, MD:Am. Physiological Society, sect.1, vol.II, part 1, pp. 345-422, 1981.

[9] Adam L, Datta A.K., Guz A., "Synchronization of motor unit firing during different respiratory and postural tasks in human sternocleidomastoid muscle: J Physiol (Land), 413: 213-231, 1989.

[10] Adrian E.D., Bronk D.W., "The discharge of impulses in motor nerve fibers, Part-II. The frequency of discharge in reflex and voluntary contractions", J. Physiol (land), 67:119-151, 1929.

[11] M.B.I. Raez, M.S. Hussain and F. Mohd-Yasin, "Techniques of EMG signal analysis: detection, processing, classification and applications", *Biol. Proced. Online*, 8:11-35, 2006.

[12] Lapatki BG, Van Dijk JP, Jonas IE, Zwarts MJ, Stegeman DF, "A thin, flexible multielectrode grid for high density surface EMG", *Journal Appl. Physiol*., 96:327-336, 2004.

[13] Mohammed Ferdjallah, Jacqueline J. Wertsch, Mohammad A. Ahad, Gulapar Phongsamart and Kevin C. McGill, "Nerve Conduction Topography in Geriatric Hand Assessment," *Journal of Rehabilitation Research and Development*, vol. 42, no. 6, pp 1-7, 2005.

[14] Mohammad A. Ahad, Abdullah Al Zaman, Mohammed Ferdjalllah and Gerald F. Harris, "Multichannel Grid Electrode Interface for EMG Mapping," *Proc. in IEEE Midwest Symp. on Circuits and Systems*, Cincinnati, OH, 2005, pp. 1770-1773, 2005

[15] Plonsey R, "Actions Potentials Sources and their Volume Conductor Fields," Proceedings of the IEEE, 65: 601-611, 1977.

[16] Plonsey R, "The Active Fiber in a Volume Conductor," IEEE Trans Biomed Eng, vol. 21, pp. 371-381, 1974.

[17] Rosenfalck P, "Intra- and Extracellular Potential Fields of Active Nerve and Muscle Fibers," Acta Physiol. Scan., suppl. 321, 1969

[18] Andreassen S, Rosenfalck A, "Ralationship of Intracellular and Extracellular Action Potentials of Skeletal Muscle Fibers," CRC Crit Rev. in Bioengineering, 6:267-306, 1981.

[19] Nandedkar SD, Stalberg E, "Simulation of Single Muscle Fiber action Potentials," Med Biol Eng Computing, vol. 21, pp. 158-165, 1983.

[20] Gootzen THJM, Stegeman DF, Van Oosterom A, "Finite Limb Dimensions and Finite Muscle Length in a Model for the Generation of Electromyographic Signals," Electroenceph Clin Neurophysiol, vol. 81:152-162, 1991.

[21] Merletti R, Conte LL, Avignone E, Guglielminotti P, "Modeling of Surface Myoelectric Signals – Part I: Model Implementation," IEEE Trans Biomed Eng, 46: 810-820, 1999.

[22] Farina D, Merletti R, "A Novel Approach for Precise Simualtion of the EMG Signal Detected by Surface Electrode," IEEE Trans Biomed Eng, 48:637-646, 2001.

[23] Burke, R.E., "Motor units: anatomy, physiology, and functional organization**.** In:" Brookhart, J.M., Mountcastle, V.B.. Brooks. V.B.. Geiger, S.R., eds. Handbook of Phvsiologv. Bethesda, MD: American Physiological Society. 345-422, 1981.

[24] Enoka, R.M., "Morphologicai features and activation patterns of motor units", *Journal of Clinical Neurophysiolo,oy*, 12, 53 8-559, 1995

[25] Henneman, E., & Mendell, L.M.**, "**Functional organization of the motoneuron pool and its inputs. In J.M Brookhart, V.V. Mountcatle (Eds.) Handbook of Phyiology: Section 1 The Nevous System (pp 423-507) Berthesda, Maryland, American Physiological Society, 1981.

[26] Heckman, C.J., & Binder, M.D., Computer simulation of the steady-state input-output function of the cat medial gastrocnernius motor-neuron pool. *Journal of Neurophvsiology*, 65,952-967, 1991

[27] Kemell, D., & Hultborn, H**.,** "Synaptic effects on recruitrnent gain: a mechanism of importance for the input-output relations of motoneurone pools", *Brain Research*. 507, 176- 179

[28] Bernardi, M., Solomonow, M., Nguyen, G., Smith, A., & Baratta, **R.**(1996).Motor unit recruitment strategy changes with skill acquisition. *European Journal of Applied Physiol.*, 74:52-59, 1996.

[29] Enoka R.M, Neural adaptations with chronic physical activity. *Journal of Biomechanics*. 30, (5),447-455, 1997.

[30] Sale GD, Neural adaptation to resistance training. *Medicine in Science and, Sports and Exercise*, 20, (5), s 135- 145,. 1988

[31] Fuglevand A.J., Winter D.A., Patla A.E., "Models of recruitment and rate coding organization in motor unit pool", J. Neurophysiol., 70:2470-2488, 1993

[32] Stashuk D.W., "Simulation of electromyographic signal", J. Electromyogr. Kinesil., 3:157-173, 1993.

[33] Zajac, F.E. "Muscle and tendon: properties, models, scaling, and application to biomechanics and motor control", *Critical Reviews in Biomedical Engineering*, -17, (4), 359-411, 1989

[34] Kernell,D., "The adaptation and the relation between discharge frequency and current strength of cat lumbosacral motoneurons stimulated by long-lasting injected currents.", Acta Physiol. Scand., 65:65-73, 1965.

[35] Stein R.B., French A.S., Mannard A. and Yemm R. “New methods for analyzing motor function in man and animals”, Brain Res, 40:187-192, 1972

[36] Goldberg L.J., and Derfler B., “Relationship among recruitment order, spike amplitude and twirch tension of single motor units in human masseter”, J. Neurophysiol., 40:879-890, 1977.

[37] Harrison, P.J., “The relationship between the distribution of motor unit mechanical properties and the force due t recruitment and to rate coding for the generation of muscle force”, Brain Res. 264: 311-315, 1983.

[38] Pan Z.S., Zhang Y., Parker P.A., “Motor unit power spectrum and firing rate”, Med. Biol. Eng. Comput., 27:14-18, 1989.

[39] Martini R, “Anatomy Physiology”, Prentice Hall Inc, 2000

[40] http://www.bergen.org/ACADEMY/Bio/molbio/AAMB5_Lesson/STRIATEDMUSC/MusclePage1.html

[41] Buchthal F., Guld C. and Rosenfalck P., “Multielectrode study of the territory of a motor unit”, Acta Physiol. Scand., 39:83-104, 1957.

[42] Gath I., Stalberg E., “On the measurement of fiber density in human muscles”, Electroenceph. Clin. Neurophysiol., 54:699-706, 1982.

[43] Lexell J., Taylor C.C., and Sjostrom M., “What is the cause of the ageing atrophy?”, J. Neurol. Sci. 84:275-294, 1988.

[44] Duchene J. and Hogrel J., “A model of EMG generation”, IEEE Trans. On Biomed. Engg., 47:192-201, 2000.

[45] Lange F, Van Weerden TW, and Van Der Hoeven JH, "A new surface electromyography analysis method to determine spread of muscle fiber conduction velocities", *J Appl Physiol* 93: 759-764, 2002

[46] C. S. Klein, G. D. Marsh, R. J. Petrella, "Muscle Fiber Number in the Biceps Brachii Muscle of Young and Old Men," Muscle & Nerve, vol. *28*, pp. 62-68, 2003.

[47] Porter M.M., Stuart S., Lexell J., "Capilary supply of the tibialis anterior muscle in young and healty and moderately active men and women", J. appl. Phyisiol. 92:1451-1457, 2002.

[48] Gordon T, Pattullo M.C., "Plasticity of muscle fiber and motor unit types", Holloszy JO, ed, Exercise and sport sciences reviews. Vol. 21. Baltimore: Williams & Wilkins, pp. 331-362, 1993

[49] Enoka R.M., Fuglevand A. J., "Motor unit physiology: some unresolved issues", Muscle Nerve, 34:4-17, 2001.

[50] Fordon D.A., Enoka R. M., Stuart D. G., "Motor unit force potentiation in adult cats during a standard fatigue test", J. Physiol. (Lond), 421:569-582, 1990.

[51] Kanda K., Hashizume K., "Factors causing difference in force output among motor units in the rat medial gastrocnemius muscle", J. Physiol. (Lond), 448:677-695, 1992.

[52] Totosy de Zepetnek J., Zung H.V., Erdebil S., Gordon T., "Innervation ratio is an important determinant of force in normal and reinnervated rat tibialis anterior muscles", J. Neuro-physiol., 67:1385-1403, 1992.

[53] http://en.wikipedia.org/wiki/Action_potential

[54] http://www.fortunecity.com/greenfield/buzzard/387/actionpot.htm

[55] Albers BA, Rutten WL, DE Jonge W, "Microscopic and macroscopic volume conduction in skeletal muscle tissue: Applied to simulation of single muscle fiber action potentials", Medical & Biological Engineering Computing, 26:605-610, 1988

[56] Brown WF, Strong MJ, Snow R, "Methods of estimiating numbers of motor units in biceps brachialis muscles and losses of motor unit with aging", Muscle & Nerve, 11:423-432, 1988

[57] Barker AT, Brown BH, Freston IL, "Modeling of an active nerve fiber in a finite volume conductor and its application to the calculation of surface action potentials", IEEE Trans on Biomedical Engineering, 26:53-56, 1979.

[58] Gath I, Stalberg E, "On the volume conduction in human skeletal muscle: In situ measurements", Electro-encephalgraphy & Clinical Neurophysiology, 43:106-110, 1977

[59] Gath I, Stalberg E, "The calculated radial decline of the extracellular action potential compared with in situ measurements in the human brachialis biceps muscle", Electro-encephalgraphy & Clinical Neurophysiology, 44:547-552, 1978

[60] Andreassen S, Rosenfalck A, "Ralationship of Intracellular and Extracellular Action Potentials of Skeletal Muscle Fibers," *CRC Critical Reviews in Bioengineering*, vol. 6, pp. 267-306, 1981.

[61] Rosenfalck P, "Intra- and Extracellular Potential Fields of Active Nerve and Muscle Fibers," Acta Physiol. Scan., suppl. 321, 1969

[62] Fleisher, S. M., "Comparative analysis of modelled extracellular potentials", Med. & Biol. Eng. & Comput. 22:440-447, 1984

[63] Albers, B A., Rutten WLC., Wallinga-de Jonge W. and Boom HBK, "Microscopic and macroscopic volume conduction in skeletal muscle tissue, applied to simulation of single fibre action potentials", Med. & Bio. Eng. & Comput. 26:605-610, 1988.

[64] Benno K. van Veen, Wolters H, Wallinga W, Rutten WLC,and Boom HBK, "The bioelectrical source in computing single muscle fiber action potentials", Journal of Biophysics, 64:1492-1498, 1993

[65] R. Plonsey, "Actions potential sources and their volume conductor fields," Proceeding of the IEEE, vol. *65*, pp. 601-611, 1977

[66] Faina D, Rainoldi A, "Compensation of the Effect of Sub-cutaneous Tissue Layers on Surface EMG: A Simulation Study," Medical Engineering and Physics, vol. 22. pp. 487-496, 1999.

[67] Rahman, MM, "Analysis of 2D spatial filtering of simulated muscle action potential using grid arrays", MS thesis, University of Tennessee, 2005.

[68] Mohammad A. Ahad, Jacqueline J. Wertsch and Mohammed Ferdjallah, "Effect of Motor Unit Distribution on Computer Generated Action Potential" *Muscle & Nerve,* 2006; 34:530.

[69] Riek S. and Bawa P. "Recruitment of motor units in human forearm extensor", J Neurophysiol., 68:100-108, 1992

[70] Zajac F.E., Faden J.S., " Relationship among recruitment order, axonal conduction velocity, and muscle unit properties of type-identified motor units in cat plantaris muscle", J Neurophysiol., 53:1303:1322, 1985.

[71] Nordstrom M.A., Miles T.A., "Discharge variability and characterization of motor units in a heterogeneous muscle (Flexor digitorum longus) of cat", Comp. Neurol, 128:475-498, 1966.

[72] Henneman E., "Functional organization of motoneuron pools: the size principle", Integration in the Nervous System, edited by H. Asunuma and V.J. Wilson. Tokyo: Igaku Shion, pp. 13-25, 1979.

[73] Monster AW, Chan H., "Isometric force production by motor units of extensor digitorum communis muscle in man", *Journal of Neurophysiol*, 40:1432-1443, 1977.

[74] Grimby L, Hannerz K, "Firing rate and recruitment order of toe extensor motor units in different models of voluntary contraction", *Journal of Physiol (land),* 264:865-879, 1977.

[75] Gilchrist J.M., Perrone M., and Ross J., "Dynamical analysis of neuromuscular transmission jitter", Muscle Nerve, 18:685-692, 1995.

[76] De Luca C.J., Forrest W.J., "Some properties of motor unit action potential trains recorded during constant force isometric contractions in man", Kybernetik, 12:160-168, 1973.

[77] Shiavi R., Negin M., "Stochastic properties of motoneuron activity and the effect of muscle length", Biol. Cybern, 19: 231-237, 1975.

[78] Clamann H.P., "Statistical analysis of motor unit firing patterns in a human skeletal muscle", Biophys. J, 9:1233-1251, 1969.

[79] Lago P. and Jones N.B., "Effect of motor unit firing time statistics on EMG spectra", Med. Biol. Eng. Comput., 15:648-655, 1977.

[80] Grimby L, Hannerz K, "Firing rate and recruitment order of toe extensor motor units in different models of voluntary contraction", *Journal of Physiol (land),* 264:865-879, 1977.

[81] Kukulka CG, Clamann HP, "Comparison of the recruitment and discharge properties of motor units in human brachial biceps and adductor pollicis during isometirc contraction*", Brain Res*, 219:45-55, 1981.

[82] De Luca CJ, LeFever RS, McCue MP, Xenakis AP, "Behavior of human motor units in different muscles during linearly varying contraction", *Journal of Physiol (Lond)*, 329:113-128, 1982.

[83] Kernell D and Sjoholm H., "Recruitment and firing rate modulation of motor unit tension in a small muscle of the cat's foot", 98:57-72, 1975.

[84] Jakobson F, Borg K, Edstrom L, Grimby L, "Use of motor units in relation of muscle fiber type and size in men", *Muscle & Nerve*, 11:1211-1218, 1988.

[85] http://www.health.uottawa.ca/biomech/courses/apa4311/biomec~3.htm#force

[86] G. N. Williams, M. J. Higgins, M. D. Lewek, "Aging skeletal muscle: Physiologic changes and the effects of training", *Physical Therapy*, *82*, 62-68, 2002.

[87] M. A. Rogers, W. J. Evans, Changes in Skeletal Muscle with Aging: Effects of exercise Training, *Exerc Sport Sci Rev*, *21*, 65-102, 1993.

[88] W. R. Frontera, V. A. Hughes, R. A. Fielding, Aging of skeletal muscle: A 12 year longitudinal study, *Journal for Applied Physiology, 88*, 1321-1326, 2000.

[89] A. C. Hooper, Length, diameter and number of ageing skeletal muscle fibers, *Gerontology, 27*, 121-126, 1981.

[90] J. Lexell, C. C. Taylor, M. Sjostrom, What is the cause of the ageing atrophy? Total number, size and proportion of different fiber types studied in whole Vastus Lateralis Muscle from 15 to 83 year-old men, *Journal of Neurol Sci*, *84*, 275-294, 1988.

[91] W. F. Brown, M. J. Strong, R. Snow, Methods for estimating numbers of motor units in biceps-brachialis muscles and losses of motor units with aging, Muscle *& Nerve 11*, 423-432, 1988.

[92] J. Lesell , C. C. Taylor, Variability in muscle fiber areas in whole human Quadriceps Muscle: Effects of increasing age, *Journal of Anatomy, 174*, 239-249, 1991.

[93] J. A. Kent-Braun, A. V. Ng, K. Young, Skeletal Muscle Contractile and Noncontractile Components in Young and Older Women and men, *Journal for Applied Physiology*, 88, 662-668, 2000.

[94] P. G. Arabadjis, R. R. Heffner, D. R. Jr, Pendergast, "Morphologic and functional alterations in Aging Rat Muscle", *Journal of Neuropathol Exp Neurol, 49*, 600-609, 1990.

[95] M. Brown, Change in fiber size, not number, in aging skeletal muscle, *Age Ageing*, *16*, 244-248, 1987.

[96] M. M. Porter, A. A. Vandervoort, J. Lexell, "Aging of human muscle: structure, function and adaptability", *Scand J Med Sci Sports*, *5*, 129-142, 1995.

[97] R. S. Schwartz, Sarcopenia and physical performance in old age: Introduction, *Muscle and Nerve*, supp 5,pp. 10-12, and 1997.

[98] C. S. Klein, G. D. Marsh, R. J. Petrella, Muscle Fiber Number in the Biceps Brachii Muscle of Young and Old Men, *Muscle & Nerve*, *28*, 62-68, 2003.

[99] G. Goldspink, Malleability of the motor system: A comparative approach, *Journal of Experimental Biology, 115*, 375-391, 1985.

[100] Kanda, K., and Hashizume, K. Changes in properties of the medial gastrocnemius motor units in aging rats. *J. Neurophysiol.* 61: 737-746, 1989.

[101] Roos, M. R., Rice, C. L., and Vandervoort, A. A. Age-related changes in motor unit function. *Muscle Nerve* 20: 679-690, 1997.

[102] Ansved, T., and Larsson, L. Effects of aging on the motor unit. *Prog. Neurobiol.* 45: 397-458, 1995.

[103] Zeynep Erim, M. Faisal Beg, David T. Burke, and Carlo J. de Luca**,** "Effects of Aging on Motor-Unit Control Properties", *J Neurophysiol* 82: 2081-2091, 1999.

[104] Campbell M.L, McComas AJ, Petito F., "Physiological changes in ageing muscles", *Journal of Neurol Neurosurg Psychiatry*, 36:174-182, 1973.

[105] Galganski ME, Fuglevand AJ, Enoka RM, "Reduced control of motro output in human hand muscle of elderly subjects during submaximal contractions", *Journal of Neurophysiol*, 69:2108-2115, 1993.

[106] Keen DA, Yue GH, Enoka RM, "Training-related enhancement in the control of motor output in elderly humans", *Journal of Applied Physiol*, 77:2648-2658, 1994.

[107] Jakobson F, Borg K, Edstrom L, Grimby L., "Use of motor units in relation of muscle fiber type and size in man", *Muscle Nerve*, 11:1211-1218, 1988.

[108] Connelly D.M., Rice CL, Roos MR, "Motor unit firing rates and contractile properties in tibialis anterior of young and old men", *J. applied Physiol*, 87:843-852, 1999.

[109] Sale DG, "Neural adaptation to resistance training*", Med Sci Sports Exerc*, 85:319-331, 1988.

[110] Duchateau J, Hainaut K, "Effects of immobilization on contractile properties, recruitment and firing rates of human motor units", *Journal of Physiol (Lond)*, 422:55-65, 1990.

[111] McNeil CJ, Doherty TJ, Stashuk DW and Rice CL, "Motor unit number estimates in the tibialis anterior muscle of young, old, and very old men", *Muscle Nerve*, 31:461-467, 2005

[112] Yamada H et al, "Effect of aging on EMG variables during fatiguing isometric contraction", *Journal Human Ergol,* 29:7-14, 2000.

VITA

Mohammad Abdul Ahad, the son of Late Abdul Munaf and Mrs. Feroza Begum, was born in Chittagong, Bangladesh. Upon completion of preliminary schooling from St. Mary's School, he went to Collegiate School, Chittagong and Chittagong College for high schooling. He secured 13th and 17th position in the combined merit list in Secondary School Certificate and Higher Secondary School Certificate Examinations respectively. He earned his Bachelor degree in Electrical and Electronic Engineering from the prestigious Bangladesh University of Engineering and Technology (BUET), Dhaka Bangladesh. He joined the University of Tennessee, Knoxville in Master's program of Electrical Engineering in 1999. He continued his higher studies in the same University and the same department and is going to get his Ph.D. in Summer 2007. He is joining the Harvard Medical School as a post-doctoral fellow from August 2007.